Università degli Studi di Milano - Bicocca
Dept. of Biotechnologies and Biosciences

Ph.D Program in Biology

Late sodium current (I_{NaL}) enhancement contributes to cardiac pathological remodeling

Candidate:
Carlotta Ronchi
Matricola 076022

Advisor:
Prof. Marcella Rocchetti

Cycle XXVIII

We never know how high we are
Till we are asked to rise
And then if we are true to plan
Our statures touch the skies ...

Emily Dickinson

Contents

Chapter 1

Introduction

1.1 Acronyms

APD	action potential duration
AP	action potential
CAD	coronary artery disease
CaM	calmodulin
CaMKII	Ca^{2+}/CaM-dependent protein kinase II
Ca$_T$	Ca^{2+} transient
DADs	delayed after depolarizations
EADs	early after depolarizations
ECC	excitation-contraction coupling
ECG	electrocardiogram
$\mathbf{E}_{NCX}$	Na^+/Ca^{2+} exchanger equilibrium potential
HF	heart failure
$\mathbf{I}_{KATP}$	ATP-sensitive K^+ current
$\mathbf{I}_{K1}$	inward rectifier K^+ current
$\mathbf{I}_{Kr}$	rapid delayed rectifier K^+ current
$\mathbf{I}_{Ks}$	slow delayed rectifier K^+ current

$\mathbf{I}_{Na}$	Na^+ current
$\mathbf{I}_{NaL}$	late sodium current
$\mathbf{I}_{NaT}$	transient sodium current
$\mathbf{I}_{NCX}$	sarcolemmal Na^+/Ca^{2+} exchanger (sNCX) current
$\mathbf{I}_{to}$	transient outward current
$\mathbf{I}CaL$	L type Ca^{2+} current
LQTS	long QT syndrome
LV	left ventricle
MI	myocardial ischemia
mNCX	mitochondria Na^+/Ca^{2+} exchanger
Nav	voltage-gated Na^+ channels
$\mathbf{Na}_{cyt}$	cytosolic Na^+
sNCX	sarcolemmal Na^+/Ca^{2+} exchanger
NHE	Na^+/H^+ exchanger
NKA	Na^+/K^+ ATPasi
NO	nitric oxide
NOS	nitric oxide synthase
PI3K	phosphoinositide 3 kinase
ROS	reactive oxygen species
RAN	ranolazine
RyR	ryanodine receptors
SERCA	SR Ca^{2+}-ATPase
SR	sarcoplasmic reticulum
TTX	tetrodotoxin

1.1.1 Late Sodium Current

late sodium current (I_{NaL}) represents a functionally relevant contributor to cardiomyocytes electrophysiology. In non-pathological conditions, although relatively small, it is sufficiently large during cardiac action potential (AP) affect the duration; it flows over hundreds of milliseconds during AP contributing to Na^+ loading [47]. In pathological conditions, enhancement of I_{NaL} is associated to increased proarrhythmic risk due to electrophysiological and mechanical impairments[89][50][33][46].

1.1.2 Cardiac Action Potential

The cardiac AP arises from a delicate balance of depolarization and repolarization coordinated through precisely timed opening and closing ion channels. Cardiomyocytes exhibit an AP morphology with 4 phases (Figure 1.1). Phase 0 is the rapid depolarizing phase that results when Na^+ channels activate and an influx of Na^+ (I_{Na}) causes the membrane potential depolarization. Phase 1 corresponds to the inactivation of Na^+ channels and outward movement of K^+ ions through outward current (I_{to}). In phase 2, a low conductance plateau phase, inward and outward ion movements are balanced mainly by L-type calcium current (I_{CaL}) and delayed rectifier K^+ channels (rapid I_{Kr} and slow I_{Ks}), respectively. Phase 3 marks the final repolarization phase of the AP, which returns to the resting potential at about -80 mV (phase 4) [28].

1.1.3 Na^+ channels

The role of voltage-gated Na^+ channels (Nav)) in excitable tissues (e.g. neurons and myocardium) is to support autogenerative impulse propagation. The most represented isoform of Na_V in the heart is the isoform Nav1.5, which has a relatively low affinity for the neuron Na^+ channels selective blocker tetrodotoxin (TTX) [13]. Nav1.5 is a macromolecular complex consisting of subunits and accessory protein in the sarcolemma membrane of cardiomyocytes. The pore-forming α-subunit protein encoded by SCN5A gene, is composed of four heterologous domains, each

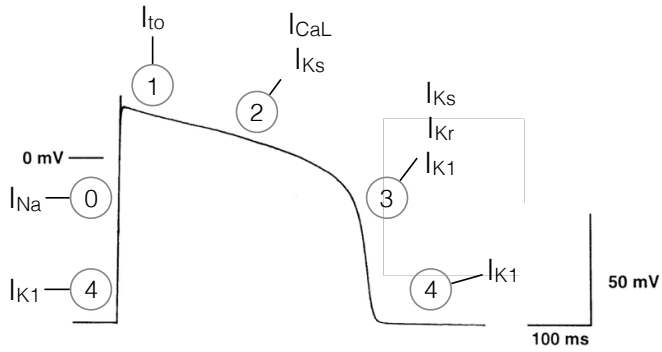

Figure 1.1: *Cardiac action potential.* The cardiac AP is generated by transmembrane inwardly and outwardly directed ion currents.

with six transmembrane segments [1]). Influx of Na^+ through Nav1.5 channels produces a large and transient sodium current (I_{NaT}) that is responsible for the initial fast upstroke of the AP (phase 0). I_{NaT} thus, determines excitability of myocardial cells and ensures proper conduction of the electrical impulse within the heart. I_{NaT} is transient because the channel once opened it is rapidly inactivated within several milliseconds by the intrinsic time dependent inactivation at the beginning of the AP plateau (phase 2) (Figure 1.3)

1.1.4 Plateau Na^+ current

In 1979 Coraboeuf et al. [20] have measured AP in dog Purkinje fibres and found that TTX reduced the action potential duration (APD) at concentrations lower than those required for the reduction of the AP upstroke velocity. These findings led them to the conclusion that there was a persistent component of Na^+ current during the AP plateau phase, which was

more sensitive to TTX than I_{NaT}. This persistent Na^+ current is somewhat involved in determining the balance of inward and outward currents that influence the AP plateau. Two mechanisms have been proposed to underlie this persistent component of Sodium current (I_{Na}): the window current and the late sodium current.

1.1.4.1 Window Plateau Current

For voltage-gated ion channels exists a voltage range (window) where the steady state inactivation curve and the activation curve overlap (Figure 1.2 A). Within this voltage range (-65 to -50 mV for Nav1.5) Na^+ channels, previously inactivated, may react and a steady-state equilibrium currents ensue [110]. The current through these channels (<1% of the peak I_{Na}) is called the window current, since it arises when the sarcolemma reaches a potential that is depolarized sufficiently to reactivate some channels, but not enough to cause complete inactivation [3]. The voltage range for the window current is very restricted in physiological conditon, granting it a small role during the cardiac AP [47]. However, an window current increment, due to delayed inactivation of cardiac Na^+ channels, has been associated with some pathological condition [103] (Figure 1.2 B-C).

1.1.4.2 Non-window plateau current (I_{NaL})

It has been observed that a lower TTX-sensitive Na^+ current with very slow or negligible inactivation was present also at potentials outside to the window current in several types of myocytes isolated from normal heart [62] [40][113][7]). This current is named late sodium current (I_{NaL}), which is much smaller than I_{NaT} in physiological condition. However, I_{NaL} may be enhanced by more than 3- to 5-fold under several pathological conditions as myocardial ischemia, heart failure and congenital long QT syndrome (described below) (Figure 1.3 B).

Expressing Nav1.5 in a heterologous system, Maltsev and Undrovinas [48] demonstrated that I_{NaL} was carried by the same molecular entity that carried I_{NaT}. The authors separated the I_{Na} into three phases (early, intermediate and late), characterized by distinct gating modalities. Two gating

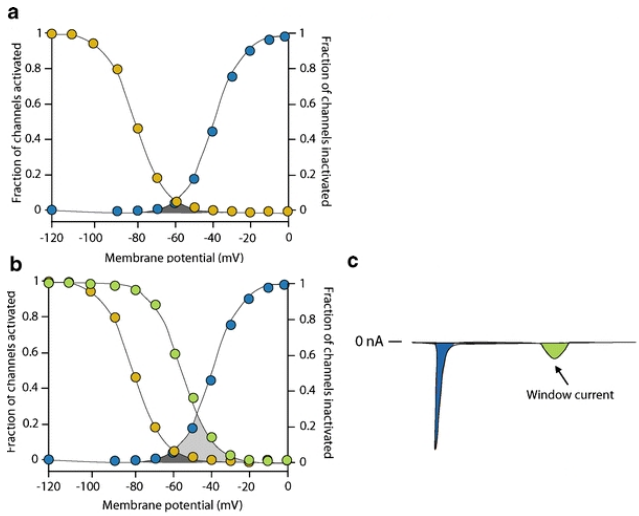

Figure 1.2: *Window plateau current.* A) The overlapping between the activation cure (blue circle) and the deactivation curve (yellow circle) determines the voltage range (dark grey area) for the window current. B-C) Window current increase (C) due to delayed inactivation of cardiac sodium channels (green circle). Modified by [3]

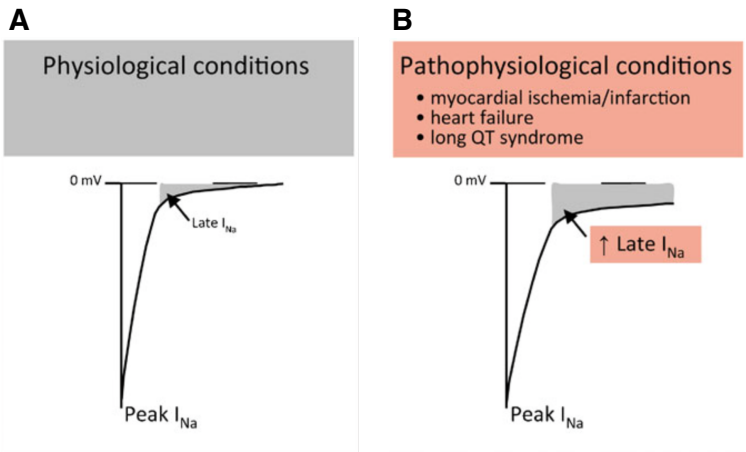

Figure 1.3: *Late Sodium Current.* I_{NaL} in physiological conditions (A) and in pathophysiological conditions (B). modified from [70]

mechanisms underlined the late phase (I_{NaL}): a burst mode openings, which undergo voltage-dependent inactivation and are not observed during I_{NaT} and a late scattered openings which inactivate extremely slowly and therefore are able to determinate a background Na^+ current. The burst mode is the principal gating mechanism of I_{NaL} and it is frequency-dependent, with a decrease in I_{NaL} during rapid heart rates [114] [57]. I_{NaL} could be also due to by an increase in the rate of channel recovery from inactivation relative to deactivation. This mechanism observed in some Nav1.5 mutations, has been referred to as reactivation under non-equilibrium conditions. This is because the excess I_{Na} can be observed only during dynamic changes of membrane potential (non-equilibrium) [18]. Since I_{NaL} is carried by the same molecular entity accounting for I_{NaT}, it is generally considered a reopening of Na^+ channels during sustained depolarization of AP and I_{NaL} enhancement may conversely reflect gating abnormalities.

1.1.5 Factors and conditions inducing I_{NaL} enhancement

I_{NaL} enhancement has been characterized under a wide variety of experimental conditions. The causes of I_{NaL} enhancement seem not be mutually exclusive but may be upstream or downstream elements in a regulatory or pathological pathway. Possible mechanisms at the cellular level for the increased I_{NaL} in cardiac disease are coming into focus, but the discovery of the mechanisms at the biophysical level appears less tractable.

1.1.5.1 Molecules

It has been showed that I_{NaL} can be induced by ischemic metabolites, oxygen free radicals and chemicals.

During ischemia/reperfusion there is an accumulation of ischemic metabolites such as palitolyl-L-carnitine, lysophosphatidylcholine that can induce an I_{NaL} enhancement [91][106]. Song et al [83] have demonstrated that I_{NaL} blockade attenuated H_2O_2-induced APD prolongation and suppressed early after depolarizations (EADs) in guinea pig and rabbit isolated ventricular myocytes. Several studies have also shown that the I_{NaL} is increased by hypoxia [88].

Several chemicals may induce an increase of I_{NaL}, such as veratridine [112] and Anemone toxin II (ATX-II) [83]. Zaza et al [110] notes that although all these compounds serves as important experimental tools, interpretation of their results must be with caution as their varied mechanisms of action producing I_{NaL} will affect the severity of repolarization abnormality and proarrhythmic potential.

1.1.5.2 Post-translational modifications

Multiple pathways regulate I_{NaL}, including the nitrosylation via nitric oxide synthase (NOS) and phosphorylation via a number of kinases. Nitrosylation for the Nav1.5 channel can be achieved because the syntriphin/dystrophin complex interacts with the c-terminus of Nav1.5 through PZD domains [59]. Furthermore, Ahern et al. [2] demonstrated that I_{NaL} was increased by nitric oxide (NO) generated enzymatically by NOS.

The I_{NaL} enhancement is also caused by a phosphorylation of Nav1.5 at specific residues through Ca^{2+}/CaM-dependent protein kinase II (CaMKII)-dependent mechanism [6] [99]. The Ca^{2+}-sensing protein calmodulin (CaM) binds near two residues on the c- terminus of Nav1.5 in a Ca^{2+}-dependent manner, where it slows inactivation of I_{Na} [87]. phosphoinositide 3 kinase (PI3K) signaling pathway, including a tyrosine kinase as an upstream activator and the protein kinase Akt as a downstream effector, has been recently reviewed as a modulator of cardiac ion channels including I_{Na} [105]. Furthermore, it has been observed that several anti-cancer and antiarrhythmic drugs may increase I_{NaL} and prolong APD through PI3K inhibition [39] [107].

1.2 Consequences of I_{NaL} enhancement

I_{NaL} enhancement, irrespective of causes, directly affects electrical activity and provides a route of sustained Na^+ influx. Furthermore, considering the role of Na^+ gradient in transmembrane transport, the I_{NaL} enhancement may affect ion homeostasis, generating indirect consequences of pathophysiological relevance.

1.2.1 Direct electrophysiological effects

Under normal condition, I_{NaL} and I_{Kr} are physiologically in balance during normal AP repolarization; whenever this balance is altered, by either I_{NaL} enhancement or I_{Kr} blockade, repolarization stability is compromised [79]. The direct contribution of I_{NaL} to repolarization course provides a first powerful mechanism linking arrhythmogenesis to I_{NaL} enhancement. The increased I_{NaL} is a persistent depolarizing force during the AP plateau, which opposes repolarizing currents and lengthens the AP. Thus, a sustained influx of Na^+ through increased I_{NaL} shifts the membrane potential toward more depolarized values, and leads to a prolongation of APD. Failed repolarization secondary to I_{NaL} enhancement is further characterized by a reactivation of I_{CaL}, which results in EADs [104]. EADs may trigger new ectopic AP and initiate ventricular tachycardia at the

tissue/organ levels and torsade de pointes [79] (Figure 1.4).

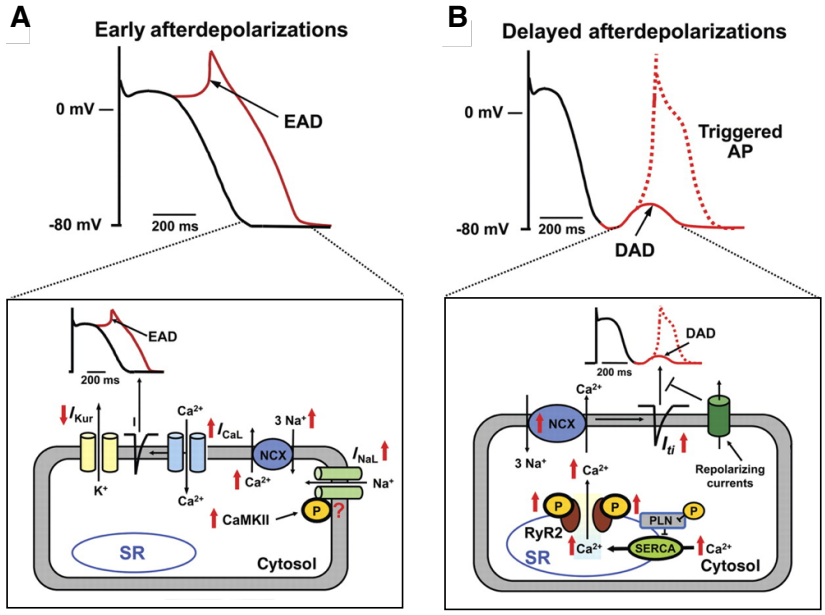

Figure 1.4: *Mechanisms of cardiac arrhythmias.* A) EADs result from excessive APD prolongation that allows I_{CaL} to depolarize the cell from the AP plateau B) DADs result from abnormal diastolic Ca^{2+} release from the sarcoplasmic reticulum viaRyRs Ca^{2+}Êrelease channels. *Modified from [56]*

1.2.2 Indirect consequences on intracellular ion homeostasis

In physiological condition, the main Na^+ influx through Na^+ channels occurs during phase 2 of AP. Even if the I_{Na} amplitude is higher during phase 0, the duration is short, so that Na^+ influx is low. Whereas, I_{Na} amplitude is lower during AP phase 2 but the duration is much longer, making phase 2 dominant in Na^+ influx [46]. An increase in I_{NaL} amplitude as found in pathological states (see below) increases the Na^+ influx by sustaining the driving force for a longer time, sufficient to raise the cytosolic Na^+ (Na_{cyt}). Na_{cyt} is normally extruded from the cell by Na^+/K^+ ATPasi pump (NKA); if Na^+ influx exceeds the maximal extrusion rate, Na^+ accumulates in the cytosol, leading to ATP consumption and dissipat-

ing Na^+ trans-membrane gradient. Because, the latter energizes many secondary membrane transport mechanisms, most importantly the sNCX and the Na^+/H^+ exchanger (NHE) (Figure 1.5), a principal consequence of an increased I_{NaL} is perturbed homeostasis of intracellular Ca^{2+} and H^+ [109]. sNCX is the main mechanism by which Ca^{2+} is extruded from cytosol and its Na^+/Ca^{2+} exchanger equilibrium potential (E_{NCX}) is mainly determined by Na_{cyt}. An increased Na_{cyt} determines a negative shift of E_{NCX}, causing less Ca^{2+} extrusion (decreased sNCX *forward mode* activity). Thus, an increased I_{NaL} may result in a significant increase in cytosolic Ca^{2+} because less energy is available in the Na^+ gradient to extrude Ca^{2+} through sNCX. If then Na_{cyt} is sufficiently high, sNCX may work in *reverse mode* with Ca^{2+} actually entering the cell (Figure 1.6). Ca^{2+} entry into the cardiomyocytes via sNCX ultimately exceeds Ca^{2+} efflux and precipitates to Ca^{2+} overload [10].

Ca^{2+} overload brings about several short and long-term changes of myocardial function [98]. Short-term changes include the spontaneous Ca^{2+} release, through RyRs, from sarcoplasmic reticulum (SR) that is directly promoted by high cytosolic and SR Ca^{2+} level [29]. When spontaneous Ca^{2+} release occurs during diastole leads to Ca^{2+} waves: part of the released Ca^{2+} is extruded through the sNCX, generating an inward current that depolarizes the membrane. This event is called delayed after depolarizations (DADs) and if it is large enough, it may reach the threshold for a premature AP, giving rise to a premature electrical activation that can propagate through the myocardium, triggering sustained arrhythmias [23] [25] (Figure 1.4 B) .

Persistent elevation of cytosolic Ca^{2+} (long-term changes) plays a pivotal role in myocardial remodelling, impairing the relaxation rate of the myocardium and causing diastolic dysfunction. I_{NaL} enhancement and therefore Na_{cyt} increase may contribute to diastolic dysfunction with different mechanisms: i) increased AP duration renders Ca^{2+} release longer and prolongs contraction: beat to beat variability of APD increases the variability of cell twitch duration in the ventricle, leading to uncoordinated relaxation; ii) increased diastolic Ca^{2+} leads to slower and incomplete my-

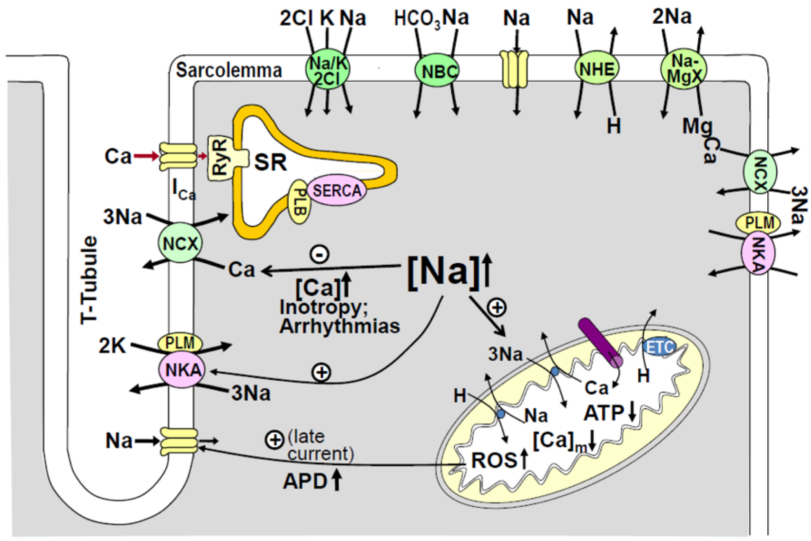

Figure 1.5: *Na_{cyt} regulation and Na^+ transport in cardiac myocytes.* The main Na^+ transporters in cardiac myocytes and the mechanisms by which an increase in Na_{cyt} affects Cacyt. [75]

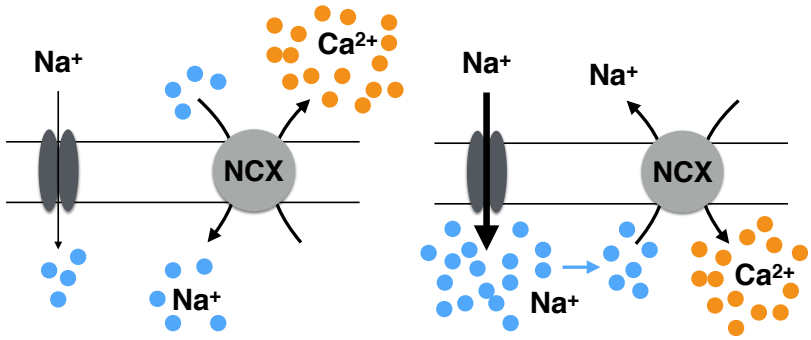

Figure 1.6: *sarcolemmal Na^+/Ca^{2+} exchanger (sNCX).* A) Forward mode activity and B) reverse mode activity of sNCX.

ofilament inactivation and relaxation: phenomenon extremely pronounced at high pacing rates, where Ca^{2+} overload extending throughout the entire diastolic period may severely impair relaxation, effectively provoking contractures [94]; iii) spontaneous SR Ca^{2+} releases induced by Ca^{2+}overload generate diastolic after- contractions that further impair and delay relaxation [93]. The concomitant increase of cytosolic Na^+ and Ca^{2+} concentration may also hamper mitochondrial Ca^{2+} uptake [41]. In particular, although elevated Na_{cyt} improves SR Ca^{2+} load and cardiac contractility, it reduces steady-state mitochondrial Ca^{2+} accumulation through activation of the mitochondrial Na^+/Ca^{2+} exchanger (mNCX), the dominant Ca^{2+} extrusion mechanism in mitochondria (Figure 1.5). This has a negative impact on the antioxidative capacity of mitochondria (NADH/NADPH), triggering oxidative stress and production of reactive oxygen species (ROS) [58] [73][41].

Elevated cytosolic Ca^{2+} activates CaMKII pathways, which enhances both SR Ca^{2+}-ATPase (SERCA) activity and RYR open probability, two actions that may contribute to spontaneous and auto-regenerative SR Ca^{2+} release [45]. Furthermore, CaMKII inducing also an I_{NaL} enhancement, may potentially supports a a positive feedback loop between Ca^{2+} overload and I_{NaL} enhancement.

High cytosolic Na^+ concentration might also decrease the driving force for extrusion of H^+ through NHE; thus, I_{NaL} enhancement may also impair control of intracellular pH, an effect of particular importance during ischemia/reperfusion [60].

1.3 Role of I_{NaL} in cardiac diseases

In recent years, the pathological increase of I_{NaL} has been linked to congenital (LQT3) and acquired (ischemia/reperfusion, hypertrophy, arrhythmias, heart failure) cardiovascular diseases and to experimentally induced conditions that mimic the pathophysiological condition. However, I_{NaL} contribution to the pathophysiology of some cardiac disease has not been clarified yet.

1.3.1 Congenital cardiac diseases

1.3.1.1 LQT syndrome

The long QT syndrome (LQTS) is a heterogeneous disorder of myocardial repolarization characterized by a prolongation of the QT interval on the electrocardiogram (ECG) and clinically manifested with episodes of arrhythmias, seizures and cardiac sudden death as consequences of physical or emotional stress [77] (Figure 1.7). LQTS are mainly originated from genetic or acquired causes. One form of LQTS (LQT3) has been linked to the *gain of function* mutations in human cardiac Nav1.5 gene (SCN5A), which typically disrupt fast inactivation of I_{Na}, leading to an increase of I_{NaL} and AP prolongation, predisposing to EADs [71]. As described before, EADs lead to trigger activity and propensity to ventricular tachycardia and torsade de pointes, the primary arrhythmia mechanism and cause of sudden death in LQT3 carriers. Some mutations in SCN5A have been identified in this subset of LQT3 patients. These include an in-frame deletion of three amino acids (Lys-1505, Pro-1506, and Glu-1507, δKPQ), and two point mutations, N1325S (Asp-1325 converted to serine) and R1644H (Arg-1644 converted to histidine) [101]. Studies on murine models of LQT3 have demonstrated that Ca^{2+} homeostasis dysregulation, secondary to an increased Na_{cyt}, provides a potentially pro-arrhythmic substrate in this congenital disease [37]. Other congenital clinical conditions associated with an enhanced I_{NaL} result from mutations in proteins that either interact with Na^+ channel directly as part of a macromolecular complex, or are important for its cellular localization. LQT10 has been related with a mutation in β4-subunit, but the mechanism for increased I_{NaL} is not known [95]. On the other hand, mutations in caveolin3 (LQT9) and syntrophyn (LQT12) has been associated with enhanced direct nitrosylation of Nav1.5 inducing I_{NaL} enhancement [17] [90].

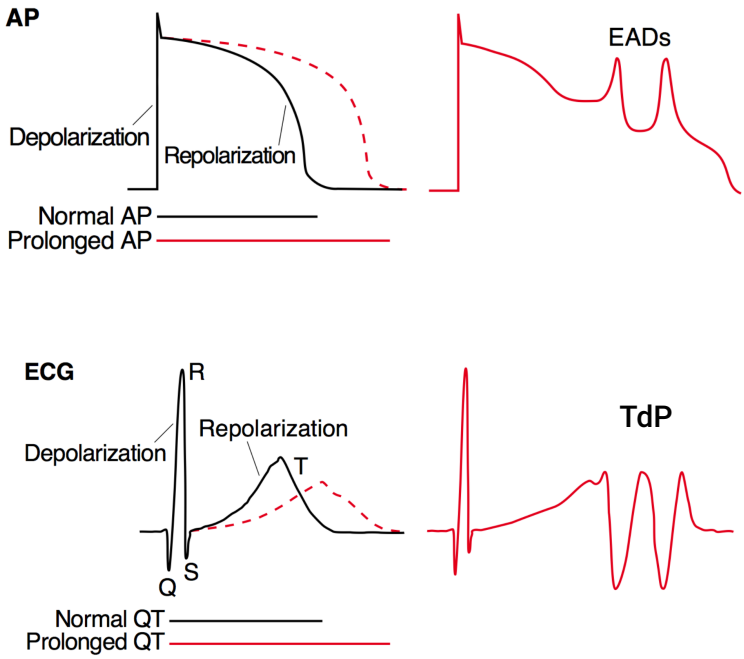

Figure 1.7: *The relationship between ventricular transmembrane APs and the surface ECG.* APs and ECG in physiological condition (black lines). An increase in the duration of the AP and consequently the QT interval prolongation (red lines). EADs occurring during the repolarization phase of a prolonged AP, giving rise to torsades de pointes (TdP) in the ECG trace. Modified by [9]

.

1.3.2 Acquired cardiac diseases

1.3.2.1 Myocardial ischemia

Myocardial ischemia (MI) is a condition of insufficient blood supply to the heart via the coronary arteries, resulting in chest pain and in some cases in *angina pectoris*. If myocardial ischemia is protracted and/or untreated, it can lead to necrosis of heart tissue (myocardial infarction)[81] (Figure 1.8). MI could be caused by several pathological conditions, such as coronary artery disease (CAD) and by some risk factors as smoking, hypertension, obesity and a strong family history [66].

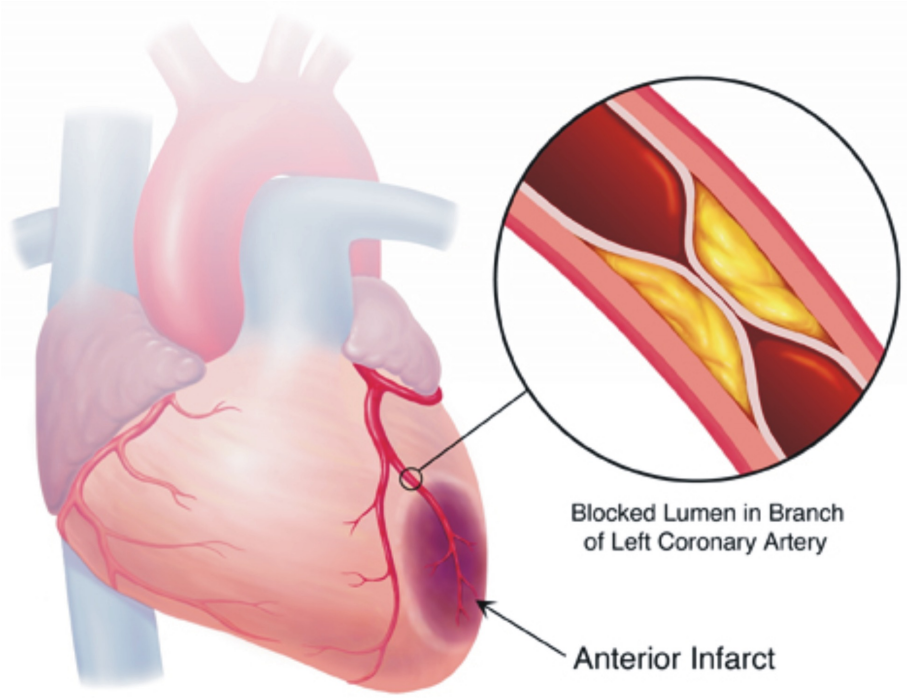

Figure 1.8: *myocardial ischemia due to coronary arteryÊblockade.*

The insufficient blood flow during MI causes an imbalance between oxygen supply and demand at the cellular level, resulting in a replacement of aerobic metabolism with anaerobic one. With the loss of oxygen (hypoxia), mitochondrial oxidative phosphorylation rapidly stops, with a resultant production of ROS and loss of ATP production. A compensatory

increase in anaerobic glycolysis for ATP production lead to H^+ and lactate accumulation, resulting in intracellular acidosis and inhibition of glycolysis (Figure 1.9).

The altered metabolic milieu leads also to a dysregulation of ionic homeostasis. The initial phase of ischemia is characterized by an increase of Na_{cyt}, likely caused by several mechanisms. Some studies proposed I_{NaL} enhancement as cause of the Na_{cyt} accumulation in myocardial ischemia. Intracellular acidification increases I_{NaL}, which therefore contributes to the rise of Na_{cyt} [12][88]. Several studies ([83] [88] [111]) demonstrated that H_2O_2 and hypoxia cause a I_{NaL} enhancement, which increases cytosolic Na^+ and Ca^{2+} in guinea pigs and rabbit ventricular myocytes. Furthermore, some ischemic metabolites, such as palmitoyl-L-carnitine and lysophosphatidylcholine, have been reported to induce I_{NaL} enhancement [92] [21]. NHE activation in response to acidosis and NKA inhibition due to the decline in ATP also lead to Na_{cyt} accumulation during ischemia [12] [42]. Together, a sustained increase of Na_{cyt} and ATP-depletion leads to intracellular Ca^{2+} overload causing the before mentioned electrical and mechanical abnormalities [30]. The progression towards an advanced stage of cardiomyocytes ischemic injury is mediated by a progressive membrane damage involving several mechanisms which result in cytoskeletal damage, alterations of contractile proteins and lipids. Collectively, these changes lead to a progressive increase in membrane permeability to ions and other small molecules, to severe derangements of ion homeostasis, and further ATP consumption, causing cardiomyocytes swelling.

After the onset of acute MI, timely myocardial reperfusion is essential to salvage viable myocardium, limit myocardial infarct size, preserve left ventricle (LV) systolic function, and prevent the onset of heart failure (HF). The blood flow restored after MI (reperfusion), delivers nutrients and oxygen to the ischemic myocardium and this produces several deleterious effects (reperfusion injury) (Figure 1.10). The major mediators of reperfusion injury are ROS, Ca^{2+} loading, and neutrophils. ROS exacerbate membrane damage while neutrophils accumulate in the microcirculation releasing inflammatory mediators and contribute to microvascular ob-

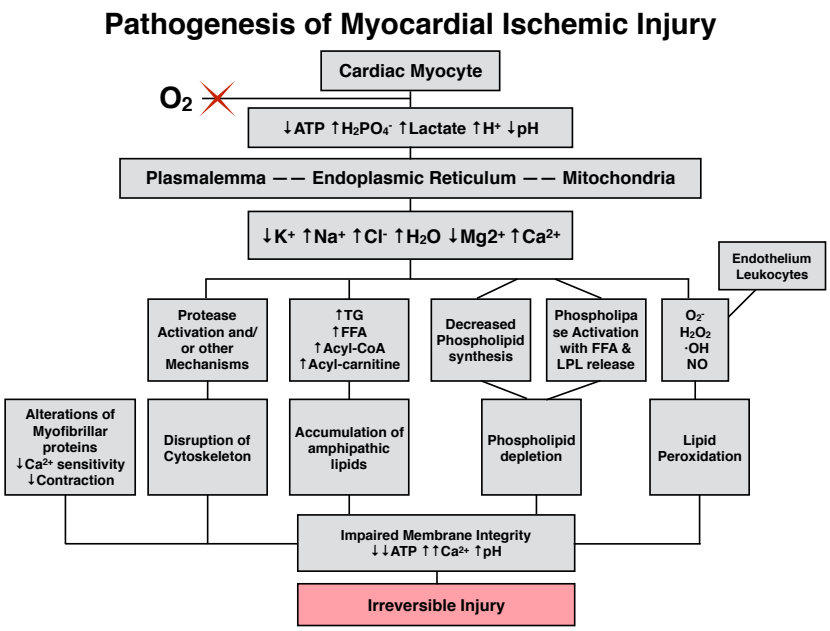

Figure 1.9: *Pathogenesis of myocardial ischemic injury.* Modified from [12]

struction [52][108]. At the same time, excellular physiological pH is rapidly restored by the washout of lactate and the normalization of intracellular pH causes a H^+ gradient, leading to NHE activation and intracellular Na^+ accumulation. The subsequent action of sNCX causes an influx of Ca^{2+}, leading to an additional intracellular and mitochondria Ca^{2+} overload via mitochondria Ca^{2+} uniporter [65][74]. Finally, reperfusion environment induce the opening of the mitochondria permeability transition pore (MTP), which leads to mitochondrial membrane depolarization and uncoupling of oxidative phosphorylation, to further ATP depletion, cell swelling with membrane rupture and, therefore, cell death [32][108].

Studies on whole-heart ischemia/reperfusion have indirectly demonstrated the presence of a I_{NaL} enhancement during the ischemic phase, showing that myocardial reperfusion injury can be prevented by blockade of I_{NaL} [27] [8] [54] (described below). However, direct evidences that I_{NaL} is effectively enhanced during ischemia phase are still missing.

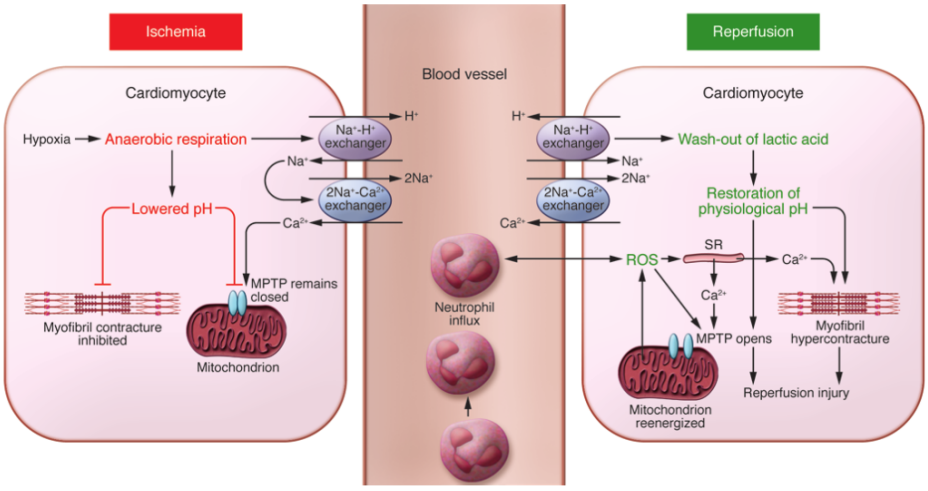

Figure 1.10: *Myocardial ischemia/reperfusion. [108]*

1.3.3 Heart Failure

Heart failure (HF) is a pathological condition characterised by a significant impairments in cardiac functions, as a consequence of compensatory and maladaptive mechanisms [34] to cardiac injury [34]. Common causes of HF include myocardial infarction, hypertension, atrial fibrillation, valvular diseases, alcohol abuse, infection and cardiomyopathy. The main consequences arising from HF are the electrophysiological alterations, which increase the propensity for cardiac arrhythmias, and excitation-contraction coupling (ECC) abnormalities, associated with severe contractile dysfunctions [19]. The major alteration that causes the contractile dysfunction is the reduction of Ca^{2+} transient amplitude (Ca_T), which is due to lower SR Ca^{2+} content. Three factors lower SR Ca^{2+} content (Ca_{SR}) in HF: 1) reduced SERCA function; 2) increased expression and function of sNCX and 3) enhanced diastolic SR Ca^{2+} leak (Figure 1.11).

Several animal and human studies have demonstrated abnormalities in Na_{cyt} homeostasis, which could lead to HF [22] [93]. The role of NKA is controversial[64][67], with its contribution to HF pathogenesis only restricted to some experimental models. The Na_{cyt} accumulation could be then largely attributed to an increased Na^+ influx. Indeed, several studies have shown that I_{NaL} is increased during HF [97] [50] [43]. Abnormally large I_{NaL} has been recorded in cardiomyocytes from patients affected by end-stage HF and following myocardial infarction [31] [51]. Despa et al. [22] have found that the majority of Na^+ influx was TTX-sensitive in cardiomyocytes from rabbits with HF induced by pressure and volume overload. Furthermore, I_{NaL} blockade prevents both electrical abnormalities (prolonged APD and EADs) and contractile dysfunctions in canine model of moderate and chronic HF [102] [68] [16]. Thus, it is now well established that I_{NaL} enhancement contributes to Na_{cyt} accumulation in HF, but the mechanisms by which I_{NaL} is increased in failing myocytes is still unclear. An increased CaM and CaMKII proteins expression has been proposed as potential explanation, since this condition increases CaMKII phosphorylation of cardiac Na^+ channels and, thus, enhancing I_{NaL}; furthermore, it has been observed as a common features of myocardial remodelling in HF

[99] [84].

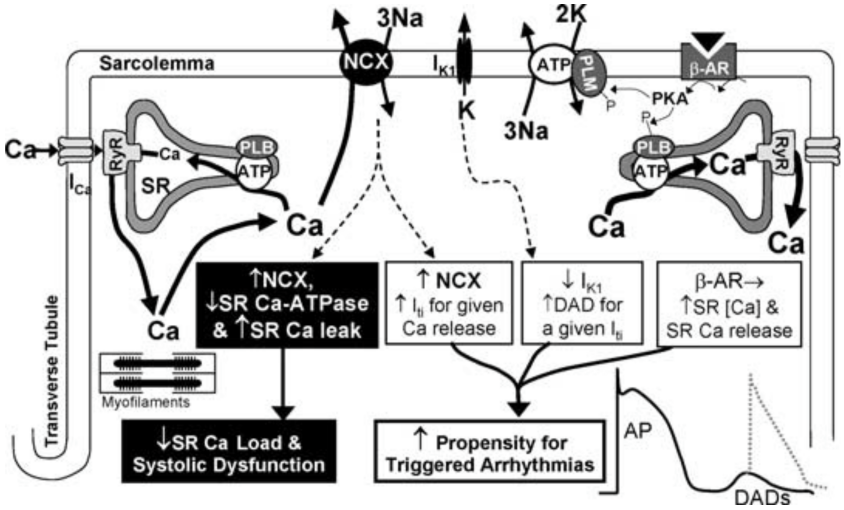

Figure 1.11: *Heart Failure* Ca^{2+} entry via Ca^{2+}current (I_{Ca}) activates SR Ca^{2+} release via RyRs, which activates the myofilaments and Ca^{2+} is cleared from the cytoplasm by the SERCA (ATP) and sNCX. Three factors contribute to reducedSRCa^{2+} load in HF (left), while enhanced NCX function, reduced I_{K1}, and residualβ adrenergic receptor (β -AR) responsiveness contribute to arrhythmogenesis via induction of delayed afterdepolarizations (DADss).

1.4 Pharmacology of I_{NaL}

Because of the role for increased I_{NaL} in the pathogenesis of arrhythmias, ischemia/reperfusion, hypertrophy and HF, I_{NaL} is an attractive target for treatment of these diseases. I_{NaL} exists as a larger target only under pathological conditions where it is increased, thus reducing the chances of on-target toxic effect. Indeed, the block of I_{NaL} in normal heart has been shown to have no deleterious effects on contractility or conduction [24].

1.4.1 Non-selective Sodium Channel Blockers

Since enhanced I_{NaL} is the consequence of dysfunctional Nav1.5, most agents with general Na^+ channel blocking effect (flecainide, lidocaine, mex-

iletine) may also inhibit I_{NaL}. A key question is the relative selectivity of the drug to block I_{NaL} versus I_{NaT}. For example, Flecainide (Class 1C Na^+ channel inhibitor) displays use-dependence block of both I_{NaT} and I_{NaL}, with 2.9- to 5-fold higher selectivity for I_{NaL} compared to peak I_{Na} [110]. Furthermore, flecainide is also an inhibitor of the delayed rectifier I_{Kr}, a major repolarizing current in repolarization phase of AP, and may therefore also prolong APD and promote torsade de pointes arrhythmias, particularly in structurally abnormal heart [61] [36]. An approximately 13-fold more potent blocking effect on I_{NaL} as compared to I_{NaT}, has been reported for the Class III anti-arrhythmic drug amiodarone. It is a mixed ion channel blocker, in addition to Na^+ channel blocking actions it also inhibits K^+ and Ca^{2+} channels, and has β-blockade-like effect [49]. Both Flecainie and amidarone display a potent off-target effects, and in particular show virtually no selectivity between I_{NaL} and I_{Kr}, which is blockaded, could further increase AP prolongation and destabilize repolarization. Because of this limitation, current research is aimed at developing selective I_{NaL} inhibitors with minimal off target and toxic side effects.

1.4.2 The I_{NaL} blocker Ranolazine

After the discovery that I_{NaL} was more sensitive to TTX than I_{NaT} in the 1970's [20], the last decade, there has been an increasing interest in a novel agent, with distinct efficacy against I_{NaL}: ranolazine (RAN). RAN, is a piperzine derivative that exhibits minimal effect on hemodynamics such heart rate and blood pressure [15]. Food Drug Administration (FDA) approves RAN in 2006 for the treatment of chronic angina pectoris. RAN at high concentration may reduce the peak of I_{Na}, but it blocks I_{NaL} over I_{NaT} with a potency ratio of 9- to 38-fold, depending on the species, cell type and the experimental conditions ([26] [94] [5]. The inhibiting effect of RAN on I_{NaT} becomes more pronounced at higher frequencies and in the setting of membrane depolarization [86], which may have clinical implication during for instance myocardial ischemia. The RAN selectivity for I_{NaL} have suggested that it may interact with different binding sites in the Na^+ channel than other I_{Na} blockers. Fredj and coworkers ([26])

has shown that a mutation in Na^+ channel reduced the potencies of both RAN and lidocaine to block I_{NaL}, implying that RAN has the same set of classical I_{Na} blockers. A different mechanism, such as a stronger state-dependency of drug access to the binding site, may account for the higher selectivity of RAN than of Lidocaine for I_{NaL}. However, RAN cannot be considered a pure I_{Na} blocker because it also inhibits other cardiac current, including I_{Ks}, I_{CaL}, inward rectifier potassium current (I_{K1}), transient outward current (I_{to}) and sNCX current (I_{NCX}) [4] (Figure 1.12). Overall, RAN exerts its therapeutic effects at concentration of 10μM, at which level it has minimal or no effect on other ion current [104] [114]. RAN inhibits I_{Kr} with an IC_{50} of approximately 12μM, close to therapeutic concentration, and the I_{NaL}/I_{Kr} block potency ratio is estimated to be around 1.5-2 [104][76]. However, it has been shown that RAN prevents APD prolongation in many pathological conditions, indicating that the I_{NaL} blocking effect of RAN prevails compared to that of I_{Kr} [44].

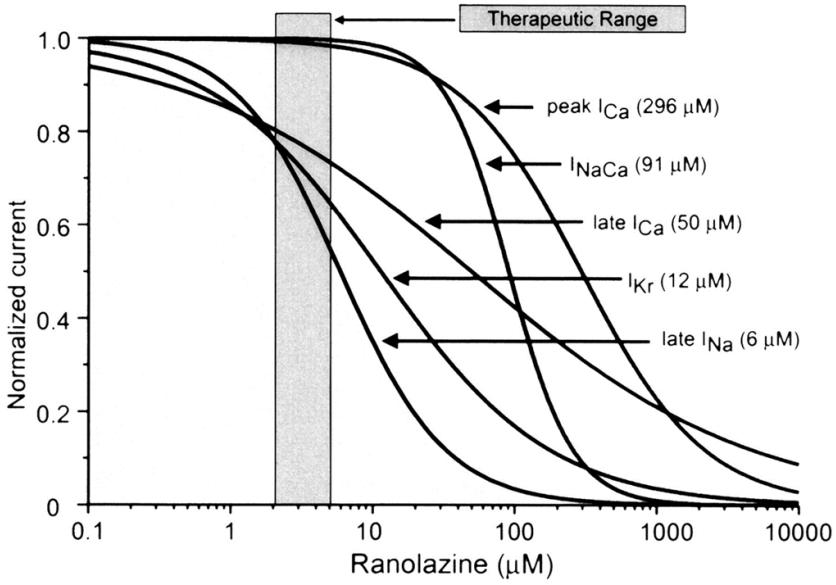

Figure 1.12: *Summary of concentration-response relationships for effect of ranolazine to inhibit inward and outward ion channel current.[4]*

Early studies have suggested that the main mechanism of anti-ischemic

and antianginal RAN effects might be through inhibition of fatty acid oxidation [27], but the experiments have been conducted at very high RAN concentrations, well in excess of therapeutic range. Furthermore, abudance of evidence from studies using RAN concentration within therapeutic range have not supported this hypothesis. Wang and coworkers [100][35] have demonstrated that ischemic protection of LV function by RAN is not mediated by inhibition of fatty acid oxidation.

The evidence that RAN, at concentrations within its proposed therapeutic range ($<10\mu$M), significantly reduces I_{NaL} and reverses or prevents the consequences of an increase of I_{NaL} has been observed in various cardiovascular diseases. Many large clinical trials have already proven the utility of RAN for the treatment of cardiac ischemia, HF and arrhythmias [44]. These pathological conditions share the commonalities of an increased I_{NaL}, resulting in ion homeostasis degeneration and mechanical impairement. Selective blockade of I_{NaL} by RAN thus diminishes intracellular Na^+ and the consequent Ca^{2+} overload and reduce contractile dysfunction.

At cellular level RAN has been found to prevent ischemia/reperfusion injury [82][83]. Song et al [83] have demonstrated that RAN attenuated H_2O_2-induced APD prolongation and suppressed EADs in guinea pig and rabbit isolated ventricular myocytes. Clinically, RAN improves diastolic function, decreasing diastolic wall tension, and extravascular compression, allowing enhanced perfusion to ischemic myocardium in patients with CAD [15] [27] [8] [54]. Importantly, the cardio-protective effects of RAN occur at a concentration that has minimal effects on heart rate, coronary blood flow and systemic arterial blood pressure [15], making RAN unique among other antianginal agents currently in use.

Several studies have been shown that RAN improves contractile function and reduce diastolic/systolic dysfunction in the setting of HF. In canine model of HF, RAN prevented progressive LV dysfunction as well as global and cellular myocardial remodeling [85][69]. RAN significantly reduced EADs, intracellular Ca^{2+} and SR Ca^{2+} content in hypertrophic cardiomyopathy and attenuated the increase in diastolic Ca^{2+} following an increase in stimulation rate [19]. RAN reduced diastolic wall tension

and LV diastolic pressure and improved coronary reperfusion [96]. Other studies argued that RAN may improve LV systolic function and provide myocardial protection during an acute myocardial infarction or heart failure [16][69].

Despite the modest QT prolongation seen with RAN in clinical trials, several in vitro and in vivo reports have reported the antiarrhythmic properties of RAN, suggesting that through reduction of I_{NaL}, it appears effective in attenuating APD prolongation and suppressing the development of EADs and DADs [44] [55] [72] . In patients with LQT3, where the underlying electrophysiological mechanism of ventricular arrhythmias is secondary to increase in I_{NaL}, RAN has been found to suppress ventricular arrhythmias by shortening the QT interval in a dose-dependent pattern and improve diastolic relaxation parameters [38]. Certainly, the most robust data investigating the potential antiarrhythmic proprieties of RAN have come from the MERLIN trial, where treatment with RAN of patients with a non ST-elevation CAD, resulted in significantly fewer episodes of ventricular tachycardia [78]. Recently, RAN has been noted to possibly impart beneficial effects in various other cardiac conditions, including new-onset, paroxysmal, and chronic atrial fibrillation, post-operative atrial fibrillation, post-revascularization coronary artery disease, chemotherapeutic cardiotoxcity, and diastolic and microvascular dysfunction [53].

1.4.3 The novel selective I_{NaL} blocker: GS967

Recently, a novel highly selective inhibitor of I_{NaL}, GS967 has been identified. GS967 inhibited ATX-II induced I_{NaL} and associated pro-arrhythmic effects in rabbit ventricular myocytes and isolated rabbit hearts, with an approximate IC50 value for I_{NaL} inhibition of 0.1-0.2 μM [80]. In addition, GS967 has been shown to exert antiarrhythmic effects on ventricular tachycardia and fibrillation [63],on atrial fibrillation [14] and on ischemia-induced atrial and ventricular repolarization alternans [11]. Although promising, the currently available data on this new compound are limited, and further experimental and pre-clinical studies will be essential to investigate its therapeutic potential.

1.5 Scope of Thesis

There is increasing evidence that I_{NaL}L plays a critical role in various cardiac pathological conditions and thus, it is a potential therapeutic target. However, I_{NaL} contribution to pathophysiology and pathological remodeling in some cardiac diseases has not been clarified yet. The scope of this thesis is to investigate the I_{Na} contribution to maladaptive cell remodelling and the benefit of I_{NaL} blockade in experimental rodent models of two cardiac diseases: acute myocardial ischemia (MI) and pulmonary arterial hypertension (PAH).

In Chapter 2 the role of I_{NaL} is evaluated in a single cell model of acute myocardial ischemia. Several studies suggest that I_{NaL} enhancement contributes to ischemia/reperfusion injury, however a direct evidence that I_{NaL} is increased during ischemia has never been showed. In addition, some ischemic conditions are opposed to the I_{NaL} occurrence: 1) depolarization of membrane diastolic potential, until inexcitability; 2) shortening of action potential duration (APD), due to the ATP-sensitive K^+ current (I_{KATP}) activation. We investigated whether I_{NaL} is increased during experimental conditions that mimic myocardial ischemia and whether it contributes to Na^+ - induced Ca^{2+} accumulation.

In Chapter 3 the role of I_{NaL} is investigated in a rat model of right ventricle (RV) hypertrophy induced by PAH. In a variety of experimental models other than RV hypertrophy, myocardial hypertrophy/failure is associated with enhancement of the late sodium current (I_{NaL}). This may, in turn, contribute to many of the functional (electrical and contractile) derangements associated with remodelled myocardium. However, whether I_{NaL} enhancement is involve in PAH-induced myocardial remodelling is still unknown. We evaluated the hypothesis that 1) constitutive I_{NaL} enhancement may occur as part of PAH-induced myocardial remodelling; 2) RAN may prevent I_{NaL} enhancement 3) RAN can prevent PAH-induced myocardial remodelling.

1.6 References

1. Abriel, H. & Kass, R. S. Regulation of the voltage-gated cardiac sodium channel Nav1.5 by interacting proteins. *Trends Cardiovasc. Med.* **15,** 35–40. ISSN: 10501738 (2005).
2. Ahern, G. P., Hsu, S.-F., Klyachko, V. A. & Jackson, M. B. Induction of Persistent Sodium Current by Exogenous and Endogenous Nitric Oxide. *J. Biol. Chem.* **275,** 28810–28815 (2000).
3. Amin, A. S., Asghari-roodsari, A. & Tan, H. L. Cardiac sodium channelopathies. **3,** 223–237 (2010).
4. Antzelevitch, C. Electrophysiological Effects of Ranolazine, a Novel Antianginal Agent With Antiarrhythmic Properties. *Circulation* **110,** 904–910. ISSN: 0009-7322 (2004).
5. Antzelevitch, C., Burashnikov, A., Sicouri, S. & Belardinelli, L. Electrophysiologic basis for the antiarrhythmic actions of ranolazine. *Hear. Rhythm* **8,** 1281–1290. ISSN: 15475271 (2011).
6. Ashpole, N. M. *et al.* Ca2+/Calmodulin-dependent Protein Kinase II (CaMKII) Regulates Cardiac Sodium Channel NaV1.5 Gating by Multiple Phosphorylation Sites. *J. Biol. Chem.* **287,** 19856–19869. ISSN: 0021-9258 (2012).
7. Baruscotti, M, DiFrancesco, D & Robinson, R. B. Na(+) current contribution to the diastolic depolarization in newborn rabbit SA node cells. *Am. J. Physiol. Heart Circ. Physiol.* **279,** H2303–H2309. ISSN: 03636135 (2000).
8. Belardinelli, L. Inhibition of the late sodium current as a potential cardioprotective principle: effects of the late sodium current inhibitor ranolazine. *Heart* **92,** iv6–iv14. ISSN: 1355-6037 (2006).
9. Belardinelli, L., Antzelevitch, C. & Vos, M. A. Assessing predictors of drug-induced torsade de pointes. *Trends Pharmacol. Sci.* **24,** 619–625. ISSN: 01656147 (2003).
10. Bers, D. M. Calcium cycling and signaling in cardiac myocytes. *Annu. Rev. Physiol.* **70,** 23–49. ISSN: 0066-4278 (2008).

11. Bonatti, R. *et al.* Selective late sodium current blockade with GS-458967 markedly reduces ischemia-induced atrial and ventricular repolarization alternans and ECG heterogeneity. *Hear. Rhythm* **11,** 1827–1835. ISSN: 15475271 (2014).

12. Buja, L. M. Myocardial ischemia and reperfusion injury. **14,** 170–175 (2005).

13. Carmeliet, E. Voltage-dependent block by tetrodotoxin of the sodium channel in rabbit cardiac Purkinje fibers. *Biophys. J.* **51,** 109–114. ISSN: 00063495 (1987).

14. CARNEIRO, J. S. *et al.* The Selective Cardiac Late Sodium Current Inhibitor GS-458967 Suppresses Autonomically Triggered Atrial Fibrillation in an Intact Porcine Model. *J. Cardiovasc. Electrophysiol.* **26,** 1364–1369. ISSN: 10453873 (2015).

15. Chaitman, B. R. Ranolazine for the treatment of chronic angina and potential use in other cardiovascular conditions. *Circulation* **113,** 2462–2472. ISSN: 00097322 (2006).

16. Chandler, M. P. *et al.* Short-Term Treatment With Ranolazine Improves Mechanical Efficiency in Dogs With Chronic Heart Failure. *Circ. Res.* **91,** 278–280. ISSN: 00097330 (2002).

17. Cheng, J. *et al.* Caveolin-3 suppresses late sodium current by inhibiting nNOS-dependent S-nitrosylation of SCN5A. *J. Mol. Cell. Cardiol.* **61,** 102–110. ISSN: 00222828 (2013).

18. Clancy, C. E. Non-Equilibrium Gating in Cardiac Na+ Channels: An Original Mechanism of Arrhythmia. *Circulation* **107,** 2233–2237. ISSN: 00097322 (2003).

19. Coppini, R. *et al.* Late Sodium Current Inhibition Reverses Electromechanical Dysfunction in Human Hypertrophic Cardiomyopathy. *Circulation* **127,** 575–584. ISSN: 0009-7322 (2013).

20. Coraboeuf, E, Deroubaix, E & Coulombe, a. Effect of tetrodotoxin on action potentials of the conducting system in the dog heart. *Am. J. Physiol.* **236,** H561–7. ISSN: 0002-9513 (1979).

21. Corr, P. B. & Corr, B. Palmitoyl transient carnitine modifies sodium currents and induces inward current in ventricular myocytes.

22. Despa, S. Intracellular Na+ Concentration Is Elevated in Heart Failure But Na/K Pump Function Is Unchanged. *Circulation* **105,** 2543–2548. ISSN: 00097322 (2002).

23. Eigel, B. N. & Hadley, R. W. Antisense inhibition of Na+/Ca2+ exchange during anoxia/reoxygenation in ventricular myocytes. *Am. J. Physiol. Heart Circ. Physiol.* **281,** H2184–90. ISSN: 0363-6135 (2001).

24. Fernandes, S. *et al.* Selective inhibition of the late sodium current has no adverse effect on electrophysiological or contractile function of the normal heart. *J. Cardiovasc. Pharmacol.* **63,** 512–9. ISSN: 1533-4023 (2014).

25. Fredj, S., Lindegger, N., Sampson, K. J., Carmeliet, P. & Kass, R. S. Altered Na+ channels promote pause-induced spontaneous diastolic activity in long QT syndrome type 3 myocytes. *Circ. Res.* **99,** 1225–32. ISSN: 1524-4571 (2006).

26. Fredj, S., Sampson, K. J., Liu, H. & Kass, R. S. Molecular basis of ranolazine block of LQT-3 mutant sodium channels: evidence for site of action. *Br. J. Pharmacol.* **148,** 16–24. ISSN: 00071188 (2009).

27. Gralinski, M. R. *et al.* Cardioprotective effects of ranolazine (RS-43285) in the isolated perfused rabbit heart. *Cardiovasc. Res.* **28,** 1231–1237. ISSN: 0008-6363 (1994).

28. Grant, A. O. Cardiac Ion Channels. *Circ. Arrhythmia Electrophysiol.* **2,** 185–194. ISSN: 1941-3149 (2009).

29. Györke, S. *et al.* Regulation of sarcoplasmic reticulum calcium release by luminal calcium in cardiac muscle. *Front. Biosci.* **7,** d1454–63. ISSN: 1093-4715 (2002).

30. Hale, S. L., Shryock, J. C., Belardinelli, L., Sweeney, M. & Kloner, R. A. Late sodium current inhibition as a new cardioprotective approach. *J. Mol. Cell. Cardiol.* **44,** 954–967. ISSN: 00222828 (2008).

31. Huang, B, El-Sherif, T, Gidh-Jain, M, Qin, D & El-Sherif, N. Alterations of sodium channel kinetics and gene expression in the postinfarction remodeled myocardium. *J. Cardiovasc. Electrophysiol.* **12,** 218–225. ISSN: 10453873 (2001).

32. Ibanez, B., Fuster, V., Jiménez-Borreguero, J. & Badimon, J. J. Lethal myocardial reperfusion injury: a necessary evil? *Int. J. Cardiol.* **151,** 3–11. ISSN: 1874-1754 (2011).

33. JC Shryock and L Belardinelli. REVIEW : Inhibition of late sodium current to reduce electrical and mechanical dysfunction of ischaemic myocardium, 1128–1132 (2008).

34. Krum, H. & Abraham, W. T. Heart failure. *Lancet* **373,** 941–955. ISSN: 0140-6736 (2009).

35. L., B., J.C., S. & H., F. The mechanism of ranolazine action to reduce ischemia-induced diastolic dysfunction. *Eur. Hear. Journal, Suppl.* **8,** A10–A13. ISSN: 1520-765X (2006).

36. Lee, H.-A., Kim, E.-J., Hyun, S.-A., Park, S.-G. & Kim, K.-S. Electrophysiological effects of the anti-cancer drug lapatinib on cardiac repolarization. *Basic Clin. Pharmacol. Toxicol.* **107,** 614–8. ISSN: 1742-7843 (2010).

37. Lindegger, N, Hagen, B. M., Marks, a. R., Lederer, W. J. & Kass, R. S. Diastolic transient inward current in long QT syndrome type 3 is caused by Ca2+ overload and inhibited by ranolazine. *J. Mol. Cell. Cardiol.* **47,** 326–34. ISSN: 1095-8584 (2009).

38. Liu, J., Moss, A. & Jons, C. Mutation-specific risk in two genetic forms of type 3 long QT syndrome. *Am. J. ...* **105.** doi:10.1016/j.amjcard.2009.08.676.Mutation-specific. <http://www.sciencedirect.com/science/article/pii/S0002914909023297> (2010).

39. Lu, Z. *et al.* Suppression of Phosphoinositide 3-Kinase Signaling and Alteration of Multiple Ion Currents in Drug-Induced Long QT

Syndrome. *Sci. Transl. Med.* **4,** 131ra50–131ra50. ISSN: 1946-6234 (2012).

40. Ma, J. *et al.* Ranolazine attenuates hypoxia- and hydrogen peroxide-induced increases in sodium channel late openings in ventricular myocytes. *J. Cardiovasc. Pharmacol.* **64,** 60–8. ISSN: 1533-4023 (2014).

41. Maack, C. *et al.* Elevated cytosolic Na+ decreases mitochondrial Ca2+ uptake during excitation-contraction coupling and impairs energetic adaptation in cardiac myocytes. *Circ. Res.* **99,** 172–182. ISSN: 00097330 (2006).

42. Madonna, R., Cevik, C. & Nasser, M. Electrical plasticity and cardioprotection in myocardial ischemia–role of selective sodium channel blockers. *Clin. Cardiol.* **36,** 255–61. ISSN: 1932-8737 (2013).

43. Maier, L. S. A novel mechanism for the treatment of angina, arrhythmias, and diastolic dysfunction: inhibition of late I(Na) using ranolazine. *J. Cardiovasc. Pharmacol.* **54,** 279–286. ISSN: 0160-2446 (2009).

44. Maier, L. S. & Sossalla, S. The late Na current as a therapeutic target: Where are we? *J. Mol. Cell. Cardiol.* **61,** 44–50. ISSN: 00222828 (2013).

45. Maier, L. S. *et al.* Transgenic CaMKIIδc overexpression uniquely alters cardiac myocyte Ca2+ handling: Reduced SR Ca2+ load and activated SR Ca2+ release. *Circ. Res.* **92,** 904–911. ISSN: 00097330 (2003).

46. Makielski, J. C. Late sodium current : A mechanism for angina , heart failure , and arrhythmia. *Trends Cardiovasc. Med.* 1–8. ISSN: 1050-1738 (2015).

47. Makielski, J. C. & Farley, A. L. Na+ current in human ventricle: Implications for sodium loading and homeostasis. *J. Cardiovasc. Electrophysiol.* **17,** 15–20. ISSN: 10453873 (2006).

48. MALTSEV, V & UNDROVINAS, A. A multi-modal composition of the late Na+ current in human ventricular cardiomyocytes. *Cardiovasc. Res.* **69,** 116–127. ISSN: 00086363 (2006).

49. Maltsev, V. a. *et al.* Novel, ultraslow inactivating sodium current in human ventricular cardiomyocytes. *Circulation* **98,** 2545–2552. ISSN: 0009-7322 (1998).

50. Maltsev, V. A. & Undrovinas, A. Late sodium current in failing heart : Friend or foe ? **96,** 421–451 (2008).

51. Maltsev, V. a., Silverman, N., Sabbah, H. N. & Undrovinas, A. I. Chronic heart failure slows late sodium current in human and canine ventricular myocytes: Implications for repolarization variability. *Eur. J. Heart Fail.* **9,** 219–227. ISSN: 13889842 (2007).

52. Maxwell, S. R. & Lip, G. Y. Reperfusion injury: a review of the pathophysiology, clinical manifestations and therapeutic options. *Int. J. Cardiol.* **58,** 95–117. ISSN: 0167-5273 (1997).

53. Mihos, C. G. *et al.* The use of ranolazine in non-anginal cardiovascular disorders: A review of current data and ongoing randomized clinical trials. *Pharmacol. Res.* **103,** 49–55. ISSN: 10436618 (2016).

54. Mohammed Aldakkaka. Ranolazine reduces Ca2+ overload and oxidative stress and improves mitochondrial integrity to protect against ischemia reperfusion injury in isolated hearts. **64,** 381–392 (2012).

55. Moreno, J. D. & Clancy, C. E. Pathophysiology of the cardiac late Na Current and its potential as a drug taghet. **52.** doi:`10.1016/j.yjmcc.2011.12.003.Pathophysiology` (2013).

56. Nattel, S. & Dobrev, D. The multidimensional role of calcium in atrial fibrillation pathophysiology: Mechanistic insights and therapeutic opportunities. *Eur. Heart J.* **33,** 1870–1877. ISSN: 0195668X (2012).

57. NĚMEC, J. *et al.* Heart Rate Dependence of the QT Interval Duration: *J. Cardiovasc. Electrophysiol.* **15,** 550–556. ISSN: 10453873 (2004).

58. Nickel, A., Kohlhaas, M. & Maack, C. Mitochondrial reactive oxygen species production and elimination. *J. Mol. Cell. Cardiol.* **73,** 26–33. ISSN: 10958584 (2014).

59. Ou, Y. *et al.* Syntrophin gamma 2 regulates SCN5A gating by a PDZ domain-mediated interaction. *J. Biol. Chem.* **278,** 1915–1923. ISSN: 0021-9258 (2003).

60. Park, C. O., Xiao, X. H. & Allen, D. G. Changes in intracellular Na+ and pH in rat heart during ischemia: role of Na+/H+ exchanger. *Am. J. Physiol.* **276,** H1581–90. ISSN: 0002-9513 (1999).

61. Paul, A. A., Witchel, H. J. & Hancox, J. C. Inhibition of the current of heterologously expressed HERG potassium channels by Âŕ ecainide and comparison with quinidine , propafenone and lignocaine, 717–729 (2002).

62. Persson, F., Andersson, B., Duker, G., Jacobson, I. & Carlsson, L. Functional effects of the late sodium current inhibition by AZD7009 and lidocaine in rabbit isolated atrial and ventricular tissue and Purkinje fibre. *Eur. J. Pharmacol.* **558,** 133–143. ISSN: 00142999 (2007).

63. Pezhouman, A *et al.* Selective Inhibition of Late Sodium Current Suppresses Ventricular Tachycardia and Fibrillation in Intact Rat Hearts. *Hear. Rhythm* **11,** 492–501. ISSN: 1878-5832 (2014).

64. Pieske, B. & Houser, S. R. [Na+]i handling in the failing human heart. *Cardiovasc. Res.* **57,** 874–86. ISSN: 0008-6363 (2003).

65. Piper, H. M. & Ovize, M. A fresh look at reperfusion injury. *Cardiovasc. Res.* **38,** 291–300. ISSN: 0008-6363 (1998).

66. Plank, B. G., Doling, J. M. & Knight, P. A. Coronary Artery Disease. *Man. Outpatient Cardiol.* 179–216. ISSN: 1555-9041 (2012).

67. Pogwizd, S. M., Sipido, K. R., Verdonck, F. & Bers, D. M. Intracellular Na in animal models of hypertrophy and heart failure: Contractile function and arrhythmogenesis. *Cardiovasc. Res.* **57,** 887–896. ISSN: 00086363 (2003).

68. Rastogi, S. *et al.* Ranolazine combined with enalapril or metoprolol prevents progressive LV dysfunction and remodeling in dogs with moderate heart failure. *AJP Hear. Circ. Physiol.* **295,** H2149–H2155. ISSN: 0363-6135 (2008).

69. Rastogi, S. *et al.* Ranolazine combined with enalapril or metoprolol prevents progressive LV dysfunction and remodeling in dogs with moderate heart failure. *Am. J. Physiol. Heart Circ. Physiol.* **295,** H2149–55. ISSN: 0363-6135 (2008).

70. Remme, C. A. & Wilde, A. A. M. Late Sodium Current Inhibition in Acquired and Inherited Ventricular (dys)function and Arrhythmias. *Cardiovasc. Drugs Ther.* **27,** 91–101. ISSN: 0920-3206 (2013).

71. Remme, C. A., Wilde, a. a. M. & Bezzina, C. R. Cardiac Sodium Channel Overlap Syndromes: Different Faces of SCN5A Mutations. *Trends Cardiovasc. Med.* **18,** 78–87. ISSN: 10501738 (2008).

72. Saad, M., Mahmoud, A., Elgendy, I. Y. & Richard Conti, C. Ranolazine in Cardiac Arrhythmia. *Clin. Cardiol.* n/a–n/a. ISSN: 01609289 (2015).

73. Sag, C. M., Wagner, S. & Maier, L. S. Role of oxidants on calcium and sodium movement in healthy and diseased cardiac myocytes. *Free Radic. Biol. Med.* **63,** 338–49. ISSN: 1873-4596 (2013).

74. Sanada, S., Komuro, I. & Kitakaze, M. Pathophysiology of myocardial reperfusion injury: preconditioning, postconditioning, and translational aspects of protective measures. *AJP Hear. Circ. Physiol.* **301,** H1723–H1741. ISSN: 0363-6135 (2011).

75. Sanda Despa;Donald M. Bers. Na+ transport in the normal and failing heart âĂŞ remember the balance, 2–10 (2013).

76. Schram, G. *et al.* Ranolazine: Ion-channel-blocking actions and in vivo electrophysiological effects. *Br. J. Pharmacol.* **142,** 1300–1308. ISSN: 00071188 (2004).

77. Schwartz, P. J. & Ackerman, M. J. The long QT syndrome: a transatlantic clinical approach to diagnosis and therapy. *Eur. Heart J.* **34,** 3109–3116. ISSN: 0195-668X (2013).

78. Scirica, B. M. *et al.* Effect of Ranolazine, an Antianginal Agent With Novel Electrophysiological Properties, on the Incidence of Arrhythmias in Patients With Non ST-Segment Elevation Acute Coronary Syndrome: Results From the Metabolic Efficiency With Ranolazine for Less Ischem. *Circulation* **116,** 1647–1652. ISSN: 0009-7322 (2007).

79. Shryock, J. C., Song, Y., Rajamani, S., Antzelevitch, C. & Belardinelli, L. The arrhythmogenic consequences of increasing late INa in the cardiomyocyte. *Cardiovasc. Res.* **99,** 600–611. ISSN: 0008-6363 (2013).

80. Sicouri, S., Belardinelli, L. & Antzelevitch, C. Antiarrhythmic effects of the highly selective late sodium channel current blocker GS-458967. *Heart Rhythm* **10,** 1036–43. ISSN: 1556-3871 (2013).

81. Silverman, H. S. & Stern, M. D. Ionic basis of ischaemic cardiac injury: insights from cellular studies. *Cardiovasc. Res.* **28,** 581–97. ISSN: 0008-6363 (1994).

82. Soliman, D. *et al.* Late sodium current inhibition alone with ranolazine is sufficient to reduce ischemia- and cardiac glycoside-induced calcium overload and contractile dysfunction mediated by reverse-mode sodium/calcium exchange. *J. Pharmacol. Exp. Ther.* **343,** 325–32. ISSN: 1521-0103 (2012).

83. Song, Y., Shryock, J. C., Wagner, S., Maier, L. S. & Belardinelli, L. Blocking Late Sodium Current Reduces Hydrogen Peroxide- Induced Arrhythmogenic Activity and Contractile Dysfunction. **318,** 214–222 (2006).

84. Sossalla, S. *et al.* Diastolic dysfunction and arrhythmias caused by overexpression of CaMKII d C can be reversed by inhibition of late Na + current, 263–272 (2011).

85. Sossalla, S. *et al.* Ranolazine improves diastolic dysfunction in isolated myocardium from failing human hearts âĂŤ Role of late sodium current and intracellular ion accumulation. *J. Mol. Cell. Cardiol.* **45,** 32–43. ISSN: 00222828 (2008).

86. Szél, T. *et al.* Class I/B antiarrhythmic property of ranolazine, a novel antianginal agent, in dog and human cardiac preparations. *Eur. J. Pharmacol.* **662,** 31–39. ISSN: 00142999 (2011).

87. Tan, H. L. *et al.* A calcium sensor in the sodium channel modulates cardiac excitability. *Nature* **415,** 442–447. ISSN: 00280836 (2002).

88. Tang, Q. *et al.* Persistent sodium current and Na+/H+ exchange contributes to the augmentation of the reverse Na+/Ca2+ exchange during hypoxia or acute ischemia in ventricular myocytes. *Pflügers Arch. - Eur. J. Physiol.* **463,** 513–522. ISSN: 0031-6768 (2012).

89. Toischer, K. *et al.* Role of late sodium current as a potential arrhythmogenic mechanism in the progression of pressure-induced heart disease. *J. Mol. Cell. Cardiol.* **61,** 111–122. ISSN: 00222828 (2013).

90. Ueda, K. *et al.* Syntrophin mutation associated with long QT syndrome through activation of the nNOS-SCN5A macromolecular complex. *Proc. Natl. Acad. Sci. U. S. A.* **105,** 9355–9360. ISSN: 0027-8424 (2008).

91. Undrovinas, a. I., Fleidervish, I. a. & Makielski, J. C. Inward sodium current at resting potentials in single cardiac myocytes induced by the ischemic metabolite lysophosphatidylcholine. *Circ. Res.* **71,** 1231–1241. ISSN: 0009-7330 (1992).

92. Undrovinas, a. I., Fleidervish, I. a. & Makielski, J. C. Inward sodium current at resting potentials in single cardiac myocytes induced by the ischemic metabolite lysophosphatidylcholine. *Circ. Res.* **71,** 1231–1241. ISSN: 0009-7330 (1992).

93. Undrovinas, A. Late Sodium Current Contributes to Diastolic Cell Ca2+ Accumulation in Chronic Heart Failure. *J Physiol Sci* **60,** 245–257 (2011).

94. Undrovinas, A. I., Belardinelli, L., Undrovinas, N. a. & Sabbah, H. N. Ranolazine improves abnormal repolarization and contraction in left ventricular myocytes of dogs with heart failure by inhibiting late sodium current. *J. Cardiovasc. Electrophysiol.* **17 Suppl 1,** S169–S177. ISSN: 1045-3873 (2006).

95. Undrovinas, N. A., Maltsev, V. A., Belardinelli, L., Sabbah, H. N. & Undrovinas, A. Late sodium current contributes to diastolic cell Ca2+ accumulation in chronic heart failure. *J. Physiol. Sci.* **60,** 245–57. ISSN: 1880-6562 (2010).

96. Vadnais, D. & Wenger, N. K. Emerging clinical role of ranolazine in the management of angina, 517–530 (2010).

97. Valdivia, C. R. *et al.* Increased late sodium current in myocytes from a canine heart failure model and from failing human heart. *J. Mol. Cell. Cardiol.* **38,** 475–483. ISSN: 00222828 (2005).

98. Vassalle, M. & Lin, C. I. Calcium overload and cardiac function. *J. Biomed. Sci.* **11,** 542–565. ISSN: 10217770 (2004).

99. Wagner, S. *et al.* Ca 2/calmodulin-dependent protein kinase II regulates cardiac Na channels. *J. Clin. Invest.* **116,** 3127–3138 (2006).

100. Wang, P., Fraser, H. & Lloyd, S. A comparison between ranolazine and CVT-4325, a novel inhibitor of fatty acid oxidation, on cardiac metabolism and left ventricular function in rat isolated perfused. ... *Pharmacol. ...* **321,** 213–220 (2007).

101. Wang, Q. *et al.* SCN5A mutations associated with an inherited cardiac arrhythmia, long QT syndrome. *Cell* **80,** 805–811. ISSN: 00928674 (1995).

102. Wasserstrom, J. A. *et al.* Ranolazine antagonizes the effects of increased late sodium current on intracellular calcium cycling in rat isolated intact heart. *J. Pharmacol. Exp. Ther.* **331,** 382–391. ISSN: 1521-0103 (2009).

103. Wedekind, H. *et al.* De Novo Mutation in the SCN5A Gene Associated With Early Onset of Sudden Infant Death. *Circulation* **104,** 1158–1164. ISSN: 0009-7322 (2001).

104. Wu, L. *et al.* Antiarrhythmic effects of ranolazine in a guinea pig in vitro model of long-QT syndrome. *J. Pharmacol. Exp. Ther.* **310,** 599–605. ISSN: 00223565 (2004).

105. Wu, Y. *et al.* Protein kinaseÂăC and Ca ²⁺ -calmodulin-dependent protein kinaseÂăII mediate the enlarged reverse I _{NCX} induced by ouabain-increased late sodium current in rabbit ventricular myocytes. *Exp. Physiol.* **100,** 399–409. ISSN: 09580670 (2015).

106. Wu, Y., Song, Y., Belardinelli, L. & Shryock, J. C. The Late Na Ïľ Current (I Na) Inhibitor Ranolazine Attenuates Effects of Palmitoyl-L -Carnitine to Increase Late I Na and Cause Ventricular Diastolic Dysfunction. **330,** 550–557 (2009).

107. Yang, T. *et al.* Screening for acute ikr block is insufficient to detect torsades de pointes liability: Role of late sodium current. *Circulation* **130,** 224–234. ISSN: 15244539 (2014).

108. Yellon, Derek M, Hausenloy, D. Myocardial reperfusion injury. *new Engl. J. o f Med.* **2,** 1121–35. ISSN: 08995885 (2007).

109. Zaza, A & Rocchetti, M. Calcium store stability as an antiarrhythmic endpoint . **21,** 2015 (2015).

110. Zaza, A., Belardinelli, L. & Shryock, J. C. Pathophysiology and pharmacology of the cardiac âĂIJ late sodium current âĂİ. **119,** 326–339 (2008).

111. Zhou, H., Ma, J.-H., Zhang, P.-H. & Luo, A.-T. Vitamin C pretreatment attenuates hypoxia-induced disturbance of sodium currents in guinea pig ventricular myocytes. *J. Membr. Biol.* **211,** 81–87. ISSN: 0022-2631 (2006).

112. Zong, X. G., Dugas, M & Honerjäger, P. Relation between veratridine reaction dynamics and macroscopic Na current in single cardiac cells. *J. Gen. Physiol.* **99,** 683–697. ISSN: 0022-1295 (1992).

113. Zygmunt, a. C., Eddlestone, G. T., Thomas, G. P., Nesterenko, V. V. & Antzelevitch, C. Larger late sodium conductance in M cells contributes to electrical heterogeneity in canine ventricle. *Am. J. Physiol. Heart Circ. Physiol.* **281,** H689–H697. ISSN: 0363-6135 (2001).

114. Zygmunt, a. C. *et al.* Mechanisms of atrial-selective block of Na+ channels by ranolazine: I. Experimental analysis of the use-dependent block. *AJP Hear. Circ. Physiol.* **301,** H1606–H1614. ISSN: 0363-6135 (2011).

Chapter 2

Role of Late Sodium Current in a single cell model of acute ischemia

Carlotta Ronchi, MSc[1]; Eleonora Torre, MSc[1]; Riccardo Rizzetto, PhD[1]; Luca Sala, PhD[1]; Gaspare Mostacciuolo, Mr[1]; Marcella Rocchetti, PhD[1]; Antonio Zaza, MD[1].

[1] Dipartimento di Biotecnologie e Bioscienze, Universitá degli Studi di Milano - Bicocca, Milano, Italy;

2.1 Acronyms

AIP	protocol of acute ischemia
ANG2	Asante Natrium Green-2
AP	action potential
APD	action potential duration
APD90	APD at 90% repolarization
$\mathbf{Ca}_{cyt}$	cytosolic Ca^{2+}
$\mathbf{Ca}_{D}$	diastolic Ca^{2+}
$\mathbf{Ca}_{FR}$	sarcoplasmic reticulum (SR) fractional release
$\mathbf{Ca}_{SR}$	SR Ca^{2+} content
$\mathbf{Ca}_{T}$	Ca^{2+} transient amplitude
CGP	CGP 31157
$\mathbf{C}_{m}$	membrane capacitance
CTRL	control
$\mathbf{dNa}_{cyt}\mathbf{/dt}$	cytosolic Na^{+} (Na_{cyt}) accumulation rate
$\mathbf{dV/dt}_{max}$	maximum depolarization rate
$\mathbf{E}_{diast}$	diastolic membrane potential
$\mathbf{I}_{KATP}$	ATP-sensitive K^{+} current
$\mathbf{I}_{Na}$	voltage gated sodium current
$\mathbf{I}_{NaL}$	late sodium current
ISC	ischemic mimic solution
$\mathbf{I}_{TTX}$	TTX-sensitive current
mNCX	mitochondrial Na^{+}/Ca^{2+} exchanger
$\mathbf{Na}_{cyt}$	cytosolic Na^{+}
NHE	Na^{+}/H^{+} exchanger
NKA	Na^{+}/K^{+} ATPasi pump
OUAB	ouabaine

RAN	ranolazine
ROS	reactive oxygen species
RyRs	Ryanodine receptors
SEA	SEA 0400
sNCX	sarcolemmal Na^+/Ca^{2+} exchanger
SR	sarcoplasmic reticulum
TA	twitch amplitude
TTX	tetrodotoxin

2.2 Abstract

Background: Myocardial ischemia is characterized by an overproduction of toxic metabolites well-known enhancers of the late sodium current (I_{NaL}). ranolazine (RAN), a blocker of I_{NaL}, improves recovery during reperfusion. However, during ischemia diastolic potential depolarization might limit Sodium current (I_{Na}) recruiting; thus, whether I_{NaL} is actually enhanced during acute ischemia is still unknown. *Aim*: To test the functional contribution of I_{NaL} in a cellular model of acute ischemia. *Methods*: Rat ventricular myocytes were exposed for 7 min to a (normoxic) ischemia-mimic solution (ISC); to evaluate the role of I_{NaL}, RAN (10 μM) or tetrodotoxin (TTX) (1μM) were added throughout the protocol. I_{NaL} was isolated as TTX-sensitive current during action potentials (APs) elicited at 1Hz. Cell shortening, cytosolic Na^+ (Na_{cyt}) and Ca^{2+} (Ca_{cyt}) were monitored in field-stimulated myocytes (1Hz). The sarcolemma (s) and mitochondrial (m) Na^+/Ca^{2+} exchanger (NCX) were blocked by SEA-0400 (1μM) and CGP37157 (1 μM) respectively. *Results*: During ischemic mimic solution (ISC), loss of contraction was followed by partial recovery. While APs persisted throughout ISC, diastolic potential markedly depolarized and AP upstroke velocity decreased. In spite of this, ISC induced I_{NaL} enhancement, which was completely prevented by RAN. ISC increased Na_{cyt} and Ca_{cyt}, which were partially prevented by RAN; TTX

affected ISC-induced Na_{cyt} enhancement only. SEA-0400 boosted cytosolic Ca_{cyt} and SR Ca^{2+} content during ISC. SEA-0400 effects were sharply curtailed by RAN, by TTX and by CGP37157 Conclusion: During ISC, I_{NaL} increased in spite of AP changes and contributed to Na_{cyt} increment. Unexpectedly, sNCX blockade unrevealed RAN and TTX effects on Ca_{cyt}. These results suggest Na^+-dependent, but sNCX-independent Ca^{2+} accumulation mechanisms during acute ischemia. Indeed, mNCX appears to be involved in the I_{NaL} induced cytosolic Ca^{2+} accumulation.

Keywords: Late Sodium Current, Myocardial Ischemia, Ranolazine

2.3 Background

Myocardial ischemia results in a characteristic pattern of metabolic and intracellular ion changes, leading to a cytosolic Na^+ (Na_{cyt}) and Ca^{2+} (Ca_{cyt}) accumulation [4][26]. The first Na^+ influx enhancement is coupled with the subsequent increase of Ca_{cyt} through sNCX working in *reverse mode* (coupled exchanger theory) [2][31][23][8].

While it is widely accepted that the Na_{cyt} accumulation is principally due to Na^+/H^+ exchanger (NHE) in post-ischemic reperfusion [18][2], there is a disagreement about the NHE activity during ischemia, because it might be partially inhibited by extracellular acidosis [2]. Furthermore, several studies have demostrated that the I_{NaL} blockade prevents Ca^{2+} overload and reduces myocardial ischemia/reperfusion injury [2][45][15][37] [27][6]. These evidences suggest that the I_{NaL} enhancement might be the mecchanism undelying the increased Na^+ influx during ischemia. Moreover, it has been observed that some pathological components of ischemia (i.e. H_2O_2, hypoxia and ischemic metabolites), induce I_{NaL} enhancement [44][38][41][21].

However, a direct evidence that I_{NaL} is increased during ischemia has never been showed. In addition, some ischemic conditions are opposed to the I_{NaL} occurrence: 1) depolarization of membrane diastolic potential, until inexcitability; 2) shortening of action potential duration (APD), due to the ATP-sensitive K^+ current (I_{KATP}) activation [48].

The aim of the present study is to directly investigate whether I_{NaL} is increased during experimental condition that mimic myocardial ischemia and whether it contributes to Na^+ - induced Ca^{2+} accumulation.

The results of the present study demonstrate that, during acute ischemia I_{NaL} is enhanced in spite of membrane potential changes and it participates to Na_{cyt} accumulation. Nevertheless, I_{NaL} blockade has a surprisingly negligible effect on Ca^{2+} accumulated in the presence of functional sNCX, whereas it prevents Ca_{cyt} accumulation in the presence of sNCX blockade, suggesting sNCX-independent mechanisms. In accordance with this, the Ca_{cyt} accumulation is also prevented by mNCX blockade. Although these evidences confirm the I_{NaL} contribution to Na^+ accumulation during ischemia, they suggest that the dysregulation of the intracellular milieu during ischemia may not be completely described by the coupled exchanger theory.

2.4 Materials and methods

The investigation conforms to the Guide of the Care and Use of Laboratory Animals published by the US National Institutes of Health (NIH publication No. 85-23, revised 1996). All the experiments were carried out according to the guidelines issued by the Animal Care Committee of the University of Milano-Bicocca. An expanded methods section is available in the Supplement.

2.4.1 Cell isolation

Male adult Sprague-Dawley rat ventricular cardiomyocytes were isolated by using a retrograde coronary perfusion method previously published except for minor modifications [54]. Measurements were performed only in quiescent rod-shaped myocytes with clear striations.

2.4.2 Acute ischemia protocol

Cardiomyocytes were placed into a recording chamber and superfused at 37 °C with Tyrode's solution containing (nM): NaCl 154, KCl 4, $CaCl_2$ 2,

$MgCl_2$ 1, HEPES 5, Glucose 5.5, adjusted to pH 7.4.

Ischemia was simulated by exposing single rat ventricular myocytes to a modified Tyrode's solution (ischemic mimic solution, ISC), which contains the major hallmarks of ischemia,previously described by [19] (mM): NaCl 134, Na-lactate 20, KCl 8, $CaCl_2$ 2, $MgCl_2$ 1, HEPES 5, Sucrose 37, adjusted to pH 6.8. ISC did not included the hypoxia, because Lu et al., [19] demonstrated that the main contributor to cardiac ischemic injury is the lactate, which leads to an extra-(first) and intra-(second) cellular acidosis. The extracellular K^+ concentration was raised to 8 mM [7] compared to the original ischemia-mimetic solution of Lu et al. [19], because extracellular K^+ accumulation is one of the major factors contributing to ischemia-induced changes [7]. Whereas, sucrose at elevated concentration was added to ISC as a hyperosmolar agent and in replacement of glucose.

All experiments were performed by using a protocol of acute ischemia (AIP) as follows: Tyrode's solution for 2 minutes to establish a steady state condition followed by ISC solution for 7 minutes (Supplemental figure 2.1). The I_{NaL} blockers RAN and TTX were used to evaluate I_{NaL} contribution. Three experimental groups were considered: control (CTRL), RAN (10μM)-treated group (RAN) and TTX(1μM)-treated group (TTX). RAN and TTX were applied throughout the duration of the AIP. The selective blockers SEA 0400 (SEA) (1μM) and CGP 31157 (CGP) (1μM) were used to test the role of sNCX and mNCX respectively. Ouabaine (OUAB,1mM)was used to inhibit Na^+/K^+ ATPasi pump (NKA). Each drug was tested by adding it to the ISC.

Data were statistically evaluated before (PRE) and at three time points: before (PRE) and at 0.5, 3 and 7 min during ISC superfusion (0.5MIN, 3MIN, 7MIN) (Supplemental figure 2.1).

2.4.3 Cell shortening

Cardiomyocytes were field stimulated at 1Hz using two parallel platinum electrodes and the single-cell shortening was measured by a video-edge detection system (Crescent Electronics). Changes in cell length between shortening and lengthening were measured using the twitch amplitude

(TA) as parameter, which represents the amplitude of myocytes contraction. TA was monitored throughout the AIP and normalized to the value measured in PRE.

2.4.4 Patch-clamp recordings

APs were recorded in current-clamp mode at 1Hz; APs waveforms recorded at baseline (PRE) and at the end of AIP were used as command signals in action potential clamp (AP-Clamp) experiments. I_{NaL} was measured by AP-clamp in PRE and at the end of AIP. I_{NaL} was isolated, by digital subtraction, as the current sensitive to 1μM TTX (TTX-sensitive current (I_{TTX})). I_{NaL} magnitude was quantified as mean inward I_{TTX} during repolarization, obtained by integrating inward I_{TTX} up to 90% repolarization and dividing the result for the integration interval.

To test whether changes in membrane potential induced by ISC may limit I_{NaL} expression, AP-clamp experiments were performed in two modalities. In the first one, the AP waveforms previously recorded in PRE or at the end of AIP were applied in the same phase,thus incorporating ISC-induced changes. In the second one, the AP waveform recorded in PRE condition was maintained throughout the AIP. Differences between I_{NaL} recorded with the two AP-clamp modalities reflects the contribution of ISC-induced membrane potential changes on I_{NaL}.

2.4.5 Measurement of intracellular ions

Na_{cyt} and Ca_{cyt} were measured in intact field-stimulated (1Hz) cardiomyocytes, loaded with the membrane -permeant form of Asante Natrium Green-2 (ANG2) for Na^+ and FLUO4 for Ca^{2+}. Cardiomyocytes were incubated with the dye for 30 min, and then washed for 15 min to allow de-esterification. ANG2 and FLUO4 emissions were collected through a 535 nm band pass filter, converted to voltage, low-pass filtered (200Hz) and digitized at 2kHz after further low-pass digital filtering (FFT, 100Hz) and subtraction of background luminescence [1].

For Na^+ measurement, fluorescence recorded during ISC (F) was nor-

malized to that recorded during PRE (F_0) and expressed as F/F_0. Because dye response is slow relative to the electrical cycle, Na^+ signal represents an average of Na_{cyt} during the cycle.

To achieve quantitative estimates, Ca^{2+} fluorescent signal was calibrated by previously described methods [35], as detailed in supplement material. Ca^{2+} signal was evaluated in terms of Ca^{2+} transient amplitude (Ca_T) and diastolic Ca^{2+} (Ca_D). The SR Ca^{2+} content (Ca_{SR}) was estimated in a subset of cardiomyocytes at protocol end, by applying an electronically timed 10 mM caffeine pulse in Ca^{2+} and Na^+ free solution (sNCX inactive). SR fractional release (Ca_{FR}) was obtained as the ratio between Ca_T and Ca_{SR}.

2.4.6 Statistical analysis

In figures, TA, Na_{cyt} and Ca_{cyt} changes during AIP are presented as the average the traces recorded from N cells, along-with their S.E. Differences between continuous variables were tested by paired T-test or ANOVA as appropriate (Bonferroni's correction in post-hoc comparisons). Statistical significance was defined as $p<0.05$ (NS, not significant). Sample size (N) is reported in figure legends.

2.5 Results

2.5.1 Cell shortening and electrical activity

ISC superfusion resulted in a significant drop of TA, followed by a slow recovery which achieved a plateau after 3 minutes (Figure 2.1 A-B). TA was minimum at 0.5MIN (-86.89±1.77% $p<0.05$ vs CTRL), then completely recovered at 3MIN further changes at 7MIN (Figure 2.1 B-C). Stimulated APs were detectable throughout ISC exposure (Figure 2.1 D), even at 0.5MIN, when mechanical activity was negligible (Figure 2.1 C). ISC induced diastolic membrane potential (E_{diast}) depolarization and maximum depolarization rate (dV/dt_{max}) reduction. APD at 90% repolarization (APD90) was prolonged at 0.5MIN and then shortened (Figure 2.1 E). In

cardiomyocytes treated with RAN, AP changes induced by ISC were comparable to those present in untreated cardiomyocytes (control (CTRL), (Supplemental figure 2.2). These data show that during ISC the cell-shortening ceases transiently while the electrical activity is always present, despite of AP changes.

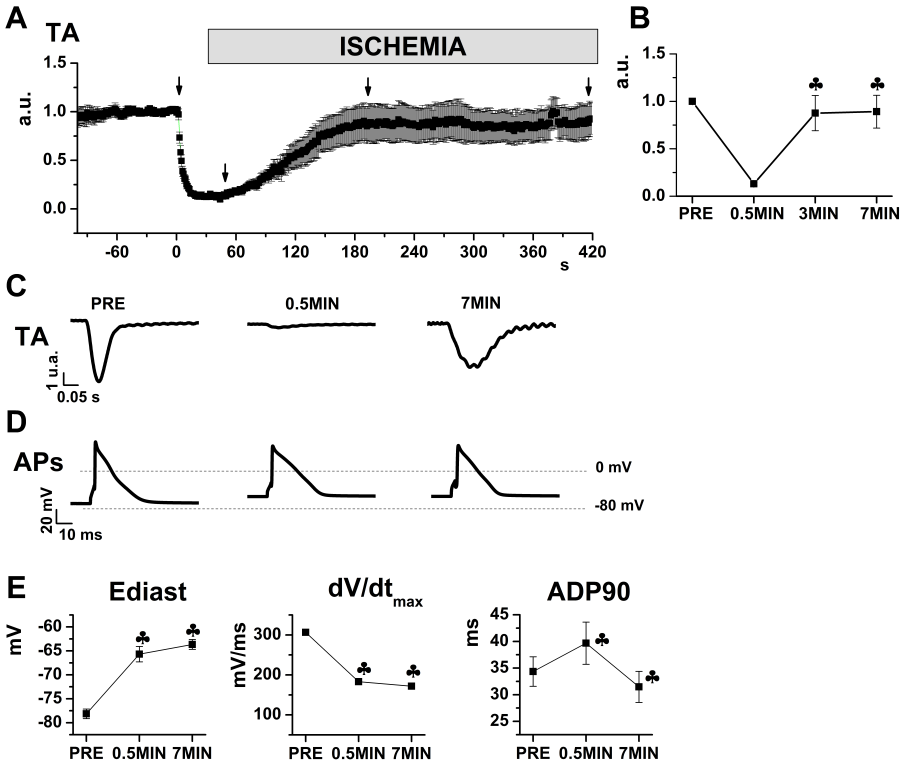

Figure 2.1: *Cell shortening and electrical activity.* A) Average traces and standard error of TA during AIP. Arrows indicate the times (PRE, 0.5MIN, 3MIN and 7MIN) considerated for statistical analysis (B). C-D) Representative traces of twitch amplitude (TA) and action potentials (APs) at PRE, 0.5MIN and 7MIN.E) Statistical analysis of diastolic membrane potential (E_{diast}), maximum depolarization rate (dV/dt_{max}) and 90% APD repolarization (APD_{90}). CTRL N=8. ♣=p<0.05 vs PRE

2.5.2 Late sodium current (I_{NaL})

To evaluate I_{NaL} contribution to AP during ISC, AP-clamp experiments were performed by using the PRE AP-waveform and the APwaveform recorded at the end of ISC (7MIN AP waveform). Under normal Tyrode's

superfusion (PRE AP waveform), small inward I_{TTX} was present during repolarization; this component was insensitive to blockade by RAN. At 7MIN (7MIN AP waveform) inward I_{TTX} during repolarization was markedly increased (+77%, p<0.05 vs PRE); the increment was almost completely blocked by RAN (Figure 2.2). The increment observed at 7MIN was larger (+88%, p<0.05 vs PRE) when the PRE AP waveform was applied (Supplemental Figure 2.3), thus indicating that during spontaneous electrical activity ISC-induced I_{NaL} increment may be partially blunted by the attending membrane potential changes.

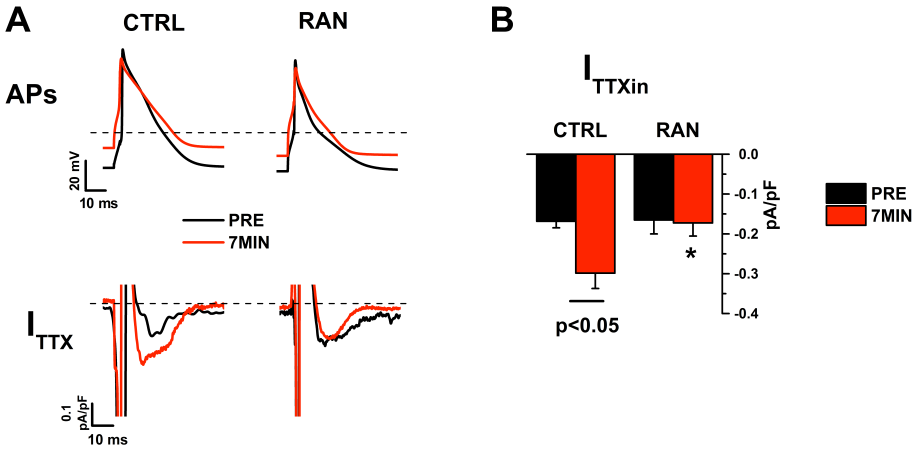

Figure 2.2: *I_{NaL} evaluation.* A) Representative APs recorded (top) and related TTX-sensative currents (I_{TTX}) (bottom)in PRE and at 7MIN in CTRL and RAN groups. B) Statistics of mean inward I_{TTX} ($ITTX_{in}$) in PRE and at 7MIN . N > 6 for both groups. ∗=p<0.05 vs CTRL.

2.5.3 Cytosolic Na^+ dynamics

Changes in Na_{cyt} during AIP were assessed in intact, field-stimulated (1Hz) cardiomyocytes in CTRL, RAN and TTX groups (Figure 2.3). After an initial dip, Na_{cyt} increased during ISC, reaching a peak at about 2 minutes, and then slowly declined (Figure 2.3 A). RAN and TTX similarly reduced the Na_{cyt} accumulation rate (dNa_{cyt}/dt), resulting in lower peak Na_{cyt} (Figure 2.3 B-C). These data indicate that I_{NaL} enhancement significantly contributed to Na_{cyt} accumulation during ISC.

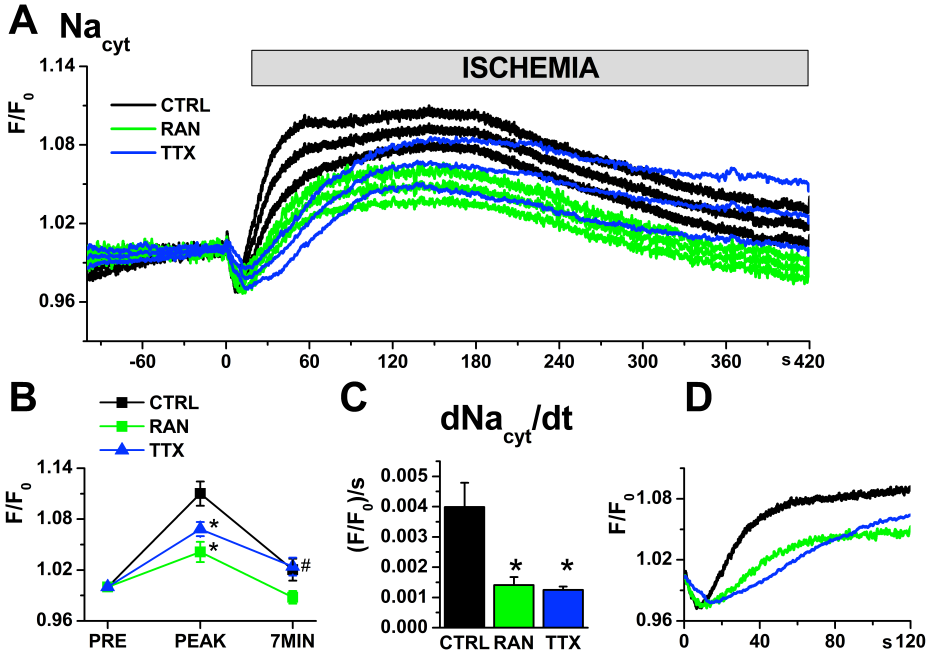

Figure 2.3: *ISC effects on cytosolic Na^+ (Na_{cyt}) dynamics* . A) Average traces and S.E. of Na_{cyt} changes during AIP in each group. B) Statistical analys of Na_{cyt} changes. C)Average and S.E. of Na_{cyt} accumulation rate (dNa_{cyt}/dt). D) Zoom of average traces reported in A. CTRL N=14; RAN N=9; TTX N=12. $*$=p$<$0.05 vs CTRL; #=p$<$0.05 vs RAN.

2.5.4 Cytosolic Ca^{2+} dynamics

Changes in Ca_{cyt} during AIP were assessed in intact, field-stimulated (1Hz) cardiomyocytes in CTRL and in the presence of RAN or TTX (Figure 2.4). Both Ca_D and Ca_T increased during ISC; the increment was initially steep and was simultaneous (or slightly preceded) that of Na_{cyt}. Ca_D monotonically increased to achieve a more or less stable plateau at about 3 mins. Ca_T increment followed a sigmoidal time course, thus lagging behind Ca_D and, achieved a peak at about 3 mins and then slowly declined (Figure 2.4 A,C). RAN slightly, but significantly decreased Ca_D; this effect was not shared by TTX (Figure 2.4 B). Both RAN and TTX not significantly affected Ca_T (Figure 2.4 D). Neither Ca_{SR} or Ca_{FR} were changed by RAN or TTX (Figure 2.4 E-F).

These data confirm a Ca_{cyt} increment during ISC; however, neither its timing with respect to Na_{cyt}, nor its unexpected insensitivity to TTX, are consistent with its dependency on enhanced Na^+ influx. Notably, Ca_{cyt} accumulation was, even if modestly, affected by RAN, possibly through a mechanism other than I_{NaL} blockade. To verify whether the sNCX contributed to Ca_{cyt} accumulation, as predicted by the coupled exchanger theory, the experiments were repeated in the presence of sNCX blockade.

2.5.5 Role of the sarcolemmal Na^+/Ca^{2+} exchanger

To assess the role of sNCX during AIP, its specific inhibitor SEA (1μM) [8] was added to the ISC solution (ISC+SEA). In presence of SEA, ISC-induced Na_{cyt} accumulation was reduced and Ca_{cyt} accumulation (Ca_D, Ca_T, Ca_{SR}) was markedly enhanced. Furthermore, peak Na_{cyt} was delayed by SEA (Supplemental figure 2.4). These unexpected results indicate that, during AIP, sNCX extruded Ca^{2+} in exchange for Na^+ (*forward mode* operation), thereby acting to compensate the rise in Ca_{cyt}. This is opposite to what predicted by the coupled exchanger theory and implies that a source other than sNCX accounted for Ca_{cyt} accumulation.

Notably, in the presence of SEA, both RAN and TTX markedly inhibited Ca_{cyt} accumulation (Figure 2.5), their effect being larger than in the

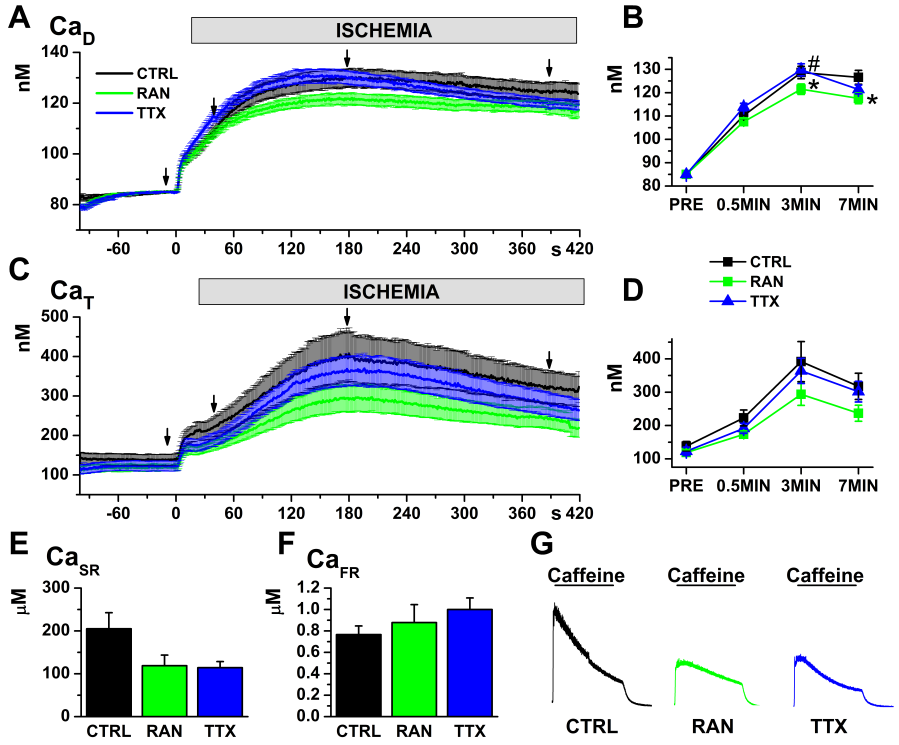

Figure 2.4: *ISC effects on cytosolic Ca^{2+} (Ca_{cyt}).* A,C) Average traces and standard errors of diastolic Ca^{2+} (Ca_D) and Ca^{2+} transient amplitude (Ca_T) changes during AIP. Arrows indicate the times (PRE, 0.5MIN, 3MIN and 7MIN) considerated for statistical analysis (B,D). E-F) Statistics of SR Ca^{2+} content (Ca_{SR}) and SR fractional release (Ca_{FR}). G) Representative Ca^{2+} transient evocated by caffeine superfusion. CTRL N=22(19); RAN N=19(13); TTXN=19(10). (N) cell numbers for Ca_{SR} and Ca_{FR} measurements. $*$=p<0.05 vs CTRL; #=p<0.05 vs RAN.

presence of active sNCX. This suggests the contribution to Ca_{cyt} accumulation of a Na^+-sensitive Ca^{2+} source, whose role was unveiled by removal of compensation by sNCX. As indicated by Ca_{SR} increment, the SR acted as a Ca^{2+} sink when sNCX was inhibited, thereby limiting Ca_{cyt} accumulation. However, TTX did not affect SEA-induced increment of Ca_{SR} (Figure 2.5 E), thus ruling out that its effect on Ca_{cyt} might depend on enhancement of SR Ca^{2+} uptake. Notably, Ca_{SR} was decreased by RAN instead, to suggest RAN modulation of a Ca^{2+} compartment insensitive to TTX. Lack of RAN (or TTX) effect on Ca_{FR} (Figure 2.5 F) argues against Ryanodine receptors (RyRs) modulation by the drugs.

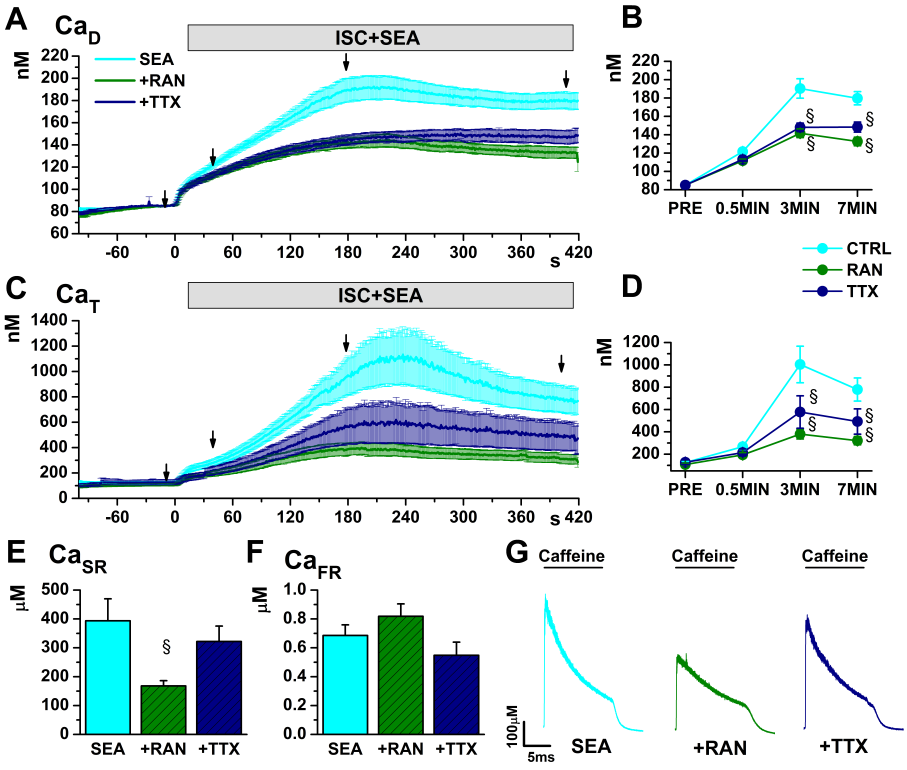

Figure 2.5: *Effects of I_{NaL} blockade on Ca_{cyt} in presence of sNCX blockade.* A-C) Average traces and standard errors of diastolic Ca^{2+} (Ca_D) and Ca^{2+} transient amplitude (Ca_T) changes during AIP. Arrows indicate the times (PRE, 0.5MIN, 3MIN and 7MIN) considered for statistical analysis (B,D). E,F) Statistics of SR Ca^{2+} content (Ca_{SR}) and SR fractional release (Ca_{FR}). G) Representative Ca^{2+} transient evocated by caffeine superfusion. SEA N=23(9); +RAN N=20(9); TTX N=18(9).(N) cell numbers for Ca_{SR} and Ca_{FR} measurements. §=p<0.05 vs SEA.

Mitochondria represent a further Ca^{2+} compartment, potentially affected by ischemia. Mitochondria normally release Ca^{2+} to cytosol through *forward mode* operation of mNCX. This release flux is proportional to Na_{cyt} and is therefore a candidate to link I_{NaL} inhibition (effect shared by TTX and RAN) to limitation of Ca_{cyt} accumulation. To test this hypothesis the experiments were repeated in the presence of mNCX blockade.

2.5.6 Role of the Na^+/Ca^{2+} exchanger

The Na^+/Ca^{2+} exchanger of the mitochondrial membrane (mNCX) was selectively blocked by 1μM CGP [32], which was added to the ISC with or without sNCX blockade. When applied in the presence of functional sNCX, CGP did not measurably affect Ca_{cyt} accumulation during ISC; however, it significantly increased Ca_{SR} (Supplemental figure 2.4 A-C), thus suggesting a shift of Ca^{2+} from the mitochondrial to the SR compartment. On the other hand, when CGP was applied in the presence of SEA (Supplemental Figure 2.5 D-F), Ca_{cyt} (Ca_D and Ca_T) accumulation was significantly reduced and Ca_{SR} also showed a trend toward reduction. These findings might suggest that during ISC, mitochondria provided a Ca^{2+} sink through *reverse mode* mNCX operation; this action was apparently reversed in the presence of sNCX blockade, when mNCX supported mitochondrial Ca^{2+} efflux (*forward mode*) instead. While the mode of mNCX operation might depend on the extent of mitochondrial Ca^{2+} load (conceivably larger in the presence of SEA), these observations altogether suggest that mNCX contributed to Ca_{cyt} buffering by mitochondria during ISC. Ca_{FR} was not affected by any of the interventions (Supplemental Figure 2.5 F), thus arguing against the involvement of RyRs modulation in their effects.

The effects of CGP, RAN and TTX on Ca_{cyt} during ISC+SEA are directly compared in Figure 2.6. Ca_D and Ca_T accumulation were similarity reduced by RAN, TTX and CGP. These data suggest that ISC+SEA-induced intracellular Ca^{2+} accumulation might depend mitochondrial Ca^{2+} efflux through mNCX and RAN and TTX effects might be through it.

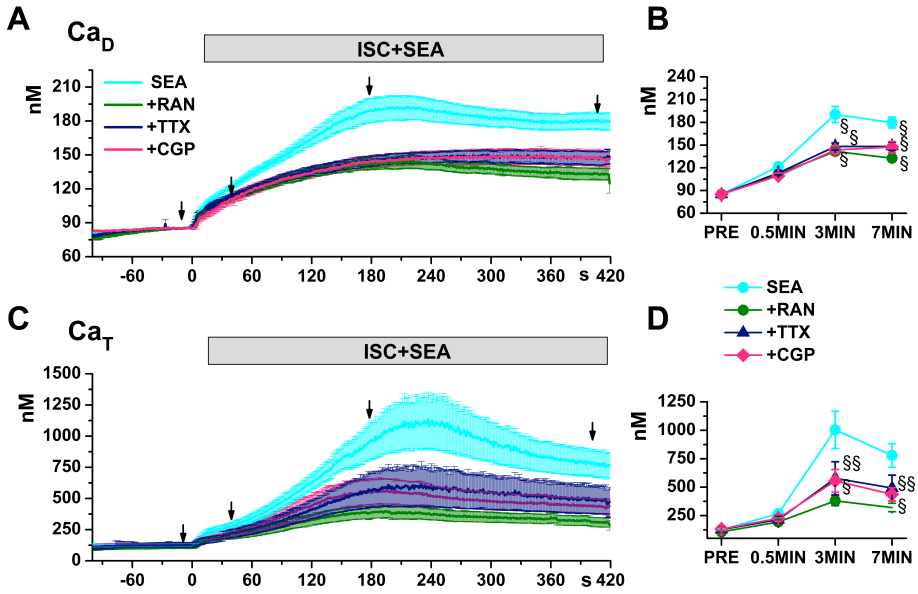

Figure 2.6: *Comparison of RAN, TTX and CGP effects on Ca_{cyt} in presence of sNCX blockade.* A-C) Average traces and standard errors of diastolic Ca^{2+} (Ca_D) and Ca^{2+} transient amplitude (Ca_T) changes during AIP. Arrows indicate the times (PRE, 0.5MIN, 3MIN and 7MIN) considered for statistical analysis (B,D). SEA N=23; +RAN N=20; TTX N=18; +CGP N=16. §=p<0.05 vs SEA.

2.6 Discussion

The main findings of this study are that during ischemia: electrical activity was present; I_{NaL} was increased in spite of AP changes; I_{NaL} contributed to Na_{cyt} accumulation, but failed to affect Ca_{cyt} accumulation in the presence of functional sNCX; sNCX worked in forward mode, thus other Ca^{2+} sources accounted for Ca_{cyt} accumulation; I_{NaL} and mNCX blockade reduced Ca_{cyt} induced by sNCX blocakde. Finally, this study suggests that mitochondria might be a source of Ca^{2+}, sensitive to Na_{cyt} and therefor, potentially affected by I_{NaL} modulation.

2.6.1 Ischemia induced-I_{NaL} enhancement

Several experimental models have indirectly linked the I_{NaL} with ischemia/ reperfusion injury. Studies on whole heart have shown that RAN prevents the ischemia-induced myocardial Ca^{2+} accumulation and improves the mechanical performance of the heart in reperfusion ([3] [6][27] [37]. Moreover, single cell studies have reported that some pathological ischemic component, such as phosphatidylcholines, reactive oxygen species (ROS), hypoxia and acidosis can induce an enhancement of I_{NaL} [38][44] [47]. However, whether I_{NaL} is increased and whether it directly contributes to ionic dysregulation during acute ischemia have not demostrated to date.

In this study I_{NaL} was directly investigated in rat ventricular cardiomyocytes exposed to ISC, which contains more hallmarks of ischemia than previous works [20] [21][38][41] (See Supplement). The present study reported that I_{NaL} enhancement is present during ISC in spite of AP changes, superseding the I_{Na} availability reduction caused by Ediast depolarization. This evidence leads to conclusion that changes in electrical activity that occur during ischemia not limit I_{NaL} enhancement, which may then contribute to the pathogenesis of ischemia/reperfusion damage.

2.6.2 I_{NaL} contribution to cytosolic Na^+ accumulation

ISC-induced Na_{cyt} accumulation was partially prevented by RAN and TTX, suggesting that the I_{NaL} contributes about 50% of increased to

Na^+ influx during ischemia. The Na_{cyt} accumulation not prevented by I_{NaL} blockade might result from Na^+ influx via NHE in response to intracellular acidosis, coupled with decreased NKA activity [34][11][16][26][29] [50]. However, ISC exposure in the presence of a selective NKA blocker (OUAB) induced a persistent rise of Na_{cyt} (Supplemental figure 2.6), indicating that the NKA activity was not abolished and suggesting that NHE was in part responsible for the Na_{cyt} accumulation. Overall, these data suggest that transient Na_{cyt} accumulation was due to increased Na^+ influx through I_{NaL} and NHE and successively compensated by NKA activity. Notably, NHE may be inhibited at end of ISC [51] [53] [13] whereas I_{NaL} enhancement was present, suggesting that I_{NaL} may partecipate to Na_{cyt} accumulation throughout ISC exposure, even if masked by NKA activity. This hypothesis is in accordance with Williams et al. [50] that have shown that the a major source of the Na^+ influx during global ischemia is the persistent component of I_{Na} and not NHE.

2.6.3 I_{NaL} contribution to cytosolic Ca^{2+} accumulation

Although, I_{NaL} enhancement participated to Na_{cyt} accumulation, surprisingly it did not contribute to Ca_{cyt} accumulation, which was insensitive to TTX and only slightly reduced by RAN (Ca_D). This result is apparently in contrast with the principal mechanism proposed to cause intracellular Ca^{2+} accumulation in ischemia/ reperfusion (coupled transport hypothesis). Indeed,sNCX blockade caused a huge Ca_{cyt} accumulation, indicating that sNCX extruded Ca^{2+} in exchange for Na^+ (*forward mode* operation), thereby acting to compensate the rise in Ca_{cyt} during ischemia. This is in contrast with other studies that have showed reverse mode sNCX activity in the development of myocardial ischemia /reperfusion injury [14][17][40][39][46][47]. In particular, Namekata et al [31] observed that the increase in cytoplasmic and mitochondrial Ca^{2+} were reduced by SEA in isolated cardiomyocytes. The discrepancy between studies might be related to the animal model used, because sNCX contribution to relaxation is higher in guinea pigs than in rat ventricular myocytes (49% vs 7%).

In the presence of sNCX blockade, both RAN and TTX markedly inhib-

ited Ca_{cyt} accumulation, suggesting that there was Na^+-dependent Ca^{2+} source that was unveiled by removal of compensation by sNCX. Mitochondria represent a further Ca^{2+} compartment, potentially affected by ischemia. It well know that elevated Nacyt reduces mitochondrial Ca^{2+} by accelerating Ca^{2+} efflux through mNCX [5] [22]. Therefore mNCX is a perfect candidate to explain why I_{NaL} inhibition by both RAN and TTX prevented Ca_{cyt} accumulation. The mNCX blockade in the presence of functional sNCX did not measurably affect Ca_{cyt} accumulation during ISC; however, it significantly increased Ca_{SR}. These evidences suggest a shift of Ca^{2+} from the mitochondrial to the SR compartment and thus, a role of mitochondria as Ca^{2+} sink during ischemia.

On the other hand, under sNCX blockade Ca_{cyt} accumulation was significantly reduced and Ca_{SR} also showed a trend toward reduction in the presence of mNCX blockade, suggesting that mitochondria provided a Ca^{2+} source for the Ca_{cyt}[42][5][36]. These findings altogether show a different mode of mNCX operation, which might depend to different direction and size of the driving force acting on mitochondrial Ca^{2+} transport systems (conceivably larger in the presence of SEA). Indeed, the comparison between RAN, TTX and CGP effects on Ca_{cyt} in the presence of sNCX blockade suggests that I_{NaL} blocked prevents ISC-induced Ca_{cyt} accumulation by modulating mNCX. However, this does not explain the total Ca_{cyt} accumulation during ISC, which is probably due to acidosis-induced Ca^{2+} debuffering [13][43]. Other experiments need to clarify this point.

2.6.4 Discrepancy between TTX and RAN effects

In the present study, RAN and TTX shared the the majority of effects during ischemia. However, in some cases RAN effects were not shared by TTX, implying the involvement of other mechanisms other than I_{NaL} blockade in RAN induced effects.

The different effect of RAN and TTX on Ca_D with functional sNCX, cannot be ascribed to RyRs stabilization by RAN [33],because the lack of RAN effects on Ca_{SR} argues against RyRs modulation by the drug.

RAN effects on Ca_{cyt} during ischemia is controversial, because studies on isolated perfused hearts report that RAN decreased systolic and diastolic Ca^{2+} concentration [3] [27] [37], while a recent study on isolated ventricular myocytes, shows that RAN not affect intracellular Ca^{2+} during simulated ischemia [6].

RAN, but not TTX, prevented the SEA-induced Ca_{SR} increment, suggesting the modulation of a Ca^{2+} compartment insensitive to TTX. RAN has been shown to stabilize mitochondrial membrane potential, (Na^{+}-mediated mechanism) [10][27][28][12],an effect not share by TTX. This intriguing point need to be further examined.

RAN might act by inhibiting fatty acid oxidation during ischemia and shifting the metabolism toward glucose oxidation [24][52], preventing myocardial damage; however much higher concentration of RAN is request (about 100 μM) compared to the one used in the present study.

2.6.5 Conclusion

The present study is the first to investigate the impact of I_{NaL} enhancement on Na^{+} and Ca^{2+} homeostasis during acute ischemia. I_{NaL} is increased in spite of AP changes, and it contributes to Na_{cyt} and Ca_{cyt} accumulation. Furthermore, Ca_{cyt} accumulation can be caused by mitochondria Ca^{2+} efflux, through mNCX, rather than by sarcolemmal Ca^{2+} influx via sNCX. I_{NaL} blockade may promote the shift form Ca^{2+} source to sink of mitochondria during acute ischemia. This is not remarked without sNCX blockade, because probably the mitochondria contribute variation is compensated by SR and sNCX; such compensation is removed by the block of sNCX.

2.6.6 Limitations

The set of conditions used to simulate ischemia in single myocytes did not include hypoxia. The work in which the ISC solution was initially described also tested hypoxia and found that its presence was not influential in determining changes in myocyte contractile function [19]. Nevertheless,

by contributing to ROS overproduction during ischemia, hypoxia might impact on I_{NaL} enhancement, thus potentially leading to its underestimation in the present setting.

2.7 Supplemental Material

2.7.1 Cell isolation

Rats weighing 125-175 g were anaesthetised with a Chloral Hydrate (400 mg/ kg at 20%), killed by cervical dislocation and exanguinated. Hearts were quickly removed, and the ascending aorta was connected to the outlet of a Langendorff column and perfused with a modified Tyrode's solution (37 °C) containing (mM): NaCl 143, KCl 5.4, $CaCl_2$ 1.8, $MgCl_2$ 0.5, NaH_2PO_4 5, HEPES NaOH 5, D-glucose 5.5, adjusted to pH 7.4. Modified Tyrode's perfusion was maintained until vigorous mechanical activity resumed and blood was completely removed. The heart was then perfused for 5 minutes with a nominally Ca^{2+}-free modified Tyrode's solution, followed by the same solution to which 140 U/ml collagenase (Worthington Type 1), 0.17 U/ml protease (Sigma, Type XIV), 0.05 mM $CaCl_2$ and 1 mg/ml bovine serum albumin were added. When the liquid became slightly viscous (after about 9 min), the heart was perfused for 5 min with Ca^{2+}-free solution (KB solution) containing (nM): KOH 70, glutammic acid 5, KCl 40, taurine 20, KH_2PO_4 20, $MgCl_2$, glucose 10, HEPES 10, EGTA 0.5, adjusted to pH 7.4. Subsequently the atria were dissected and the ventricles were chopped into 1 mm fragments, which were exposed to gentle mechanical agitation in KB solution. Samples of the suspension were collected every 5 minutes, filtered through a nylon mesh and centrifuged at 500 rpm for 3 minutes. Finally, the pellets were re-suspended in KB solution and stored at +4 °C until use. Rod shaped, Ca^{2+}-tolerant myocytes, obtained with this procedure, were used within 12 hours from dissociation.

2.7.2 Experimental model

Reproduce all aspects of myocardial acute ischemia on single cell is challenging; nevertheless, many types of ischemia-simulating solutions have been generated [6] [9][19][23][25][30]. In this study, ISC was a Tyrode's solution in which the major hallmarks of ischemia, previously described[7][9] [19][25][25][30][49],were added expect for the hypoxia: lactate accumulation; high extracellular K^+ concentration; glucose deficiency; hyperosmolarity and acidosis. The exposure of ISC induced a transient drop of cell shortening followed by a recovery; this is consistent with [19] which showed that lactate severely reduced the contractility of the cardiomyocytes and suggested that its effect was attributable to acidosis and was concentration dependent. Stimulated APs were always detectable, showing that membrane excitability persisted throughout the exposure of ISC, in spite of in AP contour changes (E_{diast} depolarization; dV/dt_{max} decrease and APD_{90} shortening), as reported previously in guinea pig cardiomyocytes [9][23].

2.7.3 Protocol of acute ischemia

In preliminary experiments, the duration of the ischemia period was varied (1, 3, 15 min). A 1-minute ischemic period resulted in a fast and complete cessation of myocytes contraction while a 3 minutes ischemic period induced a slow recovery of contraction after 2 minutes. ISC superfusion for 15 min caused a transient drop of myocytes contraction followed by a slow recovery, which tended to steady state after 3-4 minutes. Based on these preliminary experiments, we selected 7 minutes as the most appropriate duration of ischemia.

2.7.4 Patch-clamp recordings

Currents and APs were recorded from cardiomyocytes, using borosilicate glass pipettes (1.2 to 1.8 MΩ) in a whole-cell configuration of the patch-clamp technique (Digidata 1440A, Multiclamp 700b, Axon Instrument). membrane capacitance (C_m) and series resistance were measured in every cell. Traces acquisition and analysis was controlled by dedicated software

(Axon pClamp 10). The pipette solution contained (mM) K^+-aspartate 110, KCl 23, $MgCl_2$ 3, HEPES KOH 5, EGTA KOH 0.5, GTP-Na salt 0.4, ATP-Na salt 5, creatine phosphate Na^+ salt 5, $CaCl_2$ 0.2 (calculated free-Ca^{2+}= 10^{-7}M), adjusted to pH 7.3.

2.7.5 Ca_{cyt} signal calibration

The calibration of Ca^{2+} fluorescent signals was obtained with a pseudoratiometric equation (equation 1), as follows:

$$Ca_i = \frac{\frac{F}{F_0 * K_d}}{\frac{K_d}{Ca_0} - \frac{F}{F_0} + 1} \tag{2.1}$$

Where Ca_i is the value of intracellular Ca^{2+} concentration (nM), F is the raw fluorescence value, F_0 is mean diastolic fluorescence recorded in PRE phase, K_d is FLUO-4AM dissociation constant (estimated 400 nM), Ca_0 is diastolic Ca^{2+} concentration in PRE (corresponding to F_0). To provide a reliable estimate of Ca_0, saturating fluorescence (F_{max}) was measured in a subset of cells exposed to 5 mM Ca^{2+} under sNCX inhibition (nM): LiCl 154, KCl 4, $CaCl_2$ 4, $MgCl_2$ 1, HEPES 5, D-glucose 5.5, adjusted to pH 7.4) under conditions of maximal Ca^{2+} influx (upon reperfusion from 7 min of ISC). The mean Ca_0 value, estimated from the F_{max} thus obtained according to equation 2, was 85 ± 0.1 nM (N=9).

$$[Ca]_0 = \frac{K_d * F_0}{F_{max} - F_0} \tag{2.2}$$

This value was used as reference for Ca_0 in Equation 1. Total Ca_{SR} was estimated, according to published parameters of Ca^{2+} binding to intracellular buffers (B_{max} = 272 μmol/L; K_d = 0.673 μmol/L), by:

$$Ca_{SR} = \frac{B_{max}}{1 + \frac{K_d}{Ca_i}} + Ca_i \tag{2.3}$$

2.7.6 Reagents

Ranolazine (RAN) was provided by Gilead Sciences Inc (Foster City, CA); tetrodotoxin (TTX) was purchased from Tocris (Bristol, UK); all other reagents were from Sigma-Aldrich (St. Luis, MO). SEA 0400 (SEA) and CGP 31157 (CGP) were come from Clinic Sciences Srl (Rome, IT) and Abcam Plc (Cambridge UK) respectively. FLUO4 and Asante Natrium Green-2 (ANG2) were come from Life Technologies (Carlsbad, United States) and TEFlabs (Austin, TX) respectively.

2.8 Supplemental figures

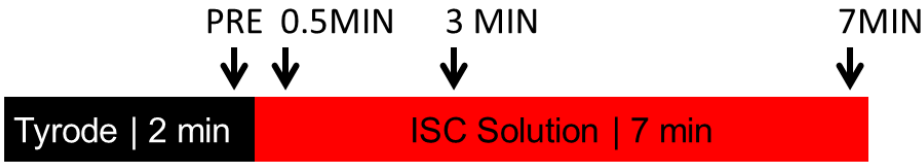

Supplemental Figure 2.1: *Protocol of acute ischemia (AIP).* Arrows indicate the times considered for statistical analyses (PRE, 0.5MIN, 3MIN and 7MIN).

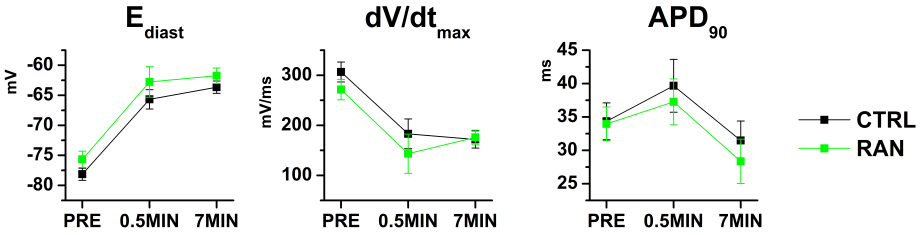

Supplemental Figure 2.2: *ISC-induced AP changes in CTRL and RAN groups.* Statistical analysis of E_{diast}; dV/dt_{max} and APD_{90}. CTRL N=8, RAN N=7

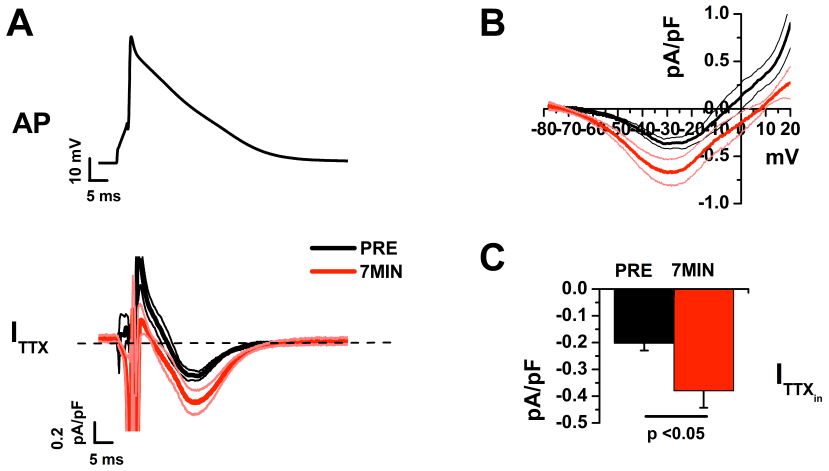

Supplemental Figure 2.3: *Late sodium current (I_{NaL}).* A) AP waveform recorded in PRE phase and average traces of TTX-sensitive current (I_{TTX}) in PRE and at 7MIN. B) Dynamic IV relationship of traces figured in A. C) Mean inward I_{TTX} in PRE and at 7MIN. N=8.

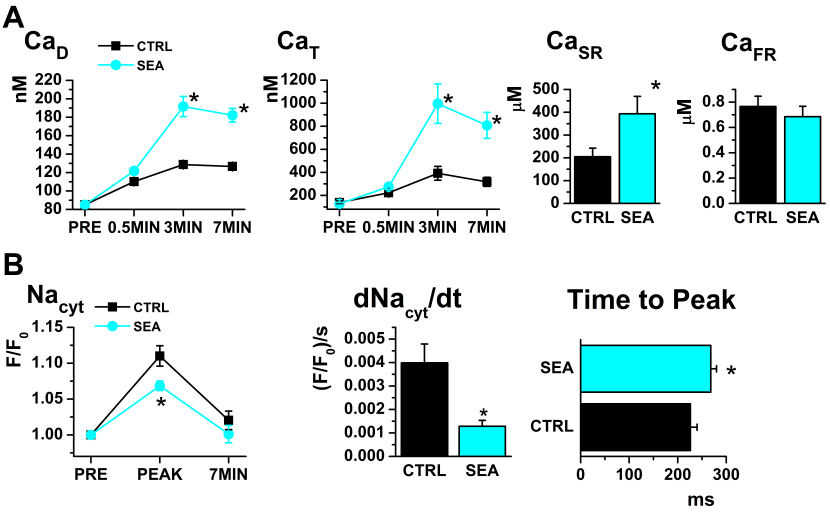

Supplemental Figure 2.4: *Effect of sNCX blockade (SEA) on cytosolic Ca^{2+} and Na^{+}.* A) Statistics of diastolic Ca^{2+} (Ca_D), Ca^{2+} transient amplitude (Ca_T), SR Ca^{2+} content (Ca_{SR}) and SR fractional release (Ca_{FR}). B) Statistics of cytosolic Na^{+} (Na_{cyt}), Na_{cyt} accumulation rate (dNa_{cyt}/dt) and time to peak. N >9 for both groups. $*$ = p<0.05 vs CTRL

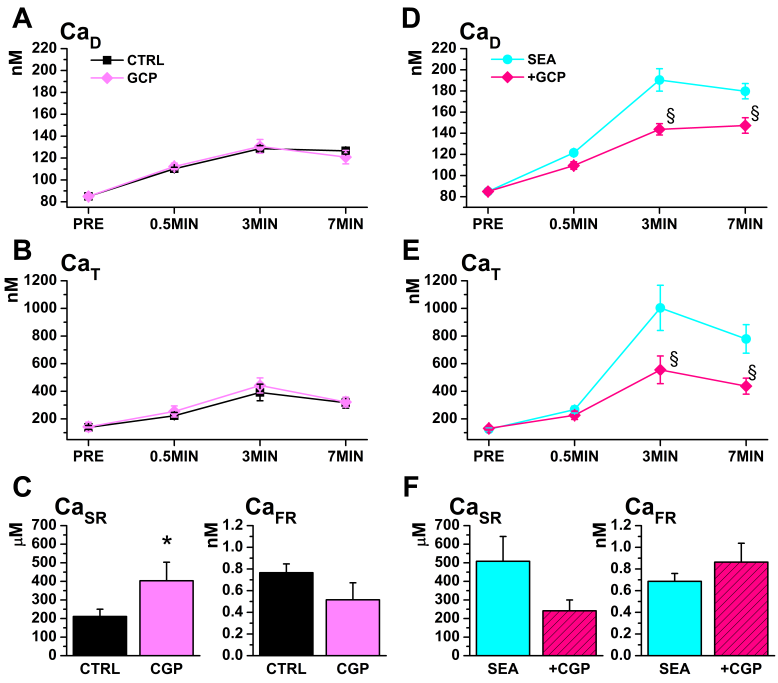

Supplemental Figure 2.5: *Effect of mNCX blockade (CGP) on cytosolic Ca^{2+} (Ca_{cyt}) in absence (left panel) or in presence (right panel) of sNCX blockade (SEA).* Statistics of diastolic Ca^{2+} (Ca_D), Ca^{2+} transient amplitude (Ca_T), SR Ca^{2+} content (Ca_{SR}) and SR fractional release (Ca_{FR}) during ischemic mimic solution (ISC) in precence of SEA (A-C) and in absences of SEA (D-F). CTRL N=22(19); CGP N=8(8);SEA N= 23(10); +CGP N=16(14). $*$ = p<0.05 vs CTRL.; § vs SEA.

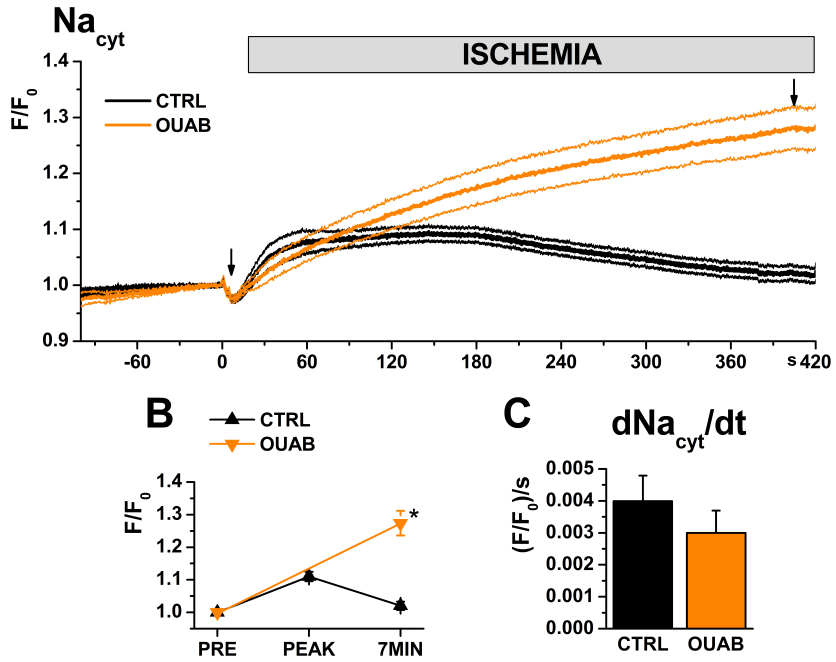

Supplemental Figure 2.6: *Effect of Na^+/K^+ ATPasi pump (NKA) blockade (OUAB) on cytosolic Na^+ (Na_{cyt}).* A) Average traces and standard error of Na_{cyt}. Arrows indicate the times (PRE, 0.5MIN, 3MIN and 7MIN) at which the statistical analysis was made (B). C) Na_{cyt} accumulation rate (dNa_{cyt}/dt). CTRL N=14, OUAB N=7 $*$ $p<0.05$ vs CTRL.

2.9 References

1. Alemanni, M., Rocchetti, M., Re, D. & Zaza, A. Role and mechanism of subcellular Ca 2+ distribution in the action of two inotropic agents with different toxicity. *J. Mol. Cell. Cardiol.* **50,** 910–918. ISSN: 00222828 (2011).

2. Allen, D. G. & Xiao, X.-H. Role of the cardiac Na+/H+ exchanger during ischemia and reperfusion. *Cardiovasc. Res.* **57,** 934–41. ISSN: 0008-6363 (2003).

3. Belardinelli, L, Shryock, J. C. & Fraser, H. Inhibition of the late sodium current as a potential cardioprotective principle: effects of the late sodium current inhibitor ranolazine. *Heart* **92 Suppl 4,** iv6–iv14. ISSN: 1468-201X (2006).

4. Bernink, F. J. P. *et al.* Progression in attenuating myocardial reperfusion injury: An overview. *Int. J. Cardiol.* **170,** 261–269. ISSN: 01675273 (2014).

5. Boyman, L., Williams, G. S. B., Khananshvili, D., Sekler, I. & Lederer, W. J. Journal of Molecular and Cellular Cardiology Review article NCLX : The mitochondrial sodium calcium exchanger. **59,** 205–213 (2013).

6. Calderon-Sanchez, A. Cardioprotective Effect of Ranolazine in the Process of Ischemia-reperfusion in Adult Rat Cardiomyocytes (2015).

7. Caldwell, J. C., Burton, F. L., Cobbe, S. M. & Smith, G. L. Amplitude Changes during Ventricular Fibrillation: A Mechanistic Insight. *Front. Physiol.* **3,** 147. ISSN: 1664-042X (2012).

8. Chen, S. & Li, S. The Na+/CaÂš+ exchanger in cardiac ischemia/reperfusion injury. *Med. Sci. Monit.* **18,** RA161–5. ISSN: 1643-3750 (2012).

9. Cordeiro, J. M., Howlett, S. E. & Ferrier, G. R. Simulated ischaemia and reperfusion in isolated guinea pig ventricular myocytes. *Cardiovasc Res* **28,** 1794–1802 (1994).

10. Dehina, L. *et al.* Protective effects of ranolazine and propranolol, alone or combined, on the structural and functional alterations of cardiomyocyte mitochondria in a pig model of ischemia/reperfusion. *Fundam. Clin. Pharmacol.* **28,** 257–267. ISSN: 07673981 (2014).

11. Fuller, W., Parmar, V., Eaton, P., Bell, J. R. & Shattock, M. J. Cardiac ischemia causes inhibition of the Na/K ATPase by a labile cytosolic compound whose production is linked to oxidant stress. *Cardiovasc. Res.* **57,** 1044–1051. ISSN: 00086363 (2003).

12. Gadicherla, A. K., Stowe, D. F., Antholine, W. E., Yang, M. & Camara, A. Damage to mitochondrial complex I during cardiac ischemia reperfusion injury is reduced indirectly by anti-anginal drug ranolazine. **18,** 1199–1216. ISSN: 1878-5832 (2013).

13. Garciarena, C. D., Youm, J. B., Swietach, P. & Vaughan-Jones, R. D. HâĄž-activated NaâĄž influx in the ventricular myocyte couples CaÂšâĄž-signalling to intracellular pH. *J. Mol. Cell. Cardiol.* **61,** 51–9. ISSN: 1095-8584 (2013).

14. Haigney, M. C., Miyata, H, Lakatta, E. G., Stern, M. D. & Silverman, H. S. Dependence of hypoxic cellular calcium loading on Na(+)-Ca2+ exchange. *Circ. Res.* **71,** 547–57. ISSN: 0009-7330 (1992).

15. Hale, S. L., Leeka, J. A. & Kloner, R. A. Improved left ventricular function and reduced necrosis after myocardial ischemia/reperfusion in rabbits treated with ranolazine, an inhibitor of the late sodium channel. *J. Pharmacol. Exp. Ther.* **318,** 418–23. ISSN: 0022-3565 (2006).

16. Hartmann, M & Decking, U. K. M. Blocking Na + âĂŞ H + Exchange by Cariporide Reduces Na + -overload in Ischemia and is Cardioprotective. **1995,** 1985–1995 (1999).

17. Imahashi, K. Cardiac-Specific Ablation of the Na+-Ca2+ Exchanger Confers Protection Against Ischemia/Reperfusion Injury. *Circ. Res.* **97,** 916–921. ISSN: 0009-7330 (2005).

18. Linz, W. J. & Busch, A. E. NHE-1 inhibition: from protection during acute ischaemia/reperfusion to prevention/reversal of myocardial remodelling. *Naunyn. Schmiedebergs. Arch. Pharmacol.* **368,** 239–46. ISSN: 0028-1298 (2003).

19. Lu, J. *et al.* Effects of ischaemia-mimetic factors on isolated rat ventricular myocytes. *Exp. Physiol.* **90,** 497–505. ISSN: 0958-0670 (2005).

20. Lu, Z., Ballou, L. M., Jiang, Y.-P., Cohen, I. S. & Lin, R. Z. Restoration of defective L-type Ca2+ current in cardiac myocytes of type 2 diabetic db/db mice by Akt and PKC-ι. *J. Cardiovasc. Pharmacol.* **58,** 439–45. ISSN: 1533-4023 (2011).

21. Ma, J. *et al.* Ranolazine attenuates hypoxia- and hydrogen peroxide-induced increases in sodium channel late openings in ventricular myocytes. *J. Cardiovasc. Pharmacol.* **64,** 60–8. ISSN: 1533-4023 (2014).

22. Maack, C. *et al.* Elevated cytosolic Na+ decreases mitochondrial Ca2+ uptake during excitation-contraction coupling and impairs energetic adaptation in cardiac myocytes. *Circ. Res.* **99,** 172–182. ISSN: 00097330 (2006).

23. MacDonald, A. C. & Howlett, S. E. Differential effects of the sodium calcium exchange inhibitor, KB-R7943, on ischemia and reperfusion injury in isolated guinea pig ventricular myocytes. *Eur. J. Pharmacol.* **580,** 214–23. ISSN: 0014-2999 (2008).

24. MacInnes, A. The Antianginal Agent Trimetazidine Does Not Exert Its Functional Benefit via Inhibition of Mitochondrial Long-Chain 3-Ketoacyl Coenzyme A Thiolase. *Circ. Res.* **93,** 26e–32. ISSN: 0009-7330 (2003).

25. Maddaford, T. G., Hurtado, C, Sobrattee, S, Czubryt, M. P. & Pierce, G. N. A model of low-flow ischemia and reperfusion in single, beating adult cardiomyocytes. *Am. J. Physiol. Circ. Physiol.* **277,** H788–H798. ISSN: 03636135 (ISSN) (1999).

26. Madonna, R., Cevik, C. & Nasser, M. Electrical plasticity and cardioprotection in myocardial ischemia–role of selective sodium channel blockers. *Clin. Cardiol.* **36,** 255–61. ISSN: 1932-8737 (2013).

27. Mohammed Aldakkaka. Ranolazine reduces Ca2+ overload and oxidative stress and improves mitochondrial integrity to protect against ischemia reperfusion injury in isolated hearts. **64,** 381–392 (2012).

28. Moreno, J. D. & Clancy, C. E. Pathophysiology of the cardiac late Na Current and its potential as a drug taghet. **52.** doi:10.1016/j.yjmcc.2011.12.003.Pathophysiology (2013).

29. Murphy, E. & Eisner, D. a. Regulation of intracellular and mitochondrial sodium in health and disease. *Circ. Res.* **104,** 292–303. ISSN: 1524-4571 (2009).

30. Nakamura, T *et al.* A single cell model of myocardial reperfusion injury: changes in intracellular Na+ and Ca2+ concentrations in guinea pig ventricular myocytes. *Mol. Cell. Biochem.* **194,** 147–57. ISSN: 0300-8177 (1999).

31. Namekata, I., Shimada, H., Kawanishi, T., Tanaka, H. & Shigenobu, K. Reduction by SEA0400 of myocardial ischemia-induced cytoplasmic and mitochondrial Ca2+ overload. *Eur. J. Pharmacol.* **543,** 108–15. ISSN: 0014-2999 (2006).

32. Palty, R. & Sekler, I. The mitochondrial Na+/Ca2+ exchanger. *Cell Calcium* **52,** 9–15. ISSN: 01434160 (2012).

33. Parikh, A. *et al.* Ranolazine stabilizes cardiac Ryanodine receptors: a novel mechanism for the suppression of Early afterdepolarization and Torsade de Pointes in Long QT type 2. **130,** 9492–9499. ISSN: 15378276 (2012).

34. Pogwizd, S. M., Sipido, K. R., Verdonck, F. & Bers, D. M. Intracellular Na in animal models of hypertrophy and heart failure: Contractile function and arrhythmogenesis. *Cardiovasc. Res.* **57,** 887–896. ISSN: 00086363 (2003).

35. Rocchetti, M. *et al.* Ranolazine prevents INaL enhancement and blunts myocardial remodelling in a model of pulmonary hypertension. *Cardiovasc. Res.* **104,** 37–48. ISSN: 0008-6363 (2014).

36. Saotome, M. *et al.* Mitochondrial membrane potential modulates regulation of mitochondrial Ca2+ in rat ventricular myocytes. *Am. J. Physiol. Hear. Circ. Physiol.* **288,** H1820–H1828 (2005).

37. Soliman, D. *et al.* Late sodium current inhibition alone with ranolazine is sufficient to reduce ischemia- and cardiac glycoside-induced calcium overload and contractile dysfunction mediated by reverse-mode sodium/calcium exchange. *J. Pharmacol. Exp. Ther.* **343,** 325–32. ISSN: 1521-0103 (2012).

38. Song, Y., Shryock, J. C., Wagner, S., Maier, L. S. & Belardinelli, L. Blocking Late Sodium Current Reduces Hydrogen Peroxide- Induced Arrhythmogenic Activity and Contractile Dysfunction. **318,** 214–222 (2006).

39. Swift, F. *et al.* Extreme sarcoplasmic reticulum volume loss and compensatory T-tubule remodeling after Serca2 knockout. *Proc. Natl. Acad. Sci.* **109,** 3997–4001. ISSN: 0027-8424 (2012).

40. Takahashi, K. *et al.* Protective effects of SEA0400, a novel and selective inhibitor of the Na+/Ca2+ exchanger, on myocardial ischemia-reperfusion injuries. *Eur. J. Pharmacol.* **458,** 155–62. ISSN: 0014-2999 (2003).

41. Tang, Q. *et al.* Persistent sodium current and Na+/H+ exchange contributes to the augmentation of the reverse Na+/Ca2+ exchange during hypoxia or acute ischemia in ventricular myocytes. *Pflügers Arch. - Eur. J. Physiol.* **463,** 513–522. ISSN: 0031-6768 (2012).

42. Tanonaka, K., Motegi, K., Arino, T., Marunouchi, T. & Takagi, N. Possible Pathway of Na Flux into Mitochondria in Ischemic Heart. **35,** 1661–1668 (2012).

43. Thompson, B. R. & Metzger, J. M. Cell biology of sarcomeric protein engineering: Disease modeling and therapeutic potential. *Anat. Rec.* **297,** 1663–1669. ISSN: 19328494 (2014).

44. Undrovinas, a. I., Fleidervish, I. a. & Makielski, J. C. Inward sodium current at resting potentials in single cardiac myocytes induced by the ischemic metabolite lysophosphatidylcholine. *Circ. Res.* **71,** 1231–1241. ISSN: 0009-7330 (1992).

45. Undrovinas, A. I., Belardinelli, L., Undrovinas, N. a. & Sabbah, H. N. Ranolazine improves abnormal repolarization and contraction in left ventricular myocytes of dogs with heart failure by inhibiting late sodium current. *J. Cardiovasc. Electrophysiol.* **17 Suppl 1,** S169–S177. ISSN: 1045-3873 (2006).

46. Wang, J. SEA0400, a novel Na+/Ca2+ exchanger inhibitor, reduces calcium overload induced by ischemia and reperfusion in mouse ventricular myocytes. *Physiol. Res.* **56,** 17–23. ISSN: 0862-8408 (2007).

47. Wang, X.-J. *et al.* Ranolazine Attenuates the Enhanced Reverse Na+-Ca2+ Exchange Current via Inhibiting Hypoxia-Increased Late Sodium Current in Ventricular Myocytes. *J. Pharmacol. Sci.* **124,** 365–373. ISSN: 1347-8613 (2014).

48. Wilde, a. a. *et al.* Potassium accumulation in the globally ischemic mammalian heart. A role for the ATP-sensitive potassium channel. *Circ. Res.* **67,** 835–843. ISSN: 0009-7330 (1990).

49. Wilde, a. a. *et al.* Potassium accumulation in the globally ischemic mammalian heart. A role for the ATP-sensitive potassium channel. *Circ. Res.* **67,** 835–843. ISSN: 0009-7330 (1990).

50. Williams, I. a., Xiao, X.-h., Ju, Y.-k. & Allen, D. G. The rise of [Na(+)] (i) during ischemia and reperfusion in the rat heart-underlying mechanisms. *Pflugers Arch.* **454,** 903–12. ISSN: 0031-6768 (2007).

51. Wu, M.-l. L. & Vaughan-Jones, R. D. Effect of metabolic inhibitors and second messengers upon Na + -H + exchange in the sheep

cardiac Purkinje fibre. *J. Physiol.* **478 (Pt 2,** 301–13. ISSN: 0022-3751 (1994).

52. Wyatt, K. M., Skene, C, Veitch, K, Hue, L & McCormack, J. G. The antianginal agent ranolazine is a weak inhibitor of the respiratory complex I, but with greater potency in broken or uncoupled than in coupled mitochondria. *Biochem. Pharmacol.* **50,** 1599–606. ISSN: 0006-2952 (1995).

53. Xiao, X.-H. & Allen, D. G. Role of Na+/H+ Exchanger During Ischemia and Preconditioning in the Isolated Rat Heart. *Circ. Res.* **85,** 723–730. ISSN: 0009-7330 (1999).

54. Zaza, a, Rocchetti, M, Brioschi, a, Cantadori, a & Ferroni, a. Dynamic Ca2+-induced inward rectification of K+ current during the ventricular action potential. *Circ. Res.* **82,** 947–56. ISSN: 0009-7330 (1998).

Chapter 3

Ranolazine prevents I_{NaL} enhancement and blunts myocardial remodelling in a model of pulmonary hypertension

Marcella Rocchetti, PhD[1,§]; Luca Sala, Dr[1,§]; Riccardo Rizzetto, PhD[1]; Lidia Irene Staszewsky, MD[2]; Matteo Alemanni, PhD[1]; Vanessa Zambelli, PhD[3]; Ilaria Russo, PhD[2]; Lucio Barile[4], PhD; Laura Cornaghi, PhD[2]; Claudia Altomare, Dr[1]; Carlotta Ronchi, Dr[1]; Gaspare Mostacciuolo, Mr[1]; Roberto Latini, MD[2]; Antonio Zaza, MD[1].

[1] Dipartimento di Biotecnologie e Bioscienze, Universitá degli Studi di Milano - Bicocca, Milano, Italy;
[2] Lab Cardiovascular Clinical Pharmacology, Dept of Cardiovascular Research, IRCCS-Istituto Mario Negri, Milano, Italy;
[3] Dipartimento di Scienze della Salute, Universitá degli studi di Milano - Bicocca, Monza, Italy;
[4] Molecular Cardiology Laboratory, Fondazione Cardiocentro Ticino, Lugano, Switzerland.

[§] Authors equally contributed to this work.

Cardiovascular Research 2014;104(1):37-48. doi:10.1093/cvr/cvu188.

3.1 Acronyms

APD	action potential duration
APD_{50}	50% APD repolarization
APD_{90}	90% APD repolarization
AP	action potential
$[Ca]_T$	Ca^{2+} transient amplitude
$[Ca]_{diast}$	diastolic Ca^{2+}
SR	sarcoplasmic reticulum
$[Ca]_{SR}$	sarcoplasmic reticulum (SR) Ca^{2+} content
C_m	membrane capacitance
E_{diast}	diastolic membrane potential
I_{NaL}	late sodium current
I_{TTX}	TTX-sensitive current
I_{CaL}	L-type calcium current
I_{Na}	Sodium current
I_{K1}	inward rectifier potassium current
I_{NaW}	sodium window current
I_{to}	transient outward current
RAN	ranolazine
TTX	tetrodotoxin
BW	body weight
CO	cardiac output
EDV	end diastolic volume
EF	ejection fraction
ESV	end systolic volume
FAC	fractional area contraction
HW	heart weight

IVRT	isovolumic relaxation time
IVS	interventricular septum
LW	lungs weight
MCT	monocrotaline
MHC	myosin heavy chain
NCX	Na^+/Ca^{2+} exchanger
PAH	pulmonary arterial hypertension
PASMC	pulmonary artery smooth muscle cells
RVSP	right ventricular systolic pressure
SPAWT	small pulmonary artery wall thickness
SV	stroke volume
TAPSE	tricuspid annular plane systolic excursion
TT	T-Tubules
RV	right ventricle
LV	left ventricle
CSA	cross sectional area

3.2 Abstract

Aims: pulmonary arterial hypertension (PAH) reflects abnormal pulmonary vascular resistance and causes right ventricle (RV) hypertrophy. Enhancement of the late sodium current (I_{NaL}), may result from hypertrophic remodeling. The study tests whether: 1) constitutive I_{NaL} enhancement may occur as part of PAH-induced myocardial remodelling; 2) ranolazine (RAN), a clinically available I_{NaL} blocker, may prevent constitutive I_{NaL} enhancement and PAH-induced myocardial remodelling.

Methods and Results: PAH was induced in rats by a single monocrotaline injection (MCT, 60 mg/Kg i.p.); studies were performed 3 weeks later. RAN (30 mg/Kg bid i.p.) was administered 48 hrs after MCT

and washed-out 15 hrs before studies. MCT increased RV systolic pressure, caused RV hypertrophy and loss of left ventricle (LV) mass. In the RV, collagen was increased, myocytes were enlarged with T-tubules disarray, displayed myosin heavy chain isoform switch. I_{NaL} was markedly enhanced; diastolic Ca^{2+} was increased and Ca^{2+} release was facilitated. K^+ currents were downregulated and action potential duration (APD) was prolonged. In the LV, I_{NaL} was enhanced to a lesser extent and cell Ca^{2+} content was strongly depressed. Electrical remodelling was less prominent than in the RV. RAN completely prevented I_{NaL} enhancement and limited most aspects of PAH-induced remodeling, but failed to affect in-vivo contractile performance. RAN blunted the MCT-induced increase in RV pressure and medial thickening in pulmonary arterioles.

Conclusions: PAH induced remodeling with chamber-specific aspects. Remodeling was associated with I_{NaL} enhancement and was largely countered by RAN. Partial mechanical unloading, resulting from an unexpected effect of RAN on pulmonary vasculature, might contribute to this effect.

3.3 Introduction

Pulmonary hypertension may develop as a consequence of chronic enhancement of pulmonary flow (e.g. in cardiac defects) or systemic hypoxia. Nevertheless, its most common and aggressive form (PAH) results from "primary" wall thickening in small pulmonary arteries, of uncertain etiology, but often observed in association with systemic diseases (autoimmune, etc.). A widely accepted experimental model of PAH is generated by systemic administration of monocrotaline (MCT), a vascular toxin that selectively affects the pulmonary microcirculation [35]. PAH imposes a high pressure load on the right ventricle (RV) and leads to progressive remodeling of this chamber. Albeit initially compensatory, the process becomes maladaptive, thus making development of RV dysfunction the turning point in PAH prognosis 2. Although PAH-induced mechanical overload mainly affects the RV, left ventricle (LV) involvement has been reported by experimental and clinical studies [13][16][4][5][2]. In a variety of experimen-

tal models other than RV hypertrophy, myocardial hypertrophy/failure is associated with enhancement of the late sodium current (I_{NaL}). This may, in turn, contribute to many of the functional (electrical and contractile) derangements associated with remodelled myocardium. Furthermore, because of its impact on homeostasis of intracellular Ca^{2+}, which is pivotal in initiating hypertrophic transcriptional regulation, I_{NaL} enhancement might also contribute to myocardial remodeling itself [41][26][40]. Recent work reports that pressure-induced RV remodeling can be opposed by ranolazine (RAN) and trimetazidine [12]. The effect has been attributed to partial inhibition of fatty acids oxidation (FAO), an action of RAN previously reported [24]. Nevertheless, RAN ability to inhibit FAO at therapeutic concentrations has been disputed [37]. More recent reports attribute cardio-protective effects of RAN to I_{NaL} blockade [3][21]. The present study evaluates the hypothesis that 1) constitutive I_{NaL} enhancement may occur as part of PAH-induced myocardial remodelling; 2) RAN may prevent I_{NaL} enhancement 3) RAN can prevent PAH-induced myocardial remodelling.

3.4 Methods

The investigation conforms to the Guide of the Care and Use of Laboratory Animals published by the US National Institutes of Health (NIH publication No. 85-23, revised 1996) and to the guidelines for animal care endorsed by the hosting institution.

3.4.1 Pulmonary arterial hypertension (PAH) model

Adult male Sprague Dawley rats (110 gr) were injected intraperitoneally (i.p.) with 2% MCT solution at a dose of 60 mg/Kg (MCT group). A subset of MCT-treated rats received RAN (30 mg/Kg, b.i.d., i.p.) for 20 days (MCT-RAN group); to avoid interference with MCT metabolism, RAN treatment was started two days after MCT injection. RAN vehicle was administered to the MCT group and to untreated littermates, which served as controls (CTRL group). To evaluate remodelling-dependent ef-

fects, all measurements had to be carried out in the absence of RAN. Thus, the time between the last RAN injection and sacrifice (blood sample collection) was 15-16 hours in all cases, i.e. adequate for complete RAN washout.

3.4.2 Echocardiography

Transthoracic echocardiography was performed on sedated rats (ketamine 80 mg/kg and midazolam 2.5 mg/kg body weight (BW) i.p.). RV systolic function was evaluated by measurement of the fractional area contraction (FAC) and the tricuspid annular plane systolic excursion (TAPSE). RV diastolic function was evaluated by measurement of isovolumic relaxation time (IVRT) by pulsed wave Tissue Doppler Imaging. LV volumes (end diastolic volume (EDV), end systolic volume (ESV)) and LV ejection fraction (EF) were measured from the parasternal long-axis view and calculated through the modified simple-plane Simpson's rule.

3.4.3 Invasive hemodynamic

right ventricular systolic pressure (RVSP) was measured with a tip-transducer catheter (Millar SPR671) introduced in the RV through the right jugular vein under anesthesia (pentobarbital 50 mg/Kg i.p.) allowing for spontaneous breathing. After ruling out pulmonary valve and RV outflow tract stenosis by echocardiography, RVSP was considered representative of pulmonary artery systolic pressure [8].

3.4.4 Quantitative RT-PCR

Relative expression of mRNAs encoding α- and β-myosin heavy chains (MHCs) was measured using RTq-PCR in RV and LV of each experimental group. Specific primers are shown in 3.3.

3.4.5 Myocytes isolation and patch clamp measurements

Rats were sacrificed by cervical dislocation under ketamine/xylazine (50 and 5 mg/Kg) anesthesia 3 weeks after MCT injection. Ventricular my-

ocytes were isolated from LV and RV free walls as previously reported [39] with minor modifications; interventricular septum (IVS) was not dissociated. Rod shaped, Ca^{2+} tolerant myocytes were used for patch clamp measurements within 6-8 hours from dissociation. Single-cell electrical activity was evaluated by action potential (AP) recordings in isolated myocytes during steady-state pacing at 2 Hz. For steady-state currents (I_{NaL} and inward rectifier potassium current (I_{K1})), I/V relationships were obtained by applying slow voltage ramps (56 mV/s). I_{NaL} was measured as tetrodotoxin (TTX), 30 μmol/L)-sensitive current (I_{TTX}). According to preliminary evidence (see Supplmental figures 3.8, 3.9), I_{TTX} at 0 mV was taken as representative of I_{NaL} and peak I_{TTX} value, occurring at more negative potentials, was assumed to reflect the Na^+ "window component" (I_{NaW}). I_{K1} was isolated by subtraction of recordings in K^+-free solution [39]. Transient currents (transient outward current (I_{to}), and L-type calcium current (I_{CaL})) were measured by standard voltage clamp protocols. To isolate I_{to} (see Supplemental figure 3.10), cadmium (0.5 mmol/L) and EGTA (4 mmol/L) were added to extracellular and intracellular solutions respectively. I_{CaL} was measured in Na^+- and K^+-free solution. To take into account the variations in cell size, current amplitude was normalized to membrane capacitance (C_m) in all measurements.

3.4.6 Calcium handling

Fluo-4 loaded intact myocytes were field-stimulated at 2 Hz (Fig S4). Fluorescence signal was converted to free Ca^{2+} concentration by an indirect method, as detailed in the Online Supplement (Supplemental figure 3.12). Ca^{2+} transient amplitude ($[Ca]_T$) and diastolic Ca^{2+} ($[Ca]_{diast}$) were measured at steady-state. SR Ca^{2+} content ($[Ca]_{SR}$) was estimated by an electronically timed 10 mmol/L caffeine pulse after 10s at resting. SR fractional release was obtained as the ratio between $[Ca]_T$ and $[Ca]_{SR}$.

3.4.7 T-tubules analysis

Sarcolemmal membranes were stained by incubating isolated ventricular myocytes with di-3-ANEPPDHQ (20 μmol/L). 8-bit grayscaled images were subjected to spatial Fast Fourier Transform analysis allowing to quantify periodic and aperiodic components of pixels variance (see Supplemental Methods). Whereas the periodic component is generated by transverse T-Tubules (TT), the aperiodic one may reflect disarray of transverse TT, but can also be generated by longitudinal TT.

3.4.8 Statistical analysis

Data are presented as mean SE. χ^2-test was used for comparison of categorical variables. Comparison between multiple means was performed by one-way ANOVA and post hoc Bonferroni's correction. A repeated measurement model was applied whenever internal comparisons were involved.The Mann-Whitney test was used for multiple comparisons of categorical variables. Statistical significance was defined as $p<0.05$ (NS = not significant). The main text reports percent changes; unless otherwise specified, a "change" is statistically significant. The respective absolute values are shown in the figures. The number of animals (N) and cells (n) are reported in figure legends.

3.5 Results

For all measurements, values obtained from RV and LV in the CTRL group are compared in 3.4. Only the changes induced by MCT and by concomitant RAN administration are described here.

3.5.1 Monocrotaline (MCT)-model: general parameters

Hematocrit was similar between CTRL and MCT rats, thus suggesting that systemic hypoxia or significant reduction of plasma volume were not present on MCT rats. MCT rats had lower BW (-27%). Lung-to-body weight ratio was increased (LW/BW, +98%), almost entirely due to an

Table 3.1: General parameters

	CTRL (*N* = 18)	MCT (*N* = 17)	+RAN (*N* = 16)	*P*-value		
				MCT vs. CTRL	RAN vs. CTRL	RAN vs. MCT
Haematocrit (%)	41.5 ± 0.8	45 ± 1.6	44 ± 1.9	NS	NS	NS
BW (kg)	0.29 ± 0.005	0.21 ± 0.007	0.22 ± 0.005	<0.05	<0.05	NS
LW/BW (g/kg)	5.65 ± 0.16	11.1 ± 0.45	10.5 ± 0.52	<0.05	<0.05	NS
HW/BW (g/kg)	4.37 ± 0.11	6.73 ± 0.27	5.87 ± 0.25	<0.05	<0.05	<0.05
RV/(LV + IVS)	0.39 ± 0.02	0.69 ± 0.04	0.58 ± 0.03	<0.05	<0.05	<0.05
RV/HW (g/g)	0.23 ± 0.008	0.33 ± 0.011	0.29 ± 0.007	<0.05	<0.05	<0.05
(LV + IVS)/HW (g/g)	0.59 ± 0.01	0.48 ± 0.01	0.52 ± 0.01	<0.05	<0.05	NS

increased water content (wet-to-dry ratio, +93%, N=5, data not shown). Heart-to-body weight ratio was increased (HW/BW, +54%), due to a substantial enhancement of the RV mass (RV/HW, +43%), partially balanced by a decrease in the LV mass (LV/HW, -19%). Overall, RV contribution to HW was markedly increased (RV/(LV+IVS), +77%) (3.1). As shown in 3.1, RAN partially prevented RV hypertrophy. BW, lung water content and LV weight were unchanged by RAN.

During the 3 weeks of treatment none of 47 animals died in the CTRL group, 5 of 46 animals died in the MCT group and 6 of 50 animals died in the MCT-RAN group (p=0.05 for overall significance).

3.5.2 Cardiac structure and function in vivo

Heart rate (measured under sedation) was significantly lower in MCT than in CTRL rats; in MCT-RAN rats heart rate did not differ from that of CTRL rats (Table 3.2). In the MCT group, RV anatomical and functional parameters were indicative of free wall hypertrophy (wall thickness +95%, see Supplemental figure 3.13), cavity enlargement (basal diameter +27%) and systolic dysfunction (FAC -63% and TAPSE -30%). Moreover, the RV isovolumetric relaxation time (IVRT) was significantly prolonged (+155%). LV function was also altered in the MCT group. All LV volumes were reduced, probably due to IVS bulging toward the LV (see Online video 1 and 2); as a result, LV stroke volume (SV) and cardiac output (CO) decreased significantly (e.g. CO -49%). LV diastolic function was also impaired, as indicated by prolonged LV IVRT (+55%) and decreased E wave deceler-

Table 3.2: *In vivo* echocardiography

	CTRL (*N* = 15)	MCT (*N* = 13)	+RAN (*N* = 10)	*P*-value		
				MCT vs. CTRL	RAN vs. CTRL	RAN vs. MCT
Heart rate (bpm)	429 ± 15	346 ± 16	373 ± 27	<0.05	NS	NS
RV						
Wall thickness (mm)	0.39 ± 0.02	0.76 ± 0.03	0.56 ± 0.03	<0.05	<0.05	<0.05
Basal diameter (mm)	3.17 ± 0.1	4.03 ± 0.1	3.19 ± 0.2	<0.05	NS	<0.05
FAC (%)	68 ± 3	25 ± 4	38 ± 5	<0.05	<0.05	NS
TAPSE (mm)	4.0 ± 0.1	2.8 ± 0.2	3.1 ± 0.3	<0.05	<0.05	NS
IRT (ms)	14.8 ± 0.73	37.8 ± 0.73	31.6 ± 3.75	<0.05	<0.05	NS
LV						
EDV (μL)	319 ± 14	157 ± 10	193 ± 20	<0.05	<0.05	NS
ESV (μL)	55 ± 6	24 ± 2	21 ± 3	<0.05	<0.05	NS
SV (μL)	368 ± 22	230 ± 30	220 ± 30	<0.05	<0.05	NS
CO (mL/min)	155 ± 9	79 ± 11	88 ± 17	<0.05	<0.05	NS
EF (%)	82 ± 2	85 ± 1	90 ± 1	NS	<0.05	NS
IRT (ms)	20 ± 1	31 ± 4	30 ± 2	<0.05	NS	NS
DT (ms)	31 ± 2	23 ± 1	37 ± 3	<0.05	NS	<0.05

ation time (DT -28%). Despite the marked changes in LV geometry, the LV EF remained unchanged. RAN partially prevented RV wall hypertrophy (wall thickness) and completely prevented chamber enlargement (basal diameter) (Table 3.2). Indexes of RV systolic (FAC and TAPSE) and diastolic (IVRT) function were not significantly affected by RAN. Impairment of LV systolic function persisted in the RAN group. For what concerns LV diastolic function, RAN failed to affect the isovolumic phase (IVRT) but sharply prevented changes in diastolic filling (DT). This pattern is consistent with prevention of septal bulging by RAN (see Online video 3), likely to affect the filling phase more than the isovolumic one.

3.5.3 Fibrosis and cellular hypertrophy

Myocyte cross sectional area (CSA) and interstitial fractional collagen content were measured to assess the relative contribution of myocyte and interstitial remodeling to muscle hypertrophy. RV interstitial collagen content was increased in MCT group (+270% vs CTRL) (Figure 3.1A), and RAN almost prevented it. LV collagen content was similar in the three experimental groups. Myocyte CSA was increased in the RV free wall of the MCT group (+68%), it did not change in the LV free wall, but it was slightly reduced (-22%) in the IVS (Supplemental figure 3.14). RAN completely

prevented myocyte CSA enhancement in the RV and partially in the IVS (Supplemental figure 3.14). Electrical and molecular indexes of myocyte hypertrophy were also evaluated. In the MCT group C_m was increased in RV myocytes (+34%) but remained unchanged in LV ones (Figure 3.1B). RAN prevented RV C_m enhancement only partially, which contrasts with complete prevention of CSA changes. Discordant changes in CSA and C_m were also seen in LV myocytes, in which RAN reduced C_m but did not affect CSA (Figure 3.1B). In the MCT group, RV α-MHC expression decreased (-0.5 times) whereas β-MHC strongly increased (+13.8 times) (3.1C). A similar pattern was observed in the LV (α-MHC -0.76 times, β-MHC +27 times), thus suggesting MCT also caused remodeling of the LV. In the MCT-RAN group α-MHC down-regulation was completely prevented in RV only and β-MHC upregulation was blunted in the LV only. Thus, although RAN counteracted MCT-induced changes in MHC in both chambers, modulation of the isoform pattern differed between RV and LV.

3.5.4 T-tubules remodeling

Disarray of the T-tubular (TT) system has been described in several hypertrophy/failure models and was generally characterized by loss of the transverse component, alone or associated with an increment of the longitudinal one [19]. Furthermore, in the present study, changes in TT were suggested by the discrepancy between myocyte CSA and C_m changes (above). Thus, the TT pattern of the three experimental groups was analyzed in isolated ventricular myocytes of both chambers (3.2). A sharp pattern of transverse striations was observed in CTRL myocytes of both chambers; accordingly, in these myocytes, pixel variance was largely represented by the periodic component, whose period (0.5 μm^{-1}) was consistent with transverse TT arrangement. RV disarray of transverse TT was visually obvious in MCT myocytes; the power under the periodic component was decreased (-49%), accompanied by an increase of the aperiodic one (+83%). The former was decreased also in the LV (-29%), but no changes were detectable in the latter. RAN partially prevented the loss of the periodic component in RV myocytes only. Changes in the aperiodic component were com-

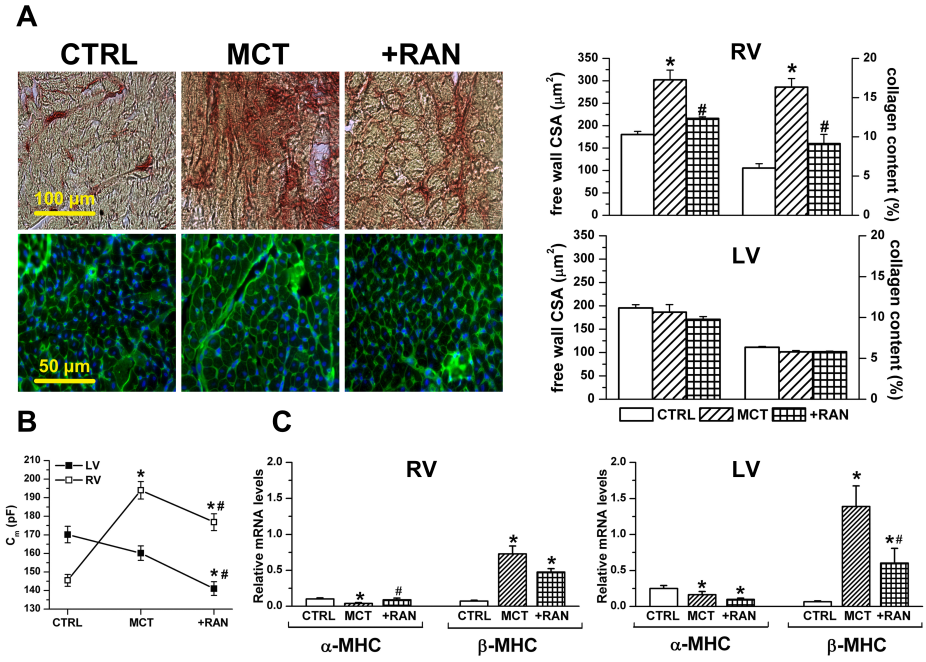

Figure 3.1: *Fibrosis and cellular hypertrophy.* A)Interstitial collagen content and myocytes CSA in each study group; comparison between RV and LV. Left: representative sections stained with 0.1% Sirius red (top) or AlexaFluor 488-conjugated wheat germ agglutinin (bottom) for collagen content and CSA measurements respectively. Right: average results for free wall CSA and collagen content. N = 5 for each group. B) membrane capacitance (C_m) in each experimental group. N >15 and n <117 for each group. C) Relative mRNA expression (vs GAPDH) of two cardiac hypertrophy-related genes (α- and β-MHC) in each study group by RTq-PCR. N >4 for each group. $*$ = p<.05 vs CTRL, # = p<0.05 vs MCT.

pletely prevented by RAN in both chambers. Overall, these results point to remodeling-induced loss of transverse TT, prevailing in the RV and effectively countered by RAN. Changes in the aperiodic component might reflect a tendency of RAN to minimize membrane structures not associated with transverse TT.

3.5.5 Remodelling of membrane currents and potential

Persistent Sodium current (I_{Na}) components were evaluated as TTX-sensitive current during slow depolarizing ramps (3.3). The "late" (I_{NaL}) and window (I_{NaW}) components were discriminated as detailed in the Methods section. MCT enhanced I_{NaL} in both chambers, but more prominently in RV myocytes (RV +149%, LV +93%). In the RV, I_{NaW} also showed an increment of borderline significance (p=0.05 vs CTRL). The contribution of the observed MCT-induced I_{NaL} enhancement to repolarization was assessed by APD measurement during acute RAN exposure (10 μmol/L). Acute RAN slightly but significantly shortened 50% APD repolarization (APD_{50}) (-6.1 $\pm$ 2.2%) in RV myocytes of the MCT group only (Supplemental figure 3.15).

RAN completely prevented I_{NaL} enhancement in both chambers. It should be stressed that RAN was completely washed out before I_{NaL} measurement; therefore, this observation indicates that chronic I_{NaL} blockade may prevent remodelling-induced, or ÒconstitutiveÓ enhancement of I_{NaL}. I_{NaL} enhancement is expected to induce Ca^{2+} overload, secondary to reduced forward operation of Na^+/Ca^{2+} exchanger (NCX). In RV MCT myocytes, $[Ca]_{diast}$ and $[Ca]_T$ were increased (+15% and +39% respectively), but $[Ca]_{SR}$ was unchanged, thus yielding a larger fractional release (+53%). In LV myocytes, Ca^{2+} handling was markedly depressed; $[Ca]_T$ and $[Ca]_{SR}$ were both reduced (-31% and -38% respectively), but fractional release was still increased (+38%); $[Ca]_{diast}$ was not significantly affected (Figure 3.4A). RAN blunted $[Ca]_{diast}$ and $[Ca]_T$ enhancement in RV myocytes; however, fractional release remained significantly higher than in CTRL myocytes. In LV myocytes, MCT- induced Ca^{2+} handling abnormalities were not affected by RAN (Figure 3.4A). Intracellular

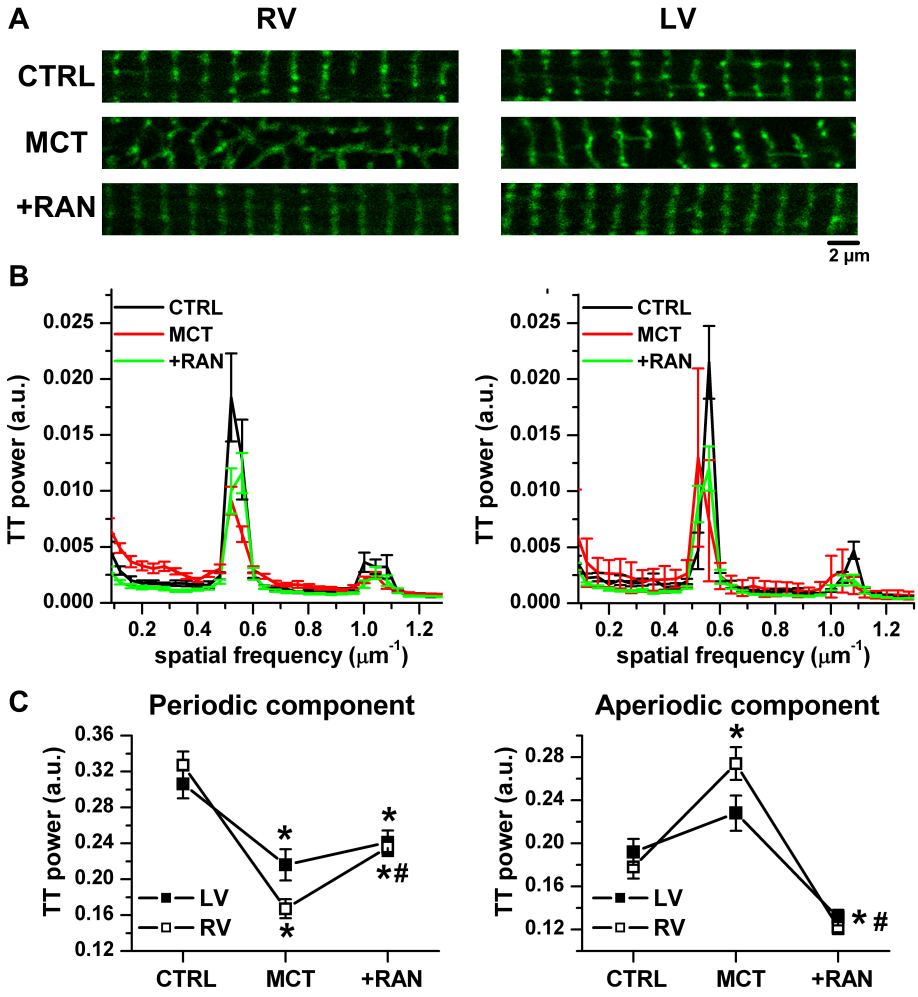

Figure 3.2: *T-Tubules (TT) remodeling* A) Confocal images of di-3-ANEPPDHQ (20 μmol/L) loaded myocytes; regions of interest of 100 pxls x 500 pxls are shown. B) Mean power spectrum of TT obtained in each experimental group. C) Average results of periodic and aperiodic components of TT. $*$ = p $<$0.05 vs CTRL, # = p $<$0.05 vs MCT. N $>$2 and $\geq$ 9 for each group.

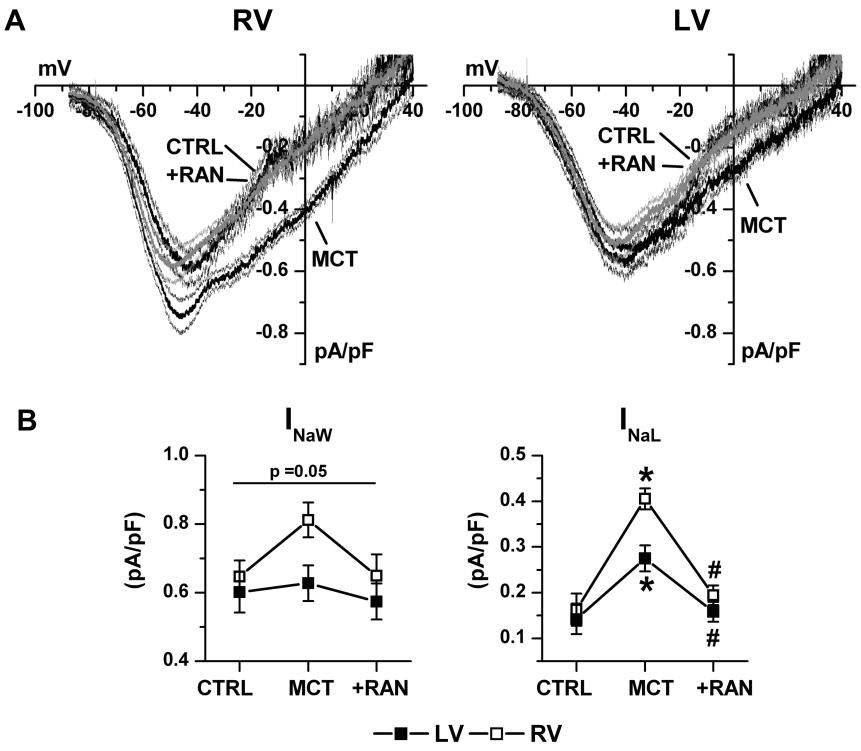

Figure 3.3: *Persistent I_{Na} components.* A) TTX-sensitive current (I_{TTX}, 30 μmol/L) activated during slow voltage ramps (56 mV/s) in each experimental group. Mean traces and confidence intervals are shown. B) average results of I_{NaW} (evaluated as peak I_{TTX}) and I_{NaL} (evaluated as current activated at 0 mV). N >3 and n >13 for each group. $*$ = p <0.05 vs CTRL, # = p<0.05 vs MCT.

Ca^{2+} overload may lead to spontaneous Ca^{2+} release from the SR; this may occur because of SR overload or, even in the presence of reduced SR Ca^{2+} content, by RyRs destabilization. Propensity to spontaneous Ca^{2+} release was evaluated by measuring the proportion of cells with delayed after-depolarizations (DADs, Figure 3.4B). In RV myocytes the increase in DADs incidence induced by MCT did not achieve significance; nevertheless, DADs incidence was significantly lower in the RAN treated group than in the MCT one. Unexpectedly, MCT-induced increment in DADs incidence was more consistent in LV myocytes, but, unlike in the RV, it was not prevented by RAN. Increments in intracellular Ca^{2+} and, in particular in fractional release, might suggest upregulation of I_{CaL} in the MCT group. However, in this group, I_{CaL} properties (Supplemental figure 3.16 and Table 3.5), including inactivation kinetics (Table 3.6), remained unchanged in RV myocytes, and only a small reduction of peak density was observed in LV myocytes (Figure 3.4C). RAN failed to affect I_{CaL} in myocytes from both chambers. I_{NaL} enhancement is expected to prolong repolarization, particularly at the plateau level (APD_{50}). In the MCT group, RV APD was prolonged and the APD_{50}/90% APD repolarization (APD_{90}) ratio was increased (+33%), to indicate that prolongation prevailed at plateau level. LV APD was also prolonged, but changes in APD_{50}/APD_{90} ratio did not achieve significance (Figure 3.5). Because of these changes, physiological APD differences between RV and LV were minimized in the MCT group.

Notably the dispersion of APD values, expressed as coefficient of variation (CV), was increased in the MCT group, particularly in RV myocytes. This observation led to evaluate the distribution of APD values. In the RV, MCT broadened the originally unimodal APD distribution and added a cluster of very long APD values. In LV myocytes, APD distribution was originally bimodal. Under MCT all LV APD values were clustered under a single larger mode (Figure 3.5A). Unexpectedly, RAN failed to prevent mean APD prolongation by MCT (Figure 3.5B). Nevertheless, consistent with a reduction of I_{NaL} contribution, RAN prevented the increase in APD_{50}/APD_{90} induced by MCT in the RV. Furthermore, in the RAN group APD distributions were restored to their control shape and very

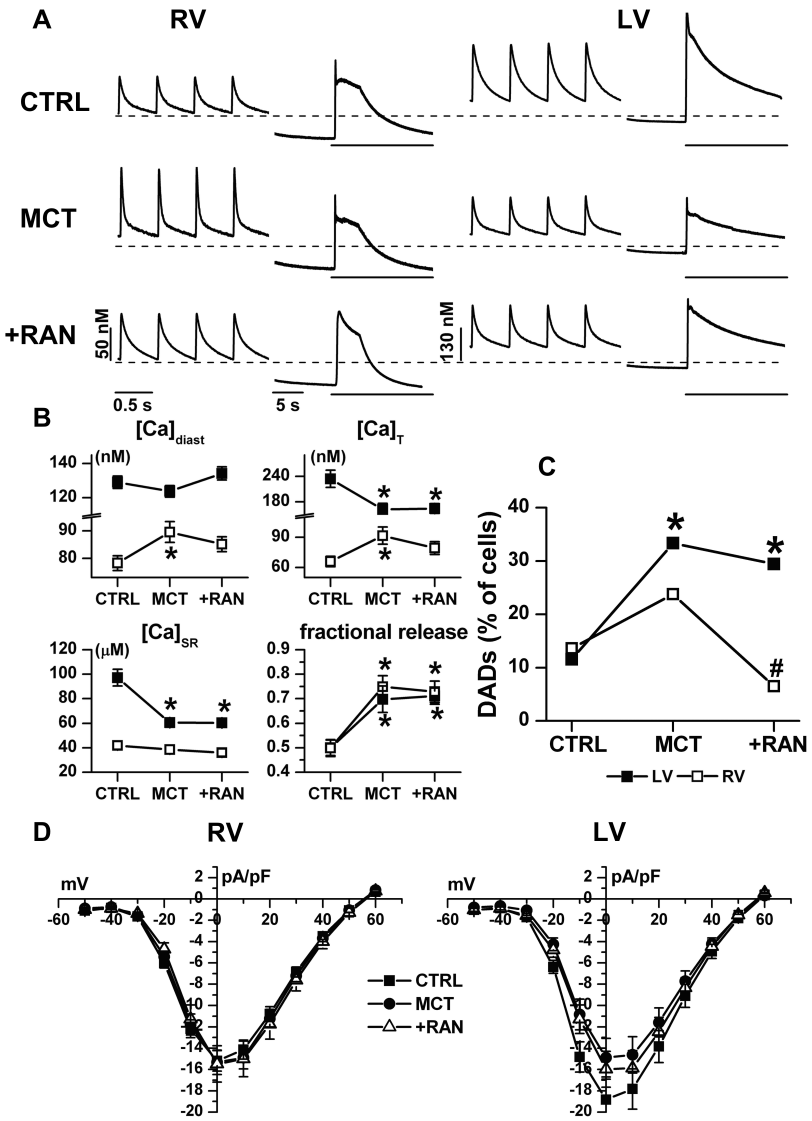

Figure 3.4: *Intracellular Ca^{2+}handling and I_{CaL}.* A) Steady-state Ca^{2+} transients evocated in field-stimulated myocytes (2 Hz) and during caffeine superfusion (shown by horizontal bars) (see protocol in Supplemental figure 3.11). Fluorescence signals were converted in free cytosolic Ca^{2+} (Supplemental figure 3.12); dotted lines refer to RV diastolic Ca^{2+} ($[Ca]_{diast}$) of the CTRL group (about 80 nM) to highlight intergroup changes. B) Statistics for $[Ca]_{diast}$, amplitude of Ca^{2+} transient amplitude (Ca_T), SR Ca^{2+} content (Ca_{SR}) and fractional release. N $\geq$ 3 and n $\geq$ 21 for each group. C) proportion of cells with delayed afterdepolarizations (DADs) in patch-clamped myocytes paced at 2 Hz. D) I_{CaL} I/V relationships in each experimental group. N $\geq$ 3 and n $\geq$ 11 for each group. $*$ = p$<$0.05 vs CTRL, # = p$<$0.05 vs MCT.

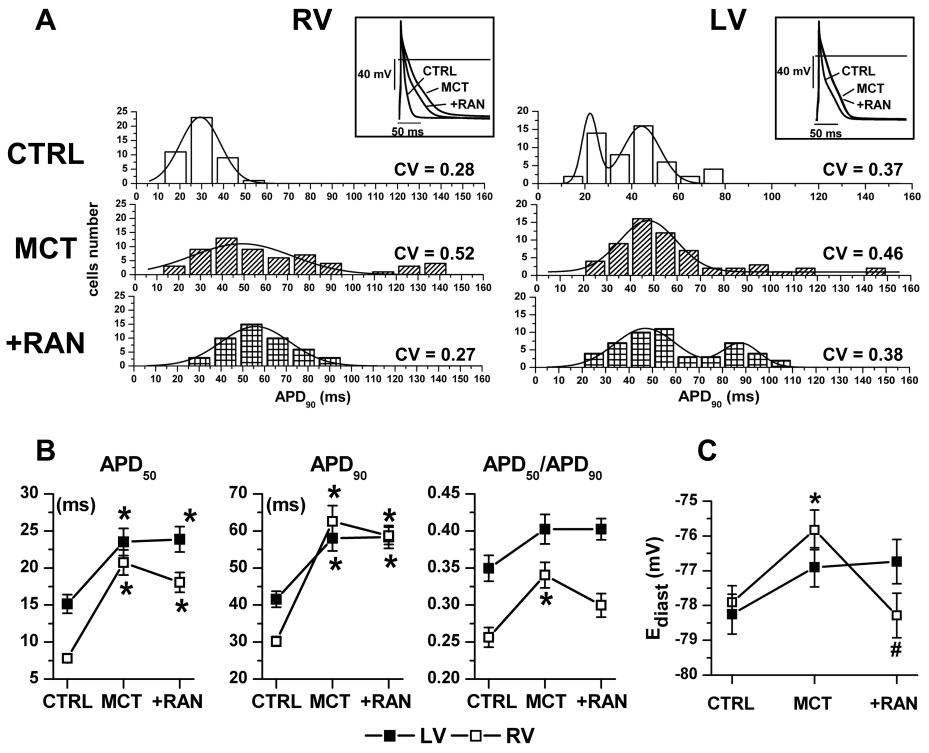

Figure 3.5: *Electrical remodeling.* A) APD_{90} distribution and its coefficient of variation (CV) in RV (left panel) and LV (right panel) myocytes of each experimental group; two or one cell populations are unveiled by Gaussian fit (black line). Representative action potentials are shown in the insets. B) Statistics for APD_{50}, APD_{90} and their ratio. C) Statistics for E_{diast}. $*$ = p<0.05 vs CTRL, # = p<0.05 vs MCT. N $\geq$ 9 and n $\geq$ 44 for each group.

long APD values were absent (Figure 3.5A). Overall, in the RAN group, albeit clustered around a higher mean, APD values were less dispersed, as reflected by the lower CV. E_{diast} was only marginally depolarized in the MCT group and in the RV only (-2 mV; $p<0.05$, Figure 3.5C); nonetheless, AP amplitude and dV/dtmax remained unchanged. The change in E_{diast} was prevented by RAN. Modulation of K^+ currents might contribute to MCT-induced changes in the AP. In the MCT group, I_{K1} conductance was reduced in RV myocytes only (-48.7%), without changes in the rectification pattern (Fig 6A). Unlike the change in E_{diast}, I_{K1} down-regulation was not prevented by RAN (Figure 3.6A).

MCT decreased I_{to} density in both chambers (Figure 3.5B), but more in RV than in LV myocytes (-46% vs -28% at +40 mV); thus, MCT minimized physiological chamber difference in I_{to}. Neither the relative weight of fast and slow I_{to} components, nor their time-constants were significantly changed by MCT (Table 3.7); thus, MCT did not affect I_{to} kinetics. RAN partially opposed I_{to} downregulation in the RV (Fig 6B) and accelerated inactivation slow component (τ_{slow} -27% vs CTRL, Table 3.7), thus further limiting the impact of I_{to} on APD. Qualitatively similar effects were observed in LV myocytes, where prevention of I_{to} downregulation by RAN was complete (Figure 3.5B).

3.5.6 Pulmonary vascular resistance and structural remodeling

To assess if mechanical unloading might contribute to RAN effects on ventricular remodeling, right ventricular systolic pressure (RVSP) was measured through right jugular vein catheterization (Figure 3.7A). RVSP was significantly increased in MCT rats (+45% vs CTRL). In the RAN group RSVP did not differ from control values. To provide preliminary information on the mechanism accounting for RAN prevention of MCT-induced increment in RVSP, small pulmonary artery wall thickness (SPAWT) was measured. As shown in Figure 3.7B, relative medial SPAWT was increased in the MCT group (+20%), a change prevented by RAN.

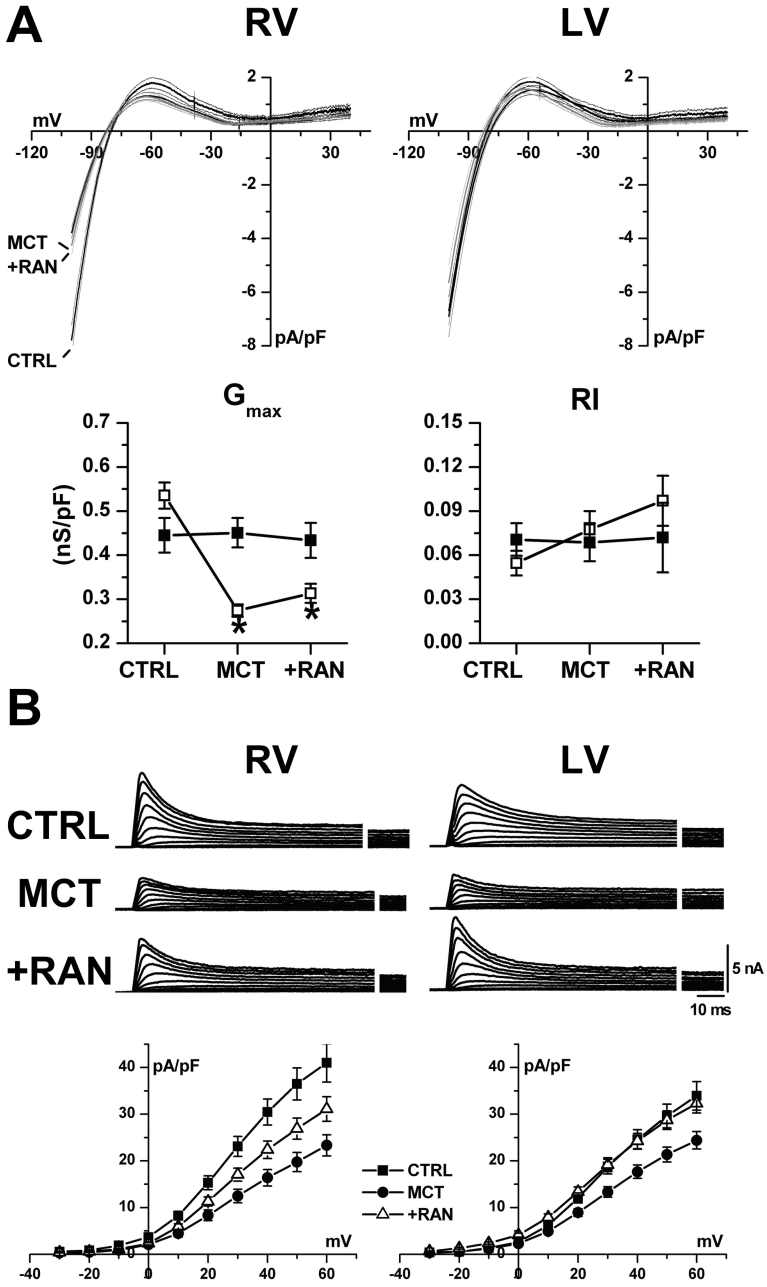

Figure 3.6: *K^+ currents down-regulation.* A) K^+ free-sensitive current (I_{K1}) activated during slow voltage ramps (56 mV/s); mean traces and confidence intervals are shown. Statistics for I_{K1} maximal conductance (G_{max}) and rectification index (RI) between 0 and -100 mV are shown. N $\geq$ 3 and n $\geq$ 14 for each group. $*$ = p<0.05 vs CTRL. B) I_{to} I/V relationships. N $\geq$ 4 and n $\geq$ 14 for each group.

3.6 Discussion

MCT-induced PAH caused substantial hypertrophy and fibrosis of the RV. Cellular structural remodelling consisted of a large increased CSA, associated with a smaller C_m increment, likely mitigated by a substantial loss of transverse TT. All structural aspects of RV structural remodelling, including fibrosis, myocyte hypertrophy and TT disarray, were countered by RAN treatment. Consistent with previous studies [13][2][9], also the LV was affected by PAH, possibly because of altered inter-ventricular interaction resulting from RV prevalence. LV abnormalities were, under many aspects, opposite to those of the RV. Loss of LV mass occurred without changes in collagen content or myocyte size. PAH has been recently reported to increase apoptosis in the LV [9], which might account for the present findings. Structural remodelling was associated with bradycardia, loss of body weight and cardiac output. This, together with the presence of initial chamber dilation, suggests that MCT-induced changes was approaching the decompensation stage.

3.6.1 Right ventricle remodeling

MCT significantly increased I_{NaL}, particularly in the pressure-overloaded RV. I_{NaL} enhancement has been extensively described as a consequence of LV remodelling. It may prolong repolarization, perturb Ca^{2+} homeostasis and thus contribute to evolution of the remodelling process 8;10. I_{NaL} enhancement may cause Ca^{2+} overload by reducing the driving force for Ca^{2+} extrusion through NCX. The significant I_{NaL} enhancement observed in the RV was associated with increased $[Ca]_{diast}$ as expected, however $[Ca]_{SR}$ was unchanged. Moreover $[Ca]_T$ was increased in spite of unchanged I_{CaL}, thus indicating a larger fractional release. Altogether, this points to facilitation of RyRs opening, which may dominate to set Ca^{2+} dynamics at this stage [5]. This pattern might represent the evolution from an initial condition of true Ca^{2+} overload, followed by Ca^{2+} -mediated activation of RyRs-destabilizing pathways (e.g. CaMKII) [10]. RyRs destabilization is also consistent with the appearance of DADs. Overall, the observed

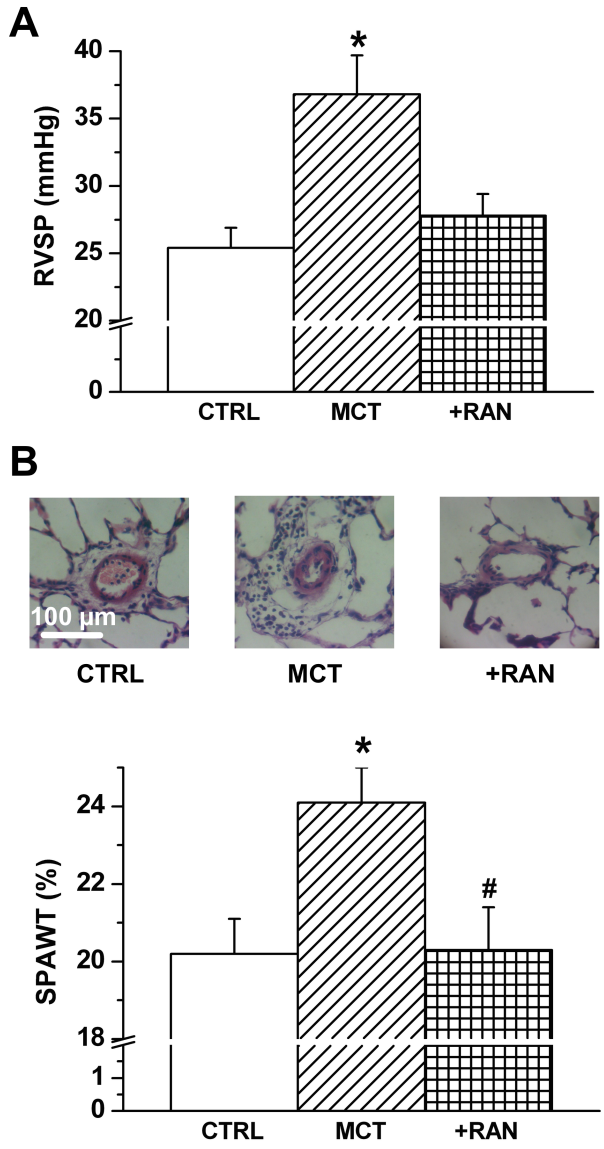

Figure 3.7: *Pulmonary vascular remodeling.* A) Statistics for right ventricular systolic pressure (RVSP) estimated through invasive right heart catheterization. N $\geq$ 5 for each group. B) Examples of hematoxylin/eosin stained lung sections and statistics for small pulmonary arterioles wall thickness (SPAWT) measurements. N $\geq$ 9 for each group. $*$ = p$<$0.05 vs CTRL, # = p$<$0.05 vs MCT.

changes in Ca^{2+} handling are such as to provide partial compensation to the increased mechanical load, but also to account for the deterioration of diastolic function. RAN completely abrogated I_{NaL} enhancement. As the drug was absent when I_{NaL} was measured, this implies that I_{NaL} blockade may prevent initiation of a remodelling loop leading to a constitutive abnormality of Na^+ channel inactivation [40]. RAN countered MCT-induced increments of $[Ca]_{diast}$ and $[Ca]_T$; thus suggesting that they were at least partially dependent on I_{NaL} enhancement. RAN also prevented MCT-induced TT disarray and this may contribute to its effect on Ca^{2+} handling [19];[36]. RAN efficacy in preventing overload-induced changes in TT organization has been recently reported [1]. RAN action on TT organization may be relevant to modulation of long term response to increased load and its mechanism deserves further investigation. RAN abolished DADs in the RV but not in the LV and this correlates with the extent of I_{NaL} enhancement in the two chambers. Thus, albeit I_{NaL} enhancement likely contributed to DADs generation in the RV, I_{NaL} independent mechanisms must be postulated for the LV. MCT increased APD and its dispersion. This is consistent with the observed down-regulation of outward currents (I_{to} and I_{K1}) and enhancement of I_{NaL}, whose direct contribution to APD became significant (Supplemental figure 3.15). RAN completely prevented I_{NaL} enhancement, partially opposed I_{to} downregulation, but failed to prevent reduction of I_{K1} conductance. APD distributions reveal that RAN prevented extremely long APDs, as expected from I_{NaL} normalization; in spite of this, mean APD was still prolonged in the RAN group, potentially contributing to the residual excess of Ca^{2+} content. This is consistent with failure of RAN to shorten QTc in a previous study on overload-induced RV remodelling [12]. This requires to postulate an additional factor delaying repolarization in the RAN group whose nature remains unclear. Indeed, RAN was absent during measurements, thus making its ancillary IKr blockade [3] irrelevant to the present measurements. Upstroke velocity (dV/dtmax) was unchanged, thus suggesting that Na^+ current enhancement was limited to its steady-state component. Previous works in MCT-induced PAH reported normal RV SCN5A tran-

script 5 and transient sodium current (I_{NaT}) density [13], but shifts of the activation curve suitable to increase I_{NaW} [13]. RAN significantly countered the development of RV hypertrophy both at the organ and cellular levels. This finding is similar to what recently reported in a pulmonary artery banding model [12]. In the latter study, RAN and trimetazidine were found to inhibit FAO and their anti-remodelling effect was attributed to this metabolic action. Concomitance with either I_{NaL} inhibition (present data), or switch in substrate utilization [12] is of course inadequate to establish which mechanism may prevail in RAN anti-remodelling effect. More conclusive in this respect are the findings of Wang et al. [37] who reported that functional recovery during reperfusion, while improved by RAN, was insensitive to FAO inhibition by a selective and more powerful agent. Even similarity between RAN and trimetazidine effects is not conclusive for a "metabolic" mechanism in prevention of RV remodelling. Indeed, trimetazidine was found to improve function in hypertrophied hearts without inhibiting FAO utilization [33]. On the other hand, improvement of cell energy balance and mitochondrial function may also be expected from I_{NaL} inhibition [20]. Notably, in the present study, prevention of hypertrophy and Ca^{2+} dynamics abnormalities by RAN was not associated with significant changes in echocardiographic indexes of RV systolic and diastolic function, which showed only "trends" toward improvement (FAC, TAPSE, IVRT in Table 3.2). This contrasts with a significant improvement in cardiac index and exercise capacity reported by Fang et al [12]. While differences in the experimental model (proximal arterial banding vs microvascular constriction) might account for this discrepancy, the objective difficulty in echocardiographic assessment of RV dynamics in small animals should also be considered.

3.6.2 Left ventricle remodeling

LV output was markedly reduced because of matching decreases in systolic and diastolic volumes, with preserved EF. This "restrictive" pattern likely reflected distortion of LV geometry secondary to RV hypertrophy and increased RV pressures (IVS bulging); nevertheless, intrinsic LV myocyte

function was also altered. I_{NaL} enhancement, although still significant, was less prominent in the LV, possibly explaining why myocyte Ca^{2+} content was more depressed than in the RV. TT disarray was present, but less obvious than in RV myocytes. Overall, changes in Ca^{2+} handling point to decreased cell Ca^{2+} content, which was nonetheless associated with DADs occurrence to suggest marked RyRs instability. In the LV of MCT myocytes APD changes were similar to those observed in the RV, but less prominent. Notably, APD distribution became unimodal due to loss of the lower cluster; since I_{to} expression underlies transmural differences in LV repolarization, this might be related to I_{to} down-regulation. According to recent reports the latter occurs at transcriptional level in PAH 5. At variance with the RV, I_{K1} was unaffected in the LV. RAN completely prevented I_{NaL} enhancement and I_{to} down-regulation, but, as occurred in the RV, it did not affect average APD (Figure 3.5). Nevertheless, RAN abolished very long APDs and reinstated the physiological bimodal distribution of APD, consistent with prevention of I_{to} down-regulation. RAN failed to affect Ca^{2+} handling abnormalities in the LV, which may be interpreted in light of the smaller extent of I_{NaL} enhancement in this chamber.

3.6.3 Pulmonary resistance and microvascular remodelling

MCT expectedly increased pulmonary vascular resistance. As reported in previous studies [35][25], medial thickening occurred in small pulmonary arteries, thus providing a structural mechanism for the increase in resistance. MCT also induced pulmonary edema, to suggest increased capillary permeability. RAN partially prevented the increase in RVSP; this was associated with less arteriolar thickening, thus suggesting a structural basis for this hemodynamic effect. Nevertheless, although failing to affect systemic vascular resistance to a significant extent, RAN has been recently reported to exert relaxing effect on vascular preparations [11][28]; thus, the contribution of functional pulmonary vasodilatation cannot be ruled out. RAN failed to affect pulmonary edema. Concerning the possibility that I_{NaL} blockade might account for RAN effect on pulmonary vasculature, only conjectures are possible thus far. Recent studies indicate that

TTX-sensitive voltage-gated Na^+ channels isoforms are expressed in human pulmonary artery smooth muscle cells (PASMC) and are blocked by RAN 27. Although their physiological role remains unresolved, their expression is enhanced in pathological states [15] [29]. Moreover, a recent cDNA microarray study found SCN1B (the Na^+ channel $\beta 1$ subunit) transcript increased in lung tissue from patients with PAH [7]. Several studies suggest that PASM remodelling is related to intracellular Ca^{2+} overload and reactive oxygen species signaling [17], components of the vicious circle supporting I_{NaL} enhancement in tissue remodeling. Thus, a role of I_{NaL} inhibition in RAN effect on pulmonary vasculature can be envisioned.

3.6.4 Study limitations

The finding of RVSP modulation raises the possibility that mechanical unloading of the RV may underlie prevention of cardiac remodelling by RAN. While this possibility cannot be ruled out, it seems unlikely that unloading may represent the sole mechanism underlying the effects of RAN. Indeed, whereas the prevention of pulmonary vascular resistance enhancement was incomplete, drug-induced changes in myocardial structure and function were rather dramatic at the organ, tissue and myocyte levels. Moreover, RAN anti-remodelling effect has been previously reported in a fixed load model [12]. Although demonstrating that I_{NaL} enhancement is part of PAH induced remodelling, the present results do not allow to discriminate between I_{NaL} blockade and FAO inhibition as the mechanism underlying anti-remodelling effect of RAN. Based on the work of Wang et al [12], we consider FAO inhibition an unlikely mechanism; nevertheless, evaluation of I_{NaL} blockade by agents devoid of effect on FAO [34] may be required to solve the controversy on this issue.

3.7 Conclusion and implications

The present observations point to a role of I_{NaL} enhancement in the maladaptive cardiac response to PAH and, unexpectedly, in the development of PAH itself. Taking this to justify the expectation of a benefit from

I_{NaL} blockade in human PAH requires caution. The first consideration, which applies to RAN effect at the pulmonary level, concerns the relevance of MCT-induced damage to human PAH. Furthermore, although countering myocardial structural remodelling, RAN was less effective in preventing cardiac function derangement. While this might depend on the extent of cardiac damage, substantial in the present model, a potentially compensatory role of I_{NaL} enhancement should also be considered. Furthermore, RAN was administered shortly after MCT administration; thus, the present results are relevant to prevention only. Specifically designed studies are required to evaluate the efficacy of I_{NaL} blockade in reversing PAH consequences and to weigh the long-term balance between benefits and drawbacks.

3.8 Fundings

This work was supported by a grant from Gilead Sciences, Inc. (Foster City, CA) and NEDD (Network Enabled Drug Design) funding to A. Zaza.

3.9 Acknowledgements

We thank Dr Luiz Belardinelli and Dr John T. Liles (Gilead Sciences) for insightful comments on the manuscript.

3.10 Conflict of interests

Gilead Sciences Inc (Foster City, CA) is patent holder for ranolazine.

3.11 Supplemental material

The investigation conforms to the Guide of the Care and Use of Laboratory Animals published by the US National Institutes of Health (NIH publication No. 85-23, revised 1996) and to the guidelines for animal care endorsed by the hosting institution.

3.11.1 Experimental procedures

Adult Sprague Dawley rats (110 gr) were injected intraperitoneally with 2% monocrotaline (MCT) solution at a dose of 60 mg/Kg (MCT group). A subset of MCT rats were treated b.i.d. intraperitoneally with ranolazine (RAN 30 mg/Kg) for 20 days (MCT-RAN group). Littermate untreated animals (CTRL group) and MCT rats received b.i.d. intraperitoneally the vehicle of RAN solution for the same period. Rats were weighed weekly to adjust drug (or vehicle) dose administration to animal growth. To achieve age uniformity, littermates accurately matched for weight were randomly assigned to the different treatment groups. MCT (Sigma-Aldrich) was dissolved in 1N HCl, neutralized with 4N NaOH, buffered to pH 7.35 and diluted with 0.9% saline to achieve a final concentration of 20 mg/ml. Blood samples were collected from each rat at the moment of the sacrifice to measure the hematocrit by centrifugation in heparinized capillaries. Heart (HW) and lung (LW) weights were measured after careful dissection from surrounding tissues. The LV, including the interventricular septum (IVS), was then dissected from the right ventricle (RV) and the two chambers were weighed separately. To estimate lung water content, in a subset of animals lungs were weighed immediately after dissection (wet weight) and after drying in a stove (70 °C for 72h). Cardiac histology, fibrosis and quantitative RT-PCR measurements were performed from portions of the same RV and LV maintained in liquid nitrogen until use. Heart and lung samples for histological staining were fixed in 4% paraformaldehyde before paraffin embedding. All patch-clamp and epifluorescence experiments were performed at 36.5 °C

3.11.2 Echocardiography

Transthoracic echocardiography was performed (ALOKA SSD-5500, Tokyo, Japan) on sedated rats (ketamine 80 mg/kg and midazolam 2.5 mg/kg BW i.p.) using a 13 MHz linear transducer at high frame rate imaging (102 Hz) and a 7.5 MHz phased array probe for pulsed-wave and continuous Doppler measurements. RV wall thickness was measured in M-mode during diastole

from the parasternal long axis view; the 2D apical four-chamber view was used to assess basal RV end-diastolic diameter. In the 2D apical four chamber view, the endocardial borders from RV end-diastolic area (RVEDA) an end-systolic area (RVESA) were traced manually and the fractional area change (FAC) was calculated as: (RVEDA-RVESA)/(RVEDA)∗100. The RV base-to-apex shortening during systole was measured as the systolic displacement of the lateral portion of the tricuspid annular plane systolic excursion (TAPSE). TAPSE was recorded as M-mode traces under 2D echocardiographic guidance [31]. RV diastolic function was evaluated using pulsed wave Tissue Doppler Imaging, obtained at the junction between the tricuspidalic annulus and the RV lateral wall. Then the isovolumetric relaxation time (IVRT) was calculated [14]. LV volumes (end diastolic volume EDV, end systolic volume ESV) and LV ejection fraction (EF) were calculated by the modified simple plane Simpson's rule from the parasternal long-axis view as previously reported [22].The long-axis and 4 and 5 apical chamber views were used for 2D and color flow imaging and spectral Doppler interrogation of the mitral valve and/or aortic outflow tract. LV stroke volume (SV), cardiac output (CO), and diastolic function parameters were obtained and calculated according to the recommendations from the American Society of Echocardiography [30][27]. All Doppler spectra were recorded for 5Ð10 cardiac cycles at a sweep speed of 100 mm/s. The color Doppler preset was at a Nyquist limit of 0.44 m/s. Echocardiographic recordings were saved on magneto-optic disk for off-line analysis by a sonographer, blind to study groups.

3.11.3 Quantitative RT-PCR

Relative expression of mRNAs encoding α- and β-myosin heavy chain (MHC) was measured by RTq-PCR in RV and LV of each experimental group as previously described [38]. Briefly, total RNA was extracted from homogenates of each ventricle by subsequent centrifugations and its concentration and purity was determined as the 260/280 nm ratio (NanoDrop Thermo Scientific). One microgram of each RNA sample was reverse transcribed to cDNA using the 5X iScriptcDNA Synthesis Kit system

(Bio-Rad Laboratories, Hercules, United States). The amplification reaction was performed with SSoFastEvaGreen(Bio-Rad Laboratories, Hercules, United States) and specific primers (Table 3.3) designed using NCBI Primer3-Blast [38]. Signal detection and analyses of results were performed using ABI Prism 7700 Sequence Detection System software (v1.6). Relative quantification was achieved with the comparative ΔCt method [18] by normalization for GAPDH or RPL29 (data not shown). All samples were amplified in triplicate from the same RNA preparation and the mean value was computed.

3.11.4 Cardiac histology

Interstitial collagen was assessed in 0.1% Sirius red-stained RV (or LV) 10 μm paraffin sections; the resulting image was processed on the Kontron KS300 image-analysis system (Kontron-Zeiss). The content of interstitial collagen (expressed as the fractional area of the entire cross section) was averaged on nine fields selected across the wall thickness in the IVS and free wall. The nature of the Sirius red-stained collagen deposit was confirmed by examining the sections under a microscope fitted with a linear cross-polarizing filter that renders collagen fibers birefringent [23]. Cardiomyocyte cross sectional area (CSA) was measured by staining plasma membranes with AlexaFluor 488-conjugated wheat germ agglutinin in 10 μm paraffin included sections. Nuclei were counterstained with bisbenzimide; CSA analysis was performed from at least 50 cardiomyocytes in each section (Analyzer IBAS 2.0, Kontron/Zeiss image analysis system) [42].

3.11.5 Patch-clamp measurements

Ventricular myocytes were voltage-clamped in the whole-cell configuration (Multiclamp 700B, Axon Instruments). membrane capacitance (C_m) and series resistance were measured in every cell and compensated to 90% before the transient outward current (I_{to}) and the L-type calcium current (I_{CaL}) measurements; the estimated voltage error was $<$5 mV in all

cases. Traces acquisition and analysis was controlled by dedicated software (Axon pClamp 10). During patch-clamp measurements myocytes were superfused at 2 ml/min with Tyrode solution containing (mmol/L) 154 NaCl, 4 KCl, 2 $CaCl_2$, 1 $MgCl_2$, 5 HEPES-NaOH, 5.5 D-glucose, adjusted to pH 7.35. The pipette solution contained (mmol/L) 110 K^+-aspartate, 23 KCl, 0.4 $CaCl_2$ (calculated free-$Ca^{2+} = 10^{-7}$ mol/L), 3 $MgCl_2$, 5 HEPES KOH, 1 EGTA KOH, 0.4 GTP-Na salt, 5 ATP-Na salt, 5 creatine phosphate Na^+ salt, pH 7.3. A thermostated manifold, allowing for fast (electronically timed) solution switch, was used for cell superfusion. I_{NaL} was evaluated as TTX-sensitive current (I_{TTX}) activated during slow voltage ramps (56 mV/s). I_{TTX} at 0 mV was taken as representative of I_{NaL} and peak I_{TTX} value, occurring at more negative potentials (-34 ± 2 mV), was assumed to reflect the I_{Na}. This was supported by results shown in Supplemental figures 3.8 and 3.9. The inward rectifier potassium current (I_{K1}) was evaluated following superfusion of K^+ free solution [39] during slow voltage ramps (56 mV/s) from -100 mV to +40 mV (Hp -100 mV). Maximal inward conductance (G_{max}) of I_{K1} was evaluated by linear fitting of the current activated at negative membrane potentials; I_{K1} rectification index (RI) was calculated as the ratio between current activated at -100 mV and 0 mV. To isolate I_{to}, cadmium (0.5 mmol/L) and EGTA (5 mmol/L) were added to extracellular and intracellular solutions respectively. I_{to} I/V relation was estimated measuring the transient outward component (see Supplemental figure 3.10) activated during depolarizing voltage steps from a holding potential of -80 mV; a brief step to -40 mV was applied to inactivate I_{Na}. I_{to} inactivation kinetics were extrapolated by fitting the current activated at +40 mV with a biexponential function. To measure I_{CaL}, Na^+- and K^+-free extracellular solution was used, containing (mmol/L): 130 NMDGCl, 20 TEACl, 1.8 $CaCl_2$, 0.5 $MgCl_2$, 5 HEPES, 5.5 glucose, pH 7.35. The internal pipette solution contained (mmol/L): 115 CsCl, 20 TEACl, 0.5 F_0MgCl_2, 10 EGTA, 5 HEPES, 0.4 GTP-tris salt, 5 ATP-Mg^{2+} salt, 5 creatine phosphate-tris salt, pH 7.3. I_{CaL} I/V relations were obtained by measuring activated current at different test potentials (300 ms) from a holding potential of -40 mV; steady state activation curves

were derived from each I/V relation. Steady-state inactivation curves were obtained by measuring the current activated at 0 mV after preconditioning voltage steps (2 sec) from -50 to 0 mV and normalizing it to the maximal current. Activation and inactivation curves were described by fitting experimental points with the Boltzmann equation to estimate the voltages of half-maximal activation and inactivation ($V_{0.5}$) and each slope^{-1} factor (k). The amplitude of window current (I_{CaLW}) was estimated as the overlapping area under the activation and inactivation curves between -50 mV and 0 mV and expressed as arbitrary units (a.u.). I_{CaL} inactivation kinetics were obtained by fitting the current activated at 0 mV with a biexponential function.

3.11.6 Calcium handling

Myocytes were incubated in Tyrode solution for 45 min with the membrane-permeant form of the dye, Fluo4-AM (10 mol/L), and then washed for 30 min to allow de-esterification. Fluo4 emission was collected through a 535 nm band pass filter, converted to voltage, low-pass filtered (200 Hz) and digitized at 2 kHz after further low-pass digital filtering (FFT, 100 Hz). Fluo4 loaded intact myocytes were field-stimulated at 2 Hz during superfusion with Tyrode solution. Stimulation was then discontinued and SR Ca^{2+} content (Ca_{SR}) was estimated after 10s by an electronically timed 10 mmol/L caffeine pulse. Fluorescence decay before caffeine application was used as reference (F_0) for signal normalization (F/F_0) after subtraction of background luminescence (Supplemental figure 3.11).

3.11.7 Fluo4 signal calibration

The experimental protocol (Supplemental figure Figure 3.11) used in the study was applied in a separate set of RV (n = 10) and LV (n = 12) myocytes of the CTRL group. Fluorescence recorded during quiescence (after the loading train) was adopted as F_0 and converted to $[Ca]_0$ according to Eq 1:

$$[Ca]_0 = \frac{K_d * F_0}{F_{max} - F_0} \tag{3.1}$$

assuming a dye Ca^{2+} dissociation constant (Kd) = 400 nmol/L. Maximum fluorescence (Fmax) was measured in the presence of 5 mmol/L Ca^{2+} after cell permeabilization with the Ca^{2+} ionophore (10 μmol/L A23187); the uncouplers carbonyl cyanide 3-chlorophenylhydrazone (5 μmol/L CCCP) and rotenone (2 μmol/L) were added to extracellular solution to block ATP synthesis (see example in Supplemental figure 3.12). Average $[Ca]_0$ value was smaller in RV myocytes than in LV myocytes (44 ± 2 nmol/L vs 60 ± 5.9 nmol/L, $p<0.05$). In each experiment F/F_0 was converted to free Ca^{2+} concentration ($[Ca]_f$) by:

$$[Ca]_f = \frac{\frac{F}{F_0} * K_d}{\frac{K_d}{[Ca]_0} - \frac{F}{F_0} + 1} \tag{3.2}$$

assuming $[Ca]_0$ equal to 45 nmol/L and 60 nmol/L in RV and LV myocytes respectively. Total SR Ca^{2+} content (Ca_{SR}) was estimated, according to published parameters of Ca^{2+} binding to intracellular buffers (B_{max} = 272 μmol/L; Kd = 0.673 μmol/L) 11, by:

$$[Ca]_{SR} = \frac{B_{max}}{1 + \frac{K_d}{[Ca]_f}} + [Ca]_f \tag{3.3}$$

3.11.8 T-Tubules analysis

Sarcolemmal membranes were stained by incubating isolated ventricular myocytes with 20 μmol/L di-3-ANEPPDHQ (Life Technologies, Carlsbad, United States) 12 dissolved in high K^+ solution (in mmol/L: 40 KCl, 3 $MgCl_2$, 70 KOH, 20 KH2PO4, 0.5 EGTA, 50 L-Glutamic acid, 20 Taurine, 10 HEPES, 10 Glucose, pH 7.4) for 10 min at room temperature. The excitation-contraction uncoupler blebbistatin (17 μmol/L) was added to inhibit cell motion. Cells were then washed before confocal analysis. T-tubules (TT) analysis was performed on images (1024 x 1024 pixels, 50μm x 50μm) collected with a Leica TCS SP2 laser-scanning confocal microscopy (Leica Microsystem GmbH, Wetzlar, Germany) equipped with

a 63x oil-immersion objective; photomultiplier gain and offset were adjusted within a small range to optimize image quality. TT organization and periodicity was evaluated by a method based on Fast Fourier Transform on 8-bit grayscaled images (modified from [32]). In brief, we generated a raw power spectrum with ImageJ (v.1.44) and normalized it to its central peak (representing the TT power value at 0 μm-1) to compensate for staining differences among samples. Then, the TT density was evaluated by two alternative methods; 1) by measuring the absolute peak at the spatial frequency of 0.5 μm-1 (first harmonic of the power spectrum), and 2) by normalizing the area under the 0.5 μm_{-1} harmonic (between 0.44 and 0.60 μm_{-1}) to the area of the entire spectrum. Because the results obtained with the two methods were similar, we report in the study only those obtained with the second method for practical reasons.

3.11.9 Hemodynamic parameters

right ventricular systolic pressure (RVSP) was measured with a tip-transducer catheter (Millar SPR671) introduced in the RV through the right jugular vein under anesthesia (pentobarbital 50 mg/Kg i.p.) allowing for spontaneous breathing. After ruling out pulmonary valve and RV outflow tract stenosis by echocardiography, RVSP was considered representative of pulmonary artery systolic pressure [8].

3.11.10 Pulmonary histology

MCT-induced pulmonary vascular remodelling was assessed by measuring wall thickness (WT) of small arterioles (diameter range 40-70 microns), an index of medial hypertrophy. Briefly, left lungs were fixed in 4% buffered formalin, embedded in paraffin and stained with hematoxylin and eosin. WT was calculated as previously reported [6].

3.11.11 Reagents

RAN was provided by Gilead Sciences Inc (Foster City, CA); TTX was purchased from Tocris (Bristol, UK); all other reagents were from Sigma-

Table 3.3: Primers for RTq-PCR analysis. (f) = forward primer, (r) = reverse primer.

Gene	Sequence
α-MHC	(f) -TGTGAAAAGATTAACCGGAGTTTAAG-
	(r) -TCTGACTTGCGGAGGTATCG-
β-MHC	(f) -AAGTCCTCCCTCAAGCTCCTAAGT-
	(r) -TTGCTTTGCCTTTGCCC-
GAPDH	(f) -ACCACGAGAAATATGACAACTCCC-
	(r) -CCAAAGTTGTCATGGATGACC-
RPL29	(f) -ACAGAAATGGCATCAAGAAACCC-
	(r) -TCTTGTTGTGCTTCTTGGCAAA-

Aldrich (St. Luis, MO). Fluo4-AM and di-3-ANEPPDHQ were from Life Technologies (Carlsbad, United States).

3.11.12 Statistical analysis

Data are presented as mean SE. χ^2-test was used for comparison of categorical variables. Comparison between multiple means was performed by one-way ANOVA and post hoc Bonferroni's correction. A repeated measurement model was applied whenever internal comparisons were involved.The Mann Whitney test was used for multiple comparisons of categorical variables. Statistical significance was defined as $p<0.05$ (NS = not significant). The main text reports percent changes; unless otherwise specified, a "change" is statistically significant. The respective absolute values are shown in the figures. The number of animals (N) and cells (n) are reported in figure legends.

Table 3.4: Physiological differences between RV and LV myocytes (CTRL group).

	RV	**LV**	**P**
C_m (pF)	145.5 ± 3.2	170.1 ± 4.5	<0.05
α-MHC mRNA	0.1 ± 0.01	0.25 ± 0.04	<0.05
β-MHC mRNA	0.07 ± 0.01	0.06 ± 0.01	NS
mean I_{TTX} (pA/pF)	0.32 ± 0.03	0.30 ± 0.02	NS
peak I_{TTX} (I_{NaW}, pA/pF)	0.65 ± 0.05	0.60 ± 0.06	NS
I_{TTX} @ 0mV (I_{NaL}, pA/pF)	0.16 ± 0.03	0.14 ± 0.03	NS
I_{CaL} (@ 0mV, pA/pF)	-15.2 ± 0.96	-18.8 ± 1.93	<0.05
I_{K1} (G_{max}, nS/pF)	0.53 ± 0.03	0.44 ± 0.04	<0.05
I_{to} (@ +40mV, pA/pF)	30.4 ± 2.8	24.6 ± 2.1	<0.05
APD_{50} (ms)	7.8 ± 0.55	15.1 ± 1.2	<0.05
APD_{90} (ms)	30.2 ± 1.29	41.6 ±2.15	<0.05
APD_{50}/APD_{90}	0.26 ± 0.01	0.35 ± 0.02	<0.05
E_{diast} (mV)	-77.9 ± 0.47	-78.2 ± 0.57	NS
dV/dt_{max} (V/s)	306.7 ± 7.7	305.5 ± 10.0	NS
$[Ca]_{resting}$ (nmol/L)	44.0 ± 2.04	60.0 ± 5.9	<0.05
$[Ca]_{diast}$ (nmol/L)	78.2 ± 2.64	129.1 ± 3.57	<0.05
$[Ca]_T$ (nmol/L)	65.8 ± 5.21	233.9 ± 20.5	<0.05
$[Ca]_{SR}$ (µmol/L)	41.9 ± 3.24	97.2 ± 6.81	<0.05
fractional release	0.49 ±0.03	0.49 ± 0.03	NS

Table 3.5: Steady-state I_{CaL} activation/inactivation properties.

	RV			LV		
	CTRL	**MCT**	**+RAN**	**CTRL**	**MCT**	**+RAN**
Activation						
$V_{0.5}$ (mV)	-12.2 ± 0.5	-11.0 ± 0.6	-10.0 ± 0.6 *	-12.0 ± 0.7	-9.6 ± 0.8	-9.2 ± 1.0
k (mV)	6.2 ± 0.1	6.3 ± 0.1	6.0 ± 0.1	6.0 ± 0.1	6.0 ± 0.1	6.1 ± 0.1
Inactivation						
$V_{0.5}$ (mV)	-33.6 ± 0.5	-33.7 ± 0.3	-34.2 ± 0.7	-32.8 ± 0.4	-31.7 ± 0.6	-30.1 ± 0.9
k (mV)	5.0 ± 0.1	5.1 ± 0.1	5.3 ± 0.1	4.7 ± 0.1 °	5.2 ± 0.1	4.9 ± 0.1
I_{CaLW}						
Area (a.u.)	1.77 ± 0.10	1.67 ± 0.14	1.71 ± 0.13	2.2 ± 0.19 °	1.99 ± 0.13	2.1 ± 0.17
Peak (mV)	-24.2 ± 0.5	-23.5 ± 0.4	-23.5 ± 0.6	-24.2 ± 0.5	-21.5 ± 0.5 *	-21.4 ± 0.9

° = p<0.05 LV vs RV (CTRL group); * = p<0.05 vs CTRL

Table 3.6: I_{CaL} inactivation kinetics at 0 mV.

	t_{fast} (ms)	**A_{fast} (pA/pF)**	**t_{slow} (ms)**	**A_{slow} (pA/pF)**	**I_{ss} (pA/pF)**
RV					
CTRL	7.9 ± 0.7	-8.9 ± 0.6	36.1 ± 1.5	-5.3 ± 0.4	-0.35 ± 0.05
MCT	7.5 ± 0.8	-9.3 ± 0.9	33.6 ± 2.2	-5.6 ± 0.7	-0.28 ± 0.05
+RAN	8.3 ± 0.7	-9.9 ± 1.2	34.7 ± 1.8	-5.2 ± 0.8	-0.43 ± 0.11
LV					
CTRL	7.6 ± 1.0	-10.3 ± 0.9	37.1 ± 2.0	-6.9 ± 0.9	-0.72 ± 0.17 °
MCT	7.4 ± 0.7	-8.7 ± 1.0	34.5 ± 1.8	-6.0 ± 0.9	-0.45 ± 0.10
+RAN	7.5 ± 1.0	-10.3 ± 1.1	35.4 ± 1.7	-7.4 ± 0.8	-0.68 ± 0.15

° = p<0.05 LV vs RV (CTRL group)

Table 3.7: I_{CaL} inactivation kinetics at +40 mV.

	t_{fast} (ms)	A_{fast} (pA/pF)	t_{slow} (ms)	A_{slow} (pA/pF)	I_{mean} (pA/pF)
RV					
CTRL	8.5 ± 0.3	22.3 ± 2.6	441.2 ± 38	7.4 ± 0.8	3.47 ± 0.5
MCT	9.0 ± 0.3	14.3 ± 1.4 *	383.1 ± 44	4.1 ± 0.3 *	1.47 ± 0.1 *
+RAN	7.7 ± 0.2 #	17.3 ± 1.5	320.6 ± 27 *	5.4 ±0.5	1.91 ± 0.2 *
LV					
CTRL	9.4 ± 0.4	19.1 ± 1.8	399.7 ± 23	6.4 ± 0.5	2.3 ± 0.2 °
MCT	7.6 ± 0.3 *	13.8 ± 1.3	349.7 ± 38	4.7 ± 0.5	1.6 ± 0.2 *
+RAN	8.3 ± 0.4	15.8 ± 2.2	298.8 ± 17 *	8.2 ±1.0 #	2.7 ± 0.3 #

° = p<0.05 LV vs RV (CTRL group); * = p<0.05 vs CTRL, # = p<0.05 vs MCT

3.12 Supplemental figures

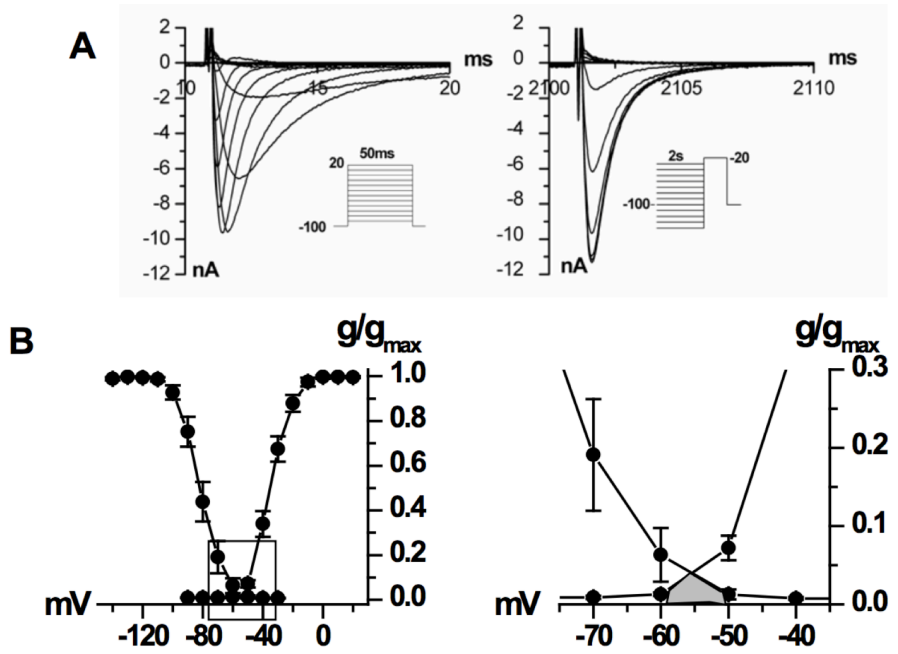

Figure 3.8: *I_{Na} steady-state activation/inactivation curves in rat ventricular myocytes:* evaluation of sodium window current (I_{NaW}). A) I_{Na} traces according to specific protocols of steady-state activation (left) and inactivation (right); recordings in the presence of 10 mmol/L NaCl in the extracellular solution (osmolarity compensated by equimolar N-Methyl-D-glucamine) and 5 mmol/L NaCl in the pipette solution. Intracellular and extracellular K^+ was replaced by equimolar Cs^+, 2 μmol/L nifedipine was used to block I_{CaL}. Measurements were performed at room temperature. B) Average I_{Na} steady-state activation/inactivation curves ($n \geq 11$). The sodium window current (I_{NaW}), grey area) represented by the overlapping between activation and inactivation curves (square box), is highlighted on the right. The window component of I_{Na} (I_{NaW}) is present between -60 and -50 mV.

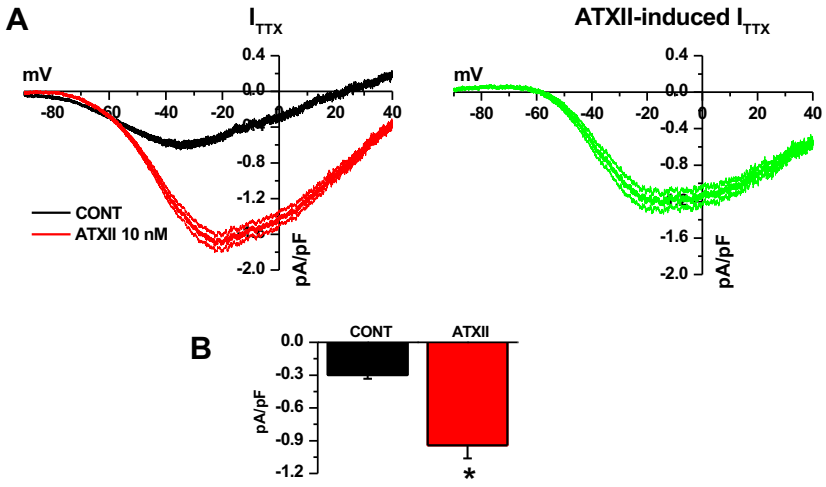

Figure 3.9: *I_{NaL} evaluation during slow voltage ramps in rat ventricular myocytes.* A) Left:TTX-sensitive current (I_{TTX}, 30 μmol/L) I/V relationships in control and in the presence of the selective I_{NaL} enhancer ATXII (10 nmol/L). Right: I/V relationship of I_{TTX} stimulated by ATXII (largely representing I_{NaL}). Average traces and confidence intervals are shown. B) Statistics of mean inward I_{TTX} (n = 8); $*$ = p$<$0.05 vs CONT. The late component of I_{Na} (I_{NaL}) activated during slow depolarizing ramps is maximal between -20 and 0 mV.

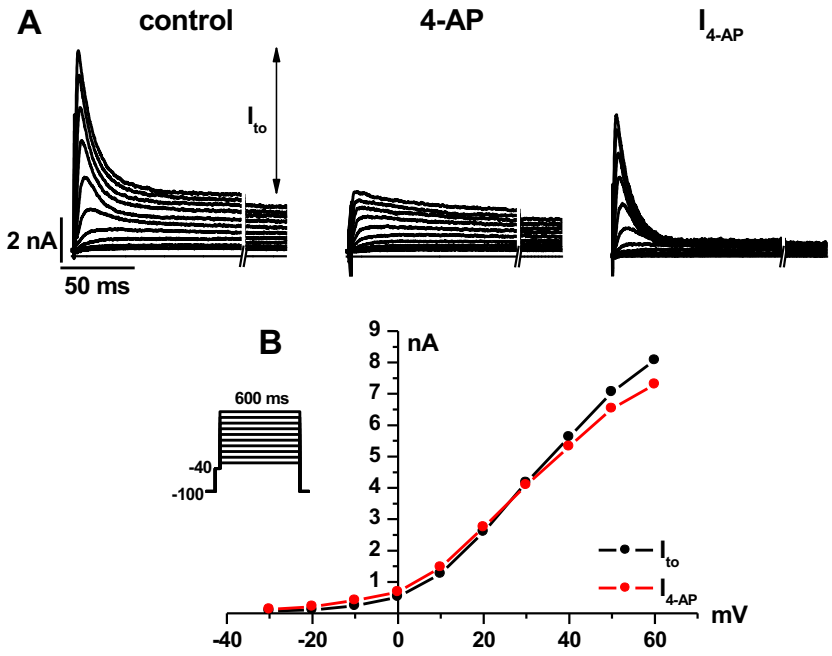

Figure 3.10: *I_{to} isolation in rat ventricular myocytes.* A) I_{to} recordings in control and after superfusion of the selective blocker 4-aminopyridine (3 mmol/L 4-AP); 4-AP-sensitive current is shown on the right (I4-AP). Cadmium (0.5 mmol/L) was added to extracellular solution to block I_{CaL}. B) Example of I_{to} I/V relationships obtained with two different methods. I_{to} I/V relationships obtained measuring the current as the transient component or the current sensitive to 4-AP (I_{4-AP}) were comparable.

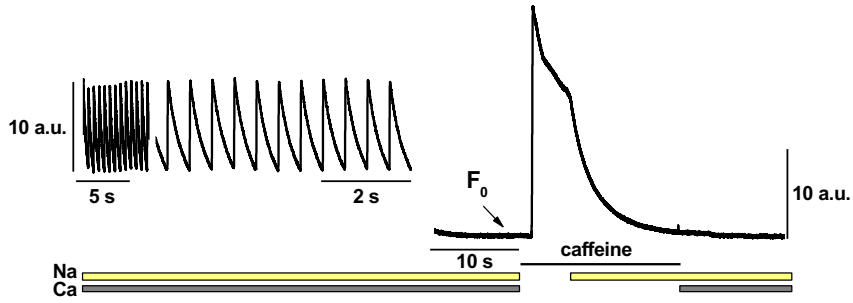

Figure 3.11: *Ca^{2+} handling protocol in field stimulated myocytes.* Fluo4 loaded intact myocytes were field-stimulated (2 Hz) at physiological temperature. SR Ca^{2+} content was estimated after 10s at resting by an electronically timed 10 mmol/L caffeine pulse. The resting fluorescence was used as reference (F_0) for signal normalization (F/F_0) after subtraction of background luminescence. Caffeine was superfused for few seconds in Na^+ and Ca^{2+} free solution to block Ca^{2+} extrusion through the Na^+/Ca^{2+} exchanger (NCX) and properly quantify the caffeine-induced Ca^{2+} transient.

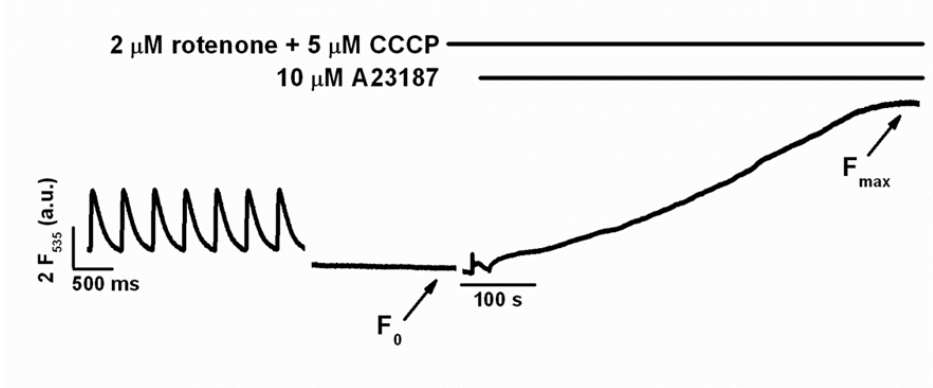

Figure 3.12: *Method for Fluo4 signal (F_{535}) calibration.* The experimental protocol used in the study (see Fig S4) was applied in a separate set of RV (n = 10) and LV (n = 12) myocytes of the CTRL group. F_{535} recorded during quiescence (after the loading train) was adopted as F_0 and converted to $[Ca]_0$ according to Eq 1 (see Supplemental Methods). Maximum fluorescence (Fmax) was measured after cell permeabilization with the Ca^{2+} ionophore (A23187); the uncouplers CCCP and rotenone were added to extracellular solution to block ATP synthesis.

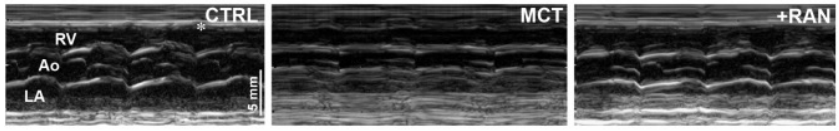

Figure 3.13: *Representative M-mode echocardiographic recordings of RV free wall thickness in each study group.* M-Mode echocardiogram of the RV from parasternal long axis view. RV= right ventricle; Ao= aorta; LA: left atrium; ∗= RV free wall.

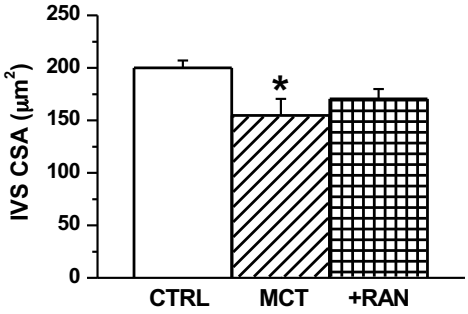

Figure 3.14: *interventricular septum (IVS) cross sectional area (CSA) changes.* Statistics of IVS CSA. ∗ = p<0.05 vs CTRL. N = 5 for each group.

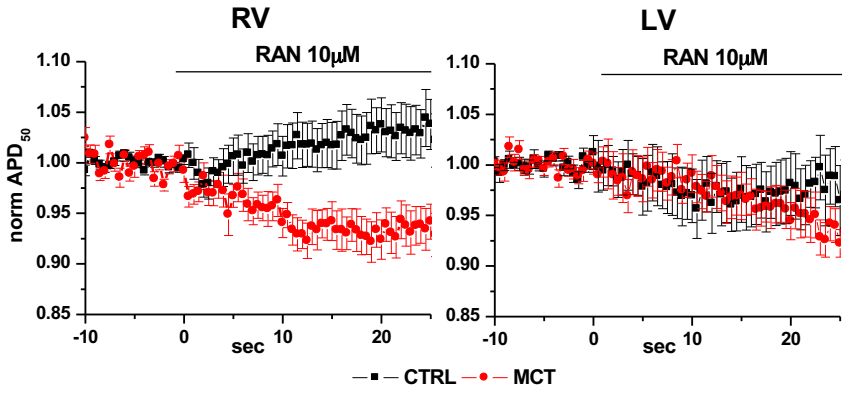

Figure 3.15: *Acute effects of RAN on APD_{50}.* Time course of APD_{50} before and after RAN (10 μmol/L) superfusion in RV (left) and LV (right) myocytes of CTRL and MCT group. Values were normalized to APD_{50} just before RAN superfusion. N $\geq$ 4 and n $\geq$ 11 for each group.

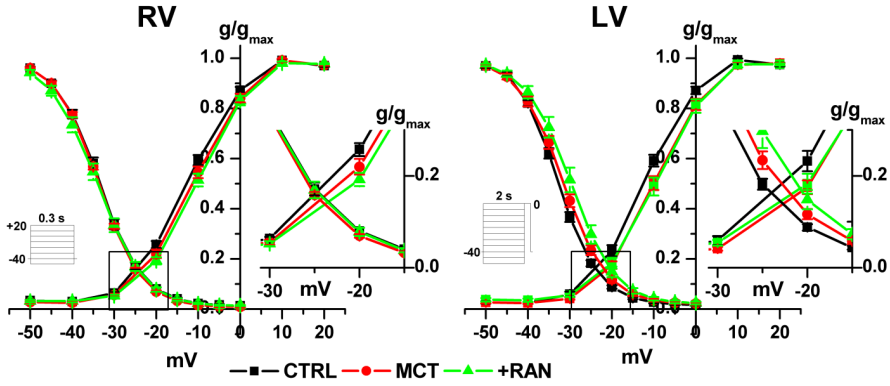

Figure 3.16: *Average I_{CaL} steady-state activation/inactivation curves in each experimental group.* The window I_{CaL}, represented by the overlapping between activation and inactivation curves (square box), is highlighted on the right. Statistics of the parameters extrapolated by Boltzmann fit are shown in Table 3.5.

3.13 References

1. Aistrup, G. L. *et al.* Inhibition of the late sodium current slows t-tubule disruption during the progression of hypertensive heart disease in the rat. *Am. J. Physiol. Heart Circ. Physiol.* **305,** H1068–79. ISSN: 1522-1539 (2013).

2. Akhavein, F, St-Michel, E. J., Seifert, E & Rohlicek, C. V. Decreased left ventricular function, myocarditis, and coronary arteriolar medial thickening following monocrotaline administration in adult rats. *J. Appl. Physiol.* **103,** 287–95. ISSN: 8750-7587 (2007).

3. Antzelevitch, C. Electrophysiological Effects of Ranolazine, a Novel Antianginal Agent With Antiarrhythmic Properties. *Circulation* **110,** 904–910. ISSN: 0009-7322 (2004).

4. Benoist, D., Stones, R., Drinkhill, M., Bernus, O. & White, E. Arrhythmogenic substrate in hearts of rats with monocrotaline-induced pulmonary hypertension and right ventricular hypertrophy. *Am. J. Physiol. Heart Circ. Physiol.* **300,** H2230–7. ISSN: 1522-1539 (2011).

5. Benoist, D. *et al.* Cardiac arrhythmia mechanisms in rats with heart failure induced by pulmonary hypertension. *Am. J. Physiol. Heart Circ. Physiol.* **302,** H2381–95. ISSN: 1522-1539 (2012).

6. Beppu, H. *et al.* BMPR-II heterozygous mice have mild pulmonary hypertension and an impaired pulmonary vascular remodeling response to prolonged hypoxia. *Am. J. Physiol. Lung Cell. Mol. Physiol.* **287,** L1241–L1247. ISSN: 1040-0605 (2004).

7. Bull, T. M. *et al.* Gene microarray analysis of peripheral blood cells in pulmonary arterial hypertension. *Am. J. Respir. Crit. Care Med.* **170,** 911–919. ISSN: 1073449X (2004).

8. Chemla, D. *et al.* New formula for predicting mean pulmonary artery pressure using systolic pulmonary artery pressure. *Chest* **126,** 1313–1317. ISSN: 0012-3692 (2004).

9. Correia-Pinto, J. *et al.* Time course and mechanisms of left ventricular systolic and diastolic dysfunction in monocrotaline-induced pulmonary hypertension. *Basic Res. Cardiol.* **104,** 535–545. ISSN: 03008428 (2009).

10. Curran, J. *et al.* Spontaneous Ca waves in ventricular myocytes from failing hearts depend on Ca2+-calmodulin-dependent protein kinase II. *J. Mol. Cell. Cardiol.* **49,** 25–32. ISSN: 00222828 (2010).

11. Deng, C.-Y. *et al.* Effect of ranolazine on rat intrarenal arteries in vitro. *Eur. J. Pharmacol.* **683,** 211–6. ISSN: 1879-0712 (2012).

12. Fang, Y.-H. *et al.* Therapeutic inhibition of fatty acid oxidation in right ventricular hypertrophy: exploiting Randle's cycle. *J. Mol. Med. (Berl).* **90,** 31–43. ISSN: 1432-1440 (2012).

13. Hardziyenka, M. *et al.* Electrophysiologic Remodeling of the Left Ventricle in Pressure Overload-Induced Right Ventricular Failure. *J. Am. Coll. Cardiol.* **59,** 2193–2202. ISSN: 07351097 (2012).

14. Horton, K. D., Meece, R. W. & Hill, J. C. Assessment of the Right Ventricle by Echocardiography: A Primer for Cardiac Sonographers. *J. Am. Soc. Echocardiogr.* **22,** 776–792. ISSN: 08947317 (2009).

15. Jo, T. *et al.* Voltage-gated sodium channel expressed in cultured human smooth muscle cells: involvement of SCN9A. *FEBS Lett.* **567,** 339–43. ISSN: 0014-5793 (2004).

16. Lamberts, R. R., Vaessen, R. J., Westerhof, N. & Stienen, G. J. M. Right ventricular hypertrophy causes impairment of left ventricular diastolic function in the rat. *Basic Res. Cardiol.* **102,** 19–27. ISSN: 0300-8428 (2007).

17. Lin, M., Yang, X., Cao, Y. & Sham, J. Hydrogen peroxide-induced Ca2+ mobilization in pulmonary arterial smooth muscle cells. *Am J Physiol Lung Cell Mol Physiol* **292,** L1598–608. ISSN: 1040-0605 (2007).

18. Livak, K. J. & Schmittgen, T. D. Analysis of relative gene expression data using real-time quantitative PCR and the 2(-Delta Delta C(T)) Method. *Methods* **25,** 402–8. ISSN: 1046-2023 (2001).

19. Louch, W. E., Sejersted, O. M. & Swift, F. There goes the neighborhood: pathological alterations in T-tubule morphology and consequences for cardiomyocyte Ca2+ handling. *J. Biomed. Biotechnol.* **2010,** 503906. ISSN: 1110-7251 (2010).

20. Maack, C. *et al.* Elevated cytosolic Na+ decreases mitochondrial Ca2+ uptake during excitation-contraction coupling and impairs energetic adaptation in cardiac myocytes. *Circ. Res.* **99,** 172–182. ISSN: 00097330 (2006).

21. Maier, L. S. A novel mechanism for the treatment of angina, arrhythmias, and diastolic dysfunction: inhibition of late I(Na) using ranolazine. *J. Cardiovasc. Pharmacol.* **54,** 279–286. ISSN: 0160-2446 (2009).

22. Masson, S *et al.* Eplerenone, a selective aldosterone blocker, improves diastolic function in aged rats with small-to-moderate myocardial infarction. *J Card Fail* **10,** 433–441. ISSN: 1071-9164 (2004).

23. Masson, S *et al.* Remodelling of cardiac extracellular matrix during beta-adrenergic stimulation: upregulation of SPARC in the myocardium of adult rats. *J Mol Cell Cardiol* **30,** 1505–1514 (1998).

24. McCormack, J. G., Barr, R. L., Wolff, A. A. & Lopaschuk, G. D. Ranolazine Stimulates Glucose Oxidation in Normoxic, Ischemic, and Reperfused Ischemic Rat Hearts. *Circulation* **93,** 135–142. ISSN: 0009-7322 (1996).

25. Michelakis, E. D., Wilkins, M. R. & Rabinovitch, M. Emerging concepts and translational priorities in pulmonary arterial hypertension. *Circulation* **118,** 1486–1495. ISSN: 1524-4539 (2008).

26. Moreno, J. D. & Clancy, C. E. Pathophysiology of the cardiac late Na current and its potential as a drug target. *J. Mol. Cell. Cardiol.* **52,** 608–619. ISSN: 00222828 (2012).

27. Nagueh, S. F. *et al.* Recommendations for the evaluation of left ventricular diastolic function by echocardiography. *J. Am. Soc. Echocardiogr.* **22,** 107–133. ISSN: 1097-6795 (2009).

28. Paredes-Carbajal, M. C. *et al.* Effects of ranolazine on vasomotor responses of rat aortic rings. *Arch. Med. Res.* **44,** 8–12. ISSN: 1873-5487 (2013).

29. Platoshyn, O., Remillard, C. V., Fantozzi, I., Sison, T. & Yuan, J. X.-J. Identification of functional voltage-gated Na+ channels in cultured human pulmonary artery smooth muscle cells. *Pflügers Arch. - Eur. J. Physiol.* **451,** 380–387. ISSN: 0031-6768 (2005).

30. Quiñones, M. a., Otto, C. M., Stoddard, M., Waggoner, A. & Zoghbi, W. a. Recommendations for quantification of Doppler echocardiography: a report from the Doppler Quantification Task Force of the Nomenclature and Standards Committee of the American Society of Echocardiography. *J. Am. Soc. Echocardiogr.* **15,** 167–184. ISSN: 08947317 (2002).

31. Rudski, L. G. *et al.* Guidelines for the Echocardiographic Assessment of the Right Heart in Adults: A Report from the American Society of Echocardiography: Endorsed by the European Association of Echocardiography, a registered branch of the European Society of Cardiology, and. *J. Am. Soc. Echocardiogr.* **23,** 685–713. ISSN: 1097-6795 (2010).

32. Sacconi, L. *et al.* Action potential propagation in transverse-axial tubular system is impaired in heart failure. *Proc. Natl. Acad. Sci.* **109,** 5815–5819. ISSN: 0027-8424 (2012).

33. Saeedi, R. & Grist, M. Trimetazidine normalizes postischemic function of hypertrophied rat hearts. ... *Pharmacol.* ... **314,** 446–454. ISSN: 00223565 (2005).

34. Sicouri, S., Belardinelli, L. & Antzelevitch, C. Antiarrhythmic effects of the highly selective late sodium channel current blocker GS-458967. *Heart Rhythm* **10,** 1036–43. ISSN: 1556-3871 (2013).

35. Stenmark, K. R., Meyrick, B., Galie, N., Mooi, W. J. & McMurtry, I. F. Animal models of pulmonary arterial hypertension: the hope for etiological discovery and pharmacological cure. *AJP Lung Cell. Mol. Physiol.* **297,** L1013–L1032. ISSN: 1040-0605 (2009).

36. Swift, F. *et al.* Extreme sarcoplasmic reticulum volume loss and compensatory T-tubule remodeling after Serca2 knockout. *Proc. Natl. Acad. Sci.* **109,** 3997–4001. ISSN: 0027-8424 (2012).

37. Wang, P. *et al.* A Comparison between Ranolazine and CVT-4325 , a Novel Inhibitor of Fatty Acid Oxidation , on Cardiac Metabolism and Left Ventricular Function in Rat Isolated Perfused Heart during Ischemia and Reperfusion. **321,** 213–220 (2007).

38. Ye, J. *et al.* Primer-BLAST: A tool to design target-specific primers for polymerase chain reaction. *BMC Bioinformatics* **13,** 134. ISSN: 1471-2105 (2012).

39. Zaza, a, Rocchetti, M, Brioschi, a, Cantadori, a & Ferroni, a. Dynamic Ca2+-induced inward rectification of K+ current during the ventricular action potential. *Circ. Res.* **82,** 947–56. ISSN: 0009-7330 (1998).

40. Zaza, A. & Rocchetti, M. The late Na+ current–origin and pathophysiological relevance. *Cardiovasc. Drugs Ther.* **27,** 61–8. ISSN: 1573-7241 (2013).

41. Zaza, A., Belardinelli, L. & Shryock, J. C. Pathophysiology and pharmacology of the cardiac âĂIJ late sodium current âĂİ. **119,** 326–339 (2008).

42. Zoja, C. & Cattaneo, S. Distinct cardiac and renal effects of ETA receptor antagonist and ACE inhibitor in experimental type 2 diabetes. . . . *Physiol.* . . . **301,** F1114–F1123. ISSN: 1522-1466 (2011).

Chapter 4

Summary and conclusion

The present thesis describes the pivotal role of I_{NaL} enhancement in cardiac pathological remodeling and the benefit of I_{NaL} blockade in experimental rodent models of two cardiac disease.

The first study investigated the role of I_{NaL} and its contribution to ionic homeostasis dysregulation during acute myocardial ischemia in rat ventricular myocytes. For the first time, an increase of I_{NaL} was directly measured in an ischemia-mimic experimental condition, in spite of the attending changes in membrane potential. This study demonstrated that I_{NaL} blockade, by RAN and TTX, prevented the ischemic mimic solution (ISC)-induced cytosolic Na^+ (Na_{cyt}) accumulation; whereas it prevented ISC-induced cytosolic Ca^{2+} (Ca_{cyt}) accumulation exclusively in the presence of sarcolemmal Na^+/Ca^{2+} exchanger (sNCX) blocked. Furthermore, this study suggested that I_{NaL} might modulate the role of mitochondria (Ca^{2+} sink/source) through mitochondrial Na^+/Ca^{2+} exchanger (mNCX) during ischemia. Thus, I_{NaL} participates, directly and via mitochondria modulation, to ion dysregulation caused by ischemia and therefore, the I_{NaL} blockade might prevent the ischemia injury.

The second study evaluated the hypothesis that an I_{NaL} enhancement may occur as part of PAH-induced myocardial remodelling and that it can be prevented by selective I_{NaL} blockade by RAN in a rat model of PAH induced by MCT. This study pointed to a role of I_{NaL} enhancement

in the development of PAH and in the maladaptive cardiac response to PAH. Furthermore, although the I_{NaL} blockade by RAN was less effective in preventing cardiac function derangement, RAN prevented constitutive I_{NaL} enhancement and most aspects of myocardial structural remodelling caused by PAH. This might depend on partial mechanical unloading resulted from an unexpected effect of RAN on pulmonary vasculature.

In conclusion, this thesis demonstrates that I_{NaL} enhancement contributes to cardiac pathological remodeling caused by acute myocardial ischemia and PAH and thus, it can be considered a potential therapeutic target in these cardiac diseases. Differences between RAN and TTX effects suggest that cardiac protective effects shown by RAN might be also due to I_{NaL} -independent effects. The development of selective I_{NaL} blockers might be crucial to better understand this point.

Chapter 5

Published papers

1. Rizzetto R, Rocchetti M, Sala L, **Ronchi C**, Villa A, Ferrandi M, Molinari I, Bertuzzi F and Zaza A (2015) *Late sodium current (I_{NaL}) in pancreatic β-cells.* Pflugers Arch - Eur J Physiol 467: 1757-1768

2. Moreno C, De La Cruz A, Oliveras A, Kharche S, Guizy M, Comes N, Stary T **Ronchi C**, Rocchetti M, Baro' I, Loussouarn G, Zaza A, Severi S, Felipe A, Valenzuela C (2015) *Marine n-3 PUFAs modulate I_{Ks} gating, channel expression, and location in membrane microdomains* Cardiovasc Res 105(2):223-232

Pflugers Arch - Eur J Physiol (2015) 467:1757–1768
DOI 10.1007/s00424-014-1613-0

ION CHANNELS, RECEPTORS AND TRANSPORTERS

Late sodium current (I_{NaL}) in pancreatic β-cells

Riccardo Rizzetto · Marcella Rocchetti · Luca Sala · Carlotta Ronchi · Alice Villa · Mara Ferrandi · Isabella Molinari · Federico Bertuzzi · Antonio Zaza

Received: 30 April 2014 / Revised: 1 September 2014 / Accepted: 8 September 2014 / Published online: 20 September 2014

Abstract Recent evidence of beneficial effects of ranolazine (RAN) in type II diabetes motivates interest in the role of the late sodium current (I_{NaL}) in glucose-stimulated insulin secretion. In the present work, we characterize I_{NaL} and its function in rat INS-1E cells and human islets cells. I_{NaL} was identified as steady-state current blocked by 10 μM RAN (I_{RAN}) or 0.5 μM tetrodotoxin (TTX) (I_{TTX}). Veratridine (VERA, 40 μM) was used as I_{NaL} enhancer. Baseline I_{NaL} was similar between INS-1E and human islet cells. In INS-1E cells, activated by glucose or tolbutamide, TTX or RAN hyperpolarized membrane potential (V_m). VERA-induced depolarization was countered by TTX or RAN. I_{TTX} and I_{RAN} reversal potentials were negative to Na^+ equilibrium one, but they approached it after Na^+ substitution with Li^+ or when K^+ channels were blocked. This revealed I_{NaL} coupling with Na^+-activated K^+ current (I_{KNa}); expression of I_{KNa} channels (*Slick*/*Slack*) was confirmed by transcript analysis and Western blot. RAN or TTX blunted cytosolic Ca^{2+} response to depolarization. Long-term incubation in high (33 mM) glucose (CHG) constitutively enhanced I_{NaL}. VERA immediately increased glucose-stimulated insulin secretion. CHG increased glucose-independent secretion instead and abolished the secretory response to glucose. RAN or TTX countered VERA- and CHG-induced changes in insulin secretion. Our study demonstrated that (1) I_{NaL} was expressed in insulin-secreting cells and coupled to I_{KNa}; I_{NaL} affected cytosolic Ca^{2+} but, unless enhanced, barely contributed to glucose-stimulated insulin secretion (GSIS); and (2) sustained hyperglycemic stress enhanced I_{NaL}, which contributed to the attending increase of glucose-independent insulin "leak" and GSIS impairment.

Keywords Late sodium current · Sodium-activated potassium current · Insulin secretion · Ranolazine · Pancreatic β-cells

Introduction

In normal conditions, increased glucose levels trigger a biphasic response of pancreatic β-cells. Whereas the first phase of glucose-induced insulin secretion primarily depends on membrane electrical activity, the second one may also require metabolic signals [31, 46]. It is widely accepted that high-glucose levels cause K_{ATP} channel closure, resulting in membrane depolarization and triggering spontaneous action potentials, driven by voltage-gated Na^+ and Ca^{2+} channels [7]. Thus, the first phase of insulin secretion depends on the functional interplay between depolarizing (Na^+ and Ca^{2+}) and hyperpolarizing (K^+) currents [7].

When evaluated for its anti-anginal efficacy, ranolazine (RAN), a blocker of the late Na^+ current (I_{NaL}), reduced fasting glucose levels and glycosylated hemoglobin (HbA1c) in type II diabetic patients [30]. RAN was also found to improve glucose homeostasis in diabetic mice by directly increasing insulin secretion from pancreatic islets [32]. Even if recent evidence indicates that inhibition of glucagon secretion may contribute to RAN action on glucose homeostasis

Electronic supplementary material The online version of this article (doi:10.1007/s00424-014-1613-0) contains supplementary material, which is available to authorized users.

R. Rizzetto · M. Rocchetti · L. Sala · C. Ronchi · A. Villa · A. Zaza (✉)
Department of Biotechnology and Biosciences, University of Milano-Bicocca, Piazza della Scienza 2, 20126 Milan, Italy
e-mail: antonio.zaza@unimib.it

M. Ferrandi · I. Molinari
Nephrology and Dialysis, Università Vita Salute San Raffaele, Milan, Italy

F. Bertuzzi
Endocrinology Unit, Niguarda Hospital, Milan, Italy

[12], the mechanism by which the drug may improve insulin secretion remains unknown.

The existing information on the role of I_{Na} in insulin secretion is limited to that of its transient component (I_{NaT}) and seemingly opposite to that potentially accounting for a beneficial effect of I_{Na} blockade on glucose homeostasis [3, 7, 33]. Nonetheless, RAN may preferentially block the late component of I_{Na} (I_{NaL}) whose pathological enhancement has been shown to contribute, albeit in different cell types, to damage progression [39, 49]. Furthermore, reactive oxygen species, a known factor in the pathogenesis of insulin deficiency [11, 44], are powerful I_{NaL} enhancers [38]. Thus, the beneficial effects of RAN on insulin secretion might be related to I_{NaL} inhibition, thus indirectly suggesting I_{NaL} enhancement as a mechanism contributing to insulin deficiency.

The (multicellular) pancreatic "islet" works as an integrated system; indeed, insulin secretion is ultimately regulated by an interaction between its α- and β-cells, which are linked by reciprocal paracrine modulation. Therefore, based on observations on pancreatic islets, it is difficult to discriminate whether RAN acts primarily on α- or β-cells. Furthermore, albeit I_{NaL} blockade is the main effect of RAN, the drug might still act through ancillary effects [27, 36]; thus, I_{NaL} involvement in β-cells pathophysiology remains to be established.

The aim of this work was to investigate I_{NaL} and its functional role in a pure population of insulin-secreting cells, representative of pancreatic β-cells (INS-1E). Considering that pathological I_{NaL} enhancement is known to promote maladaptive cell remodeling in other tissues [4, 41], we also tested if sustained hyperglycemic stress might enhance I_{NaL} in these cells and whether this might contribute to insulin secretion deficiency.

Materials and methods

INS-1E and human islet cell culture

INS-1E cells, kindly supplied by Dr. Wollheim (University of Geneva, Switzerland), were cultured in RPMI medium supplemented with 10 % fetal bovine serum (FBS), 2 mM L-glutamine, 1 mM Na-pyruvate, 50 μM 2-mercaptoethanol, and 10 mM glucose.

Human islets were obtained by four non-diabetic donors from Ospedale Niguarda Ca' Granda (Milan), according to the principles outlined in the Declaration of Helsinki. Dispersed islets were cultured in M199 supplemented with 10 % FBS and 2 mM L-glutamine. They were gently dissociated in single cells in the presence of accutase solution at 37 °C; digestion was stopped by adding FBS. Cells were collected by gentle centrifugation and resuspended in complete islet culture medium. Dispersed cells were allowed to attach at 37 °C in polylysine-covered Petri dishes overnight; patch clamp studies were performed the day after plating.

Electrophysiology

All measurements were performed at 35 °C. RAN (10 μM) and tetrodotoxin (0.5 μM, TTX) were alternatively used as I_{Na} blockers, and veratridine (40 μM, VERA) was used as I_{NaL} enhancer [12, 51].

Membrane potential (V_m) recordings were performed in the perforated-patch configuration (series resistance<20 MΩ). Steady-state membrane current was measured by applying slow voltage ramps (0.056 V/s) under ruptured-patch (series resistance<5 MΩ); its TTX- and RAN-sensitive components (I_{TTX} and I_{RAN}) were isolated by digital subtraction. Close similarity between I_{TTX} amplitude between ramp and steady-state depolarization protocols (Fig. S1) indicates that I_{NaT} was largely inactivated during the ramp protocol; thus, its contribution to I_{TTX} and I_{RAN} was negligible. Throughout the manuscript, current recordings are presented as "mean *I*/*V* relationship," obtained by averaging recordings from multiple cells, along with their 95 % confidence intervals. Current density was obtained by normalizing current to membrane capacitance. The inward component of I_{TTX} and I_{RAN} was quantified as "mean inward current" (Mean I_{IN}), obtained by integrating the current over the relevant time interval and dividing the result by the latter.

Standard extracellular solution (Krebs) contained (in mM) 140 NaCl, 3.6 KCl, 2 $NaHCO_3$, 0.5 NaH_2PO_4, 0.5 $MgSO_4$, 5 4-(2-hydroxyethyl)-1-piperazineethanesulfonic acid (HEPES), 1.5 $CaCl_2$, and 2.5 glucose (pH 7.4). K^+ channels were blocked by adding tolbutamide (TOLB, 50 μM), tetraethylammonium chloride (TEACl, 10 mM), and 4-aminopyridine (4-AP, 0.5 mM) to extracellular solution (KBK solution).

Pipette solution contained (in mM) 76 K_2SO_4, 10 NaCl, 10 KCl, 1 $MgCl_2$, 5 HEPES (pH 7.35), and 0.3 mM amphotericin-B for perforated-patch and 95 K-gluconate, 30 KCl, 1 $MgCl_2$, 5 HEPES, 5 Na_2ATP, 1 Na_2GTP, 1 EGTA, and 0.4 $CaCl_2$ (pH 7.2), for ruptured-patch. In Na^+-free pipette solution (0 Na_i, see Supplement), Na_2ATP and Na_2GTP were replaced by equimolar MgATP and TrisGTP, respectively.

Intracellular Ca^{2+} measurements

INS-1E cells were incubated with 10 μM Fluo4-AM for 45 min. Emitted fluorescence was measured at 535 nm; raw fluorescence (*F*) signals were normalized to the baseline fluorescence before initiation of the depolarization protocol (F_0).

In I-clamp measurements, V_m and $[Ca]_I$ were simultaneously recorded during exposures to different experimental solutions.

In V-clamp experiments, $[Ca^{2+}]_I$ increments were evoked by 1-s step depolarizations from −80 to 0 mV in the perforated-patch configuration and quantified as the $\Delta F/F_0$ ratio averaged during the last 10 ms before repolarization.

All experiments were performed in Krebs solution plus 50 μM tolbutamide.

Real-Time qPCR (RTq-PCR)

Relative quantification of mRNAs encoding *Slick* (Slo2.1), *Slack* (Slo2.2), and Na_V isoforms was measured in triplicates from three different INS-1E cell lysates with the comparative ΔΔCt method [25] and normalized for β-actin.

Western blotting analysis

Western blot analysis with Anti-*Slick* and Anti-*Slack* antibodies (Alomone Labs, Israel) was performed on three different microsome preparations from INS-1E cells. Samples (15 μg protein/lane) were separated by SDS–polyacrylamide gel electrophoresis (Criterion XT, Bio-Rad), blotted on nitrocellulose membrane (Bio-Rad) for 90 min, and incubated overnight at 4 °C with specific primary antibodies followed by 1-h incubation with fluorescent secondary antibodies (Alexa Fluor, 680 nm, red, Invitrogen; IRDye, 800 nm, green, Rockland). Western blotting was analyzed and quantified by Odyssey Infrared Imaging Detection System (LI-COR Biosciences).

Insulin secretion

Secretion was measured 2 days after cell plating in multi-wells containing culture cell medium at a density of 50,000 cells/well. Forty-five minutes before secretion measurements, the medium was replaced by the same extracellular solution used for electrophysiology (Krebs) supplemented with 0.1 % BSA (glucose-free). Glucose concentration was then increased from 2.5 to 20 mM for 1 h in the presence of test drugs. Insulin was measured in wells supernatant by a FRET-based assay (HTRF Cisbio). Glucose-stimulated insulin secretion (GSIS) was defined as insulin concentration at 1 h after switching to 20 mM glucose.

Chronic hyperglycemia model

Chronic hyperglycemia (CHG) was simulated as described by Wang et al. [45]. Briefly, after plating, INS-1E cells were kept in glucose-free medium overnight and then switched to complete medium containing either normal (10 mM) glucose (CNG group), high (33 mM) glucose (CHG group), 33 mM glucose+10 μM RAN (CHG+RAN group), or 33 mM glucose+0.5 μM TTX (CHG+TTX) for 24 h. Because potentially contributing to the effects of hyperglycemia, the osmolarity increment between CNG and CHG solutions was not compensated. Before measurements, preparations were rinsed twice with Krebs (2.5 mM glucose). Insulin concentrations were measured at 2.5 and 20 mM glucose. Because in the setting of CHG the number of cells could vary significantly, for each well, insulin concentrations were normalized to total protein content (Bradford assay).

Substances

The RTq-PCR reagents were purchased from Bio-Rad (USA), the HTRF assay kit from Cisbio (France), and Fluo4-AM from Molecular Probes (Italy). RAN was provided by Gilead (USA) and TTX and VERA by Alomone Labs (Israel); all the remaining substances were supplied by Sigma (Italy). Anti-*Slick* and anti-*Slack* antibodies were purchased from Alomone Labs (Israel). RAN was dissolved in HCl 0.1 M (titrated to pH 7.4 in final solution); VERA, TOLB, and bithionol were dissolved in DMSO, whose concentration was kept below 0.2 % and constant throughout solutions.

Statistical analysis

All data were analyzed using paired or unpaired *t* test, as appropriate. Multiple comparisons were performed by one-way ANOVA with Tukey's correction. P values<0.05 were considered as significant.

Results

Except for I_{NaL} comparison between INS-1E and human islet cells, experiments were performed in INS-1E cells.

I_{NaL} impact on glucose- and tolbutamide-stimulated electrical activity

Exposure to either 20 mM glucose (HG) or the I_{KATP} blocker TOLB (50 μM) was used as the "activatory" stimuli. The effect of TTX and RAN on V_m was tested under normal conditions in activated cells at baseline and during I_{NaL} enhancement by VERA.

V_m response to activation (either by HG or TOLB) was variable among cells, including initiation of sustained action potential (AP) firing, generally superimposed on weaker depolarization or, more frequently, stronger depolarizations with null or only transient AP firing (Fig. 1). The dual response pattern was exploited to test modulation of V_m and AP firing rate separately. When AP firing was absent, TTX and RAN slightly but consistently hyperpolarized V_m (Fig. 1a). When sustained AP firing was present, it was abolished, or its frequency reduced, by both agents (Fig. 1b, c). In few cases, AP firing, found to be insensitive to RAN, was promptly abolished by nifedipine (not shown), thus suggesting the occasional presence of Ca^{2+}-dependent excitability.

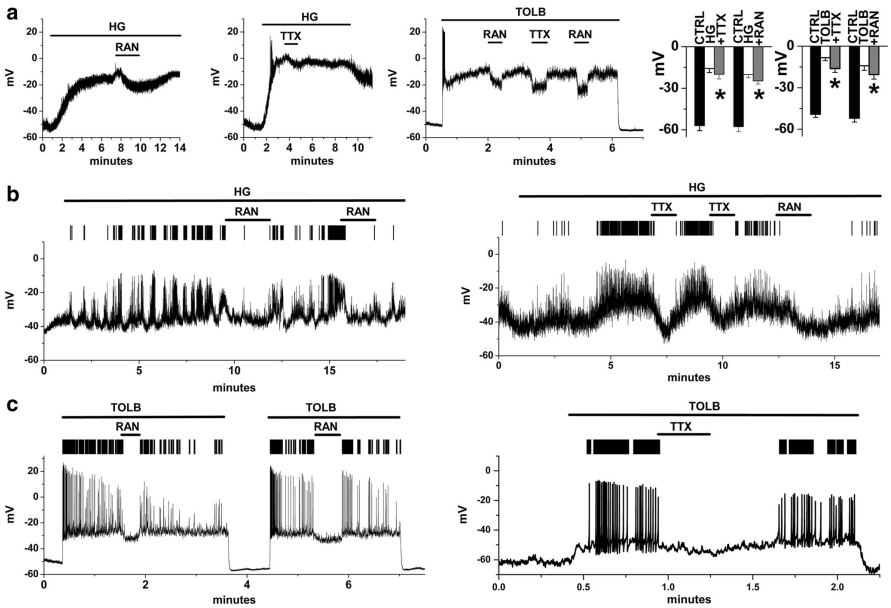

Fig. 1 Effect of RAN and TTX on glucose- and tolbutamide-induced electrical activity. **a** Examples of TTX (0.5 μM) and RAN (10 μM) effect on membrane potential in INS-1E cells responding to activation by glucose (*HG*) or tolbutamide (*TOLB*) with membrane depolarization only (no AP firing); the histogram shows statistics from $N \geq 6$ for each group; $^*p<0.05$ vs control. **b**, **c** TTX and RAN effect on AP firing induced by HG or TOLB; APs were detected with a threshold of −20 mV and are highlighted on the *top of each panel*. Experiments were performed in perforated-patch condition

During TOLB-induced activation, VERA strongly depolarized V_m and abolished AP firing. TTX and, to a lesser extent, RAN opposed VERA-induced depolarization (Fig. S2).

Na_V isoform expression pattern in INS-1E cells

RT-qPCR analysis, performed on INS-1E cells, revealed transcripts for several voltage-gated Na^+ channel isoforms, mainly represented by Na_V 1.3 and Na_V 1.6 (Fig. 2).

Steady-state I_{TTX} and I_{RAN} in INS-1E and human islet cells

I_{TTX} and I_{RAN} were isolated as subtraction currents in the whole-cell (ruptured-patch) configuration during the voltage ramp protocol; therefore, they largely reflect I_{NaL} only (see "Materials and methods").

In INS-1E cells, I_{TTX} and I_{RAN} displayed similar inward current density (Mean I_{IN}) and reversal potential (E_{REV}), but current activation threshold (E_{TH}) was significantly more negative for I_{TTX} than for I_{RAN} (Fig. 3a). In human islet cells, I_{RAN} was smaller than I_{TTX} but, at variance with INS-1E cells, E_{TH} was similar between the two currents (Fig. 3b). Despite these small differences, possibly suggestive of a different balance in the expression of Na_V isoforms, overall current profile was similar between the two cell types.

E_{REV} values of I_{RAN} and I_{TTX} were markedly negative to the one expected for a pure Na^+ conductance (E_{Na}=+64 mV) (Fig. 3). This suggests contribution to subtraction currents of a conductance with a negative E_{REV}. This may imply either incomplete selectivity of channel blockers or functional coupling of I_{Na} with another current.

Nature of the outward component of I_{TTX} and I_{RAN}

We tested whether a Na^+-activated current contributed to the outward component of I_{TTX} and I_{RAN}; to this end, we exploited the property of Li^+ to permeate Na^+ channels without affecting Na^+-activated ones [15]. Thus, I_{TTX} and I_{RAN} were measured after substitution of bath Na^+ with equimolar Li^+. As shown in Fig. 4, substitution with Li^+ strongly shifted the E_{REV} of I_{TTX} and I_{RAN} toward E_{Na} and increased their inward components

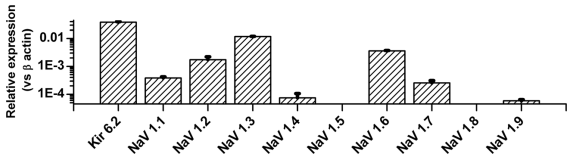

Fig. 2 Na_V channel isoform expression pattern in INS-1E cells. Relative mRNA level expression (vs β-actin) of Na_V channel isoforms quantified by RT-qPCR. The K_{ATP} channel α-subunit K_{ir} 6.2 was used as a positive reference. Experiments were run in triplicates from three RNA extracts

(Mean I_{IN} in Fig. 4a, b). These findings confirm that I_{TTX} and I_{RAN} included an outward component activated by Na^+ influx.

K^+ currents are strongly represented in the global steady-state *I/V* relationship of INS-1E cells (Fig. S3) and are thus candidates to account for outward component of I_{TTX} and I_{RAN}. To test for K^+ channel involvement, I_{TTX} and I_{RAN} were measured in the presence of a cocktail blocking a wide spectrum of K^+ channels (KBK solution). As shown in Fig. S3b, KBK abolished I_{TTX} and I_{RAN} outward components, thus shifting their E_{REV} toward the theoretical E_{Na}. By unveiling the Na^+ component, KBK should have increased the inward components of I_{TTX} and I_{RAN}, as indeed observed in the Li^+ substitution experiment. Contrary to this expectation, KBK did not increase Mean I_{IN} of I_{TTX} and I_{RAN}, thus suggesting ancillary Na^+ channel blockade by KBK components [26, 28]. Nevertheless, E_{REV} sensitivity to KBK indicates that the outward component of I_{TTX} and I_{RAN} was carried by K^+. As an attempt to block K^+ channels more selectively, K^+ was replaced with Cs^+ in intra- and extracellular solutions; unfortunately, this destabilized pipette seal and killed cells shortly after patch rupture.

If considered together, the results of Li^+ replacement and KBK experiments strongly suggest Na^+-activated K^+ channels (KNaC) to be responsible for the outward component of I_{TTX} and contribute to that of I_{RAN}. Such a Na^+-dependent outward component is therefore referred to as I_{KNa}.

Whereas TTX is highly specific for Na^+ channels, RAN ancillary blockade of ERG-type K^+ channels has been reported at concentrations partially overlapping those required to block I_{NaL} (as reviewed in ref. [49]) and might partially contribute to the outward component of I_{RAN}. To test this hypothesis, I_{RAN} was recorded in the presence of Na^+ channel blockade by TTX. Indeed, this approach unveiled a TTX-resistant, outward I_{RAN} component (Fig. S4). Evidence, presented and discussed in the supplement, suggests that this I_{RAN} component is likely to reflect direct I_{KNa} blockade by the drug, previously reported for quinidine [48].

I_{KNa} molecular identity and functional contribution

Slick and *Slack* proteins are putative candidates to represent the molecular identity of KNaC. Therefore, transcripts of their genes were measured by RTq-PCR on INS-1E cell lysates. Both *Slick* and *Slack* transcripts were clearly detected (Fig. 4c). Robust expression of *Slick* and *Slack* proteins was confirmed by Western blot analysis of INS-1E membrane fractions (Fig. 4d).

Although I_{KNa} is non-selectively inhibited by KBK components [1, 24], tools for its selective blockade are not available. As an alternative approach, I_{KNa} functional expression was evaluated through its enhancement by the specific *Slack*

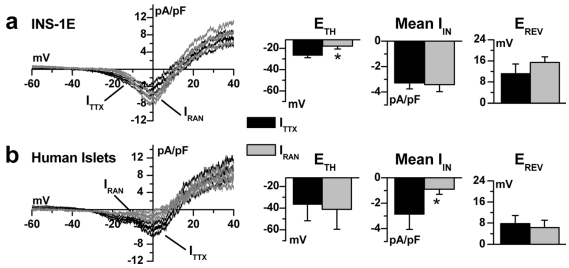

Fig. 3 I_{TTX} and I_{RAN} in INS-1E cells and human islet cells. **a** Average traces±confidence intervals for INS-1E cells (N=16 for I_{TTX} and N=15 for I_{RAN}) and statistics for curve parameters: E_{TH} threshold potential; *Mean* I_{IN} mean inward current; E_{REV} reversal potential. **b** Average traces± SE for cells derived from human islets (N=7 for I_{TTX} and N=6 for I_{RAN}) and statistics for curve parameters. *p<0.05 vs I_{TTX}. E_{TH} of both I_{TTX} and I_{RAN} was more negative in human islet than in INS-1E cells (p<0.05); Mean I_{RAN} was smaller in human islet cells than in INS-1E cells (p<0.05)

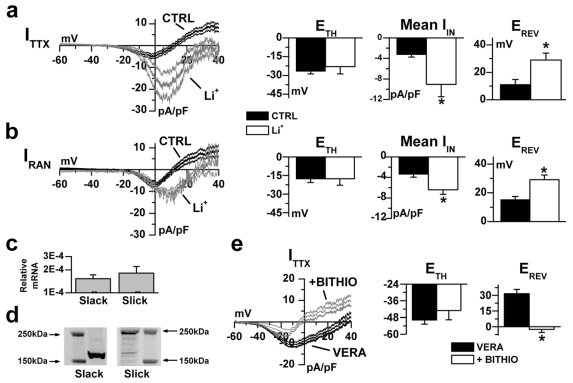

Fig. 4 Nature of the outward component of I_{TTX} and I_{RAN}. I_{TTX} (**a**) and I_{RAN} (**b**) in control (*CTRL*, *black*) and after Na^+ replacement with Li^+ (*gray*). In each panel, mean steady-state *I/V* curves±confidence intervals are shown on the *left*; statistics for curve parameters are shown on the *right*. Abbreviations as in Fig. 3 (I_{TTX}: N=16 for CTRL and 6 for Li^+; I_{RAN}: N=11 for CTRL and 5 for Li^+). *p<0.05 vs CTRL. **c** Relative mRNA level expression (vs β-actin) of *Slick* (Slo2.1) and *Slack* (Slo2.2) channels. Experiments were run in triplicates from three different mRNA extracts. **d** Western blot analysis of *Slick* and *Slack* proteins from INS-1E microsomal fractions. **e** I_{TTX} mean steady-state *I/V* curves±confidence intervals and statistics of curve parameters in 40 μM VERA alone and after I_{KNa} enhancement by 10 μM bithionol (+*BITHIO*) (VERA N=11; + BITHIO N=6). *p<0.05 vs VERA

channel activator bithionol (10 μM) [48]. To ensure sufficient influx of activating Na^+, bithionol effect on I_{TTX} and V_m was tested in the presence of 40 μM VERA. The *I/V* relationship of I_{TTX} was modified by bithionol in a way compatible to the activation of a large K^+ conductance (Fig. 4e). In spite of its remarkable impact on *I/V* contour, bithionol did not affect I_{TTX} activation threshold (E_{TH}), thus suggesting that I_{KNa} threshold is either equal to or more positive than I_{NaL} one. Bithionol significantly hyperpolarized V_m (Fig. S3c).

I_{Na}-dependent modulation of intracellular Ca^{2+}

Insulin secretion process is triggered by increments of cytosolic Ca^{2+}, potentially resulting from enhanced Na^+ influx.

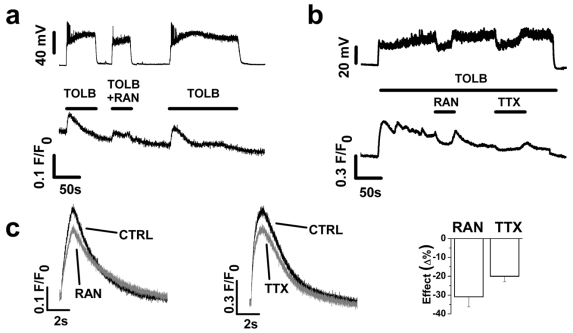

Fig. 5 Effect of RAN and TTX on intracellular Ca^{2+}. Examples of response of V_m and intracellular Ca^{2+} ($[Ca]_I$) to I_{NaL} blockade during TOLB-induced activation. **a** TOLB was repeatedly applied/washed out (*horizontal bars*) in control conditions and in the presence of RAN. **b** TTX or RAN was subsequently applied/washed out (*horizontal bars*) during sustained TOLB-induced activation (*horizontal bar*). **c** Effect of RAN and TTX on $[Ca]_I$ responses to depolarization at a constant potential (from −80 to 0 mV for 1 s). Statistics of RAN (N=6) and TTX (N=6) effects on $[Ca]_I$ amplitude are shown on the *right*. Experiments were performed in perforated-patch condition

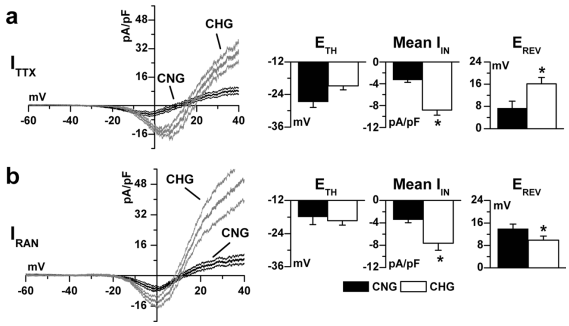

Fig. 6 Effect of chronic exposure to high glucose (*CHG*) on I_{TTX} and I_{RAN}. I_{TTX} (**a**) and I_{RAN} (**b**) after 24-h incubation in normal glucose (10 mM; *CNG*, *black*) or high glucose (33 mM, *CHG*, *gray*). In each panel, mean steady-state *I*/*V* curves±confidence intervals are shown on the *left*; statistics for curve parameters are shown on the *right* (abbreviations as in Fig. 3). (I_{TTX} CTRL N=16, CHG N=9; I_{RAN} CTRL N=11, CHG N=11). *p<0.05 vs CNG

Thus, the effect of I_{Na} modulation on intracellular Ca^{2+} ($[Ca^{2+}]_I$) was tested in Fluo4-AM (10 μM)-loaded INS-1E cells. In several TOLB-activated cells, V_m and $[Ca]_I$ were simultaneously measured under I-clamp conditions (Fig. 5). TOLB-induced depolarization, whether or not triggering AP firing, consistently increased $[Ca]_I$. RAN partially blunted TOLB-induced V_m and $[Ca]_I$ changes (Fig. 5a). When applied during sustained TOLB challenge (Fig. 5b), RAN (or TTX) hyperpolarized V_m and reduced $[Ca]_I$ reversibly; $[Ca]_I$ overshoot followed V_m depolarization upon washout.

To assess whether RAN- and TTX-induced changes in $[Ca]_I$ were just the consequence of V_m changes, depolarization-induced $[Ca^{2+}]_I$ accumulation was tested under V-clamp conditions. RAN or TTX significantly blunted $[Ca^{2+}]_I$ accumulation during steps at a constant V_m (Fig. 5c).

I_{NaL} modulation by chronic exposure to high glucose (CHG)

The above findings indicate that I_{NaL} is normally expressed in β-cells and may thus be involved in their physiology. Nevertheless, as in other tissues, pathophysiological significance of I_{NaL} may require its enhancement under clinically relevant conditions [4, 40], which in diabetes may be represented by chronic cell exposure to high glucose [45]. Thus, INS-1E cells incubated for 24 h in a medium containing 33 mM glucose (CHG) [45] were compared to cells incubated for the same period in 10 mM glucose (CNG) (Fig. 6). For both treatment groups, I_{TTX} and I_{RAN} were then measured in 2.5 mM glucose+50 μM TOLB.

CHG increased both I_{TTX} and I_{RAN}; nevertheless, minor details distinguished their response to CHG (Fig. 6). In particular, while the E_{REV} of I_{TTX} shifted by about +8 mV, I_{RAN} reversal tended to change in the opposite direction.

Modulation of insulin secretion after normal- and high-glucose incubation

The effect of I_{NaL} modulation was initially tested on insulin secretion triggered by 20 mM glucose. Under these conditions, secretion was slightly reduced by TTX only. VERA sharply increased insulin secretion, an effect significantly, but incompletely, countered by both RAN and TTX (Fig. 7a). Then, the effect of long-term exposure to high glucose (CHG) was evaluated. To this end, cells were subjected to 24 h incubation in normal (10 mM) glucose (CNG) or high glucose (33 mM, CHG); RAN or TTX was added to the CHG incubation media. To ensure that CHG effect did not reflect a massive loss of cell mass, insulin concentration was normalized to total protein content of each well. CHG was apparently without effect on insulin secretion at 20 mM glucose; thus, its effect was further evaluated by measuring the change in insulin concentration (Δ_{Ins}, normalized to total protein content) when glucose was stepped from 2.5 to 20 mM (Fig. 7b). A robust Δ_{Ins} was observed in the CNG group. In the CHG group, baseline insulin concentration was doubled (0.43 vs 0.19 ng/μg protein; p<0.05 vs CNG), but Δ_{Ins} was completely abolished. When RAN or TTX was added to the CHG incubation medium, Δ_{Ins} was restored because of a reduction in baseline insulin concentration. Notably, neither RAN nor TTX significantly affected absolute insulin concentration at 20 mM glucose in the CHG group, to suggest that under this condition, secretion was already maximized at baseline (2.5 mM glucose).

Discussion

The observations most relevant to β-cell pathophysiology and pharmacology can be summarized as follows: (1) I_{NaL} was significantly expressed in INS-1E and human islet cells with similar density and V dependency; (2) I_{NaL} was coupled,

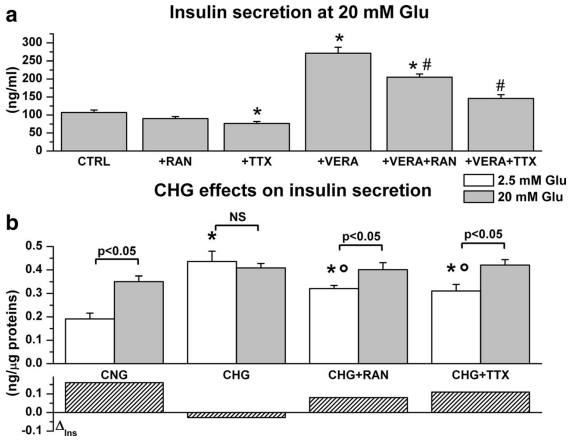

Fig. 7 Effect of CHG on insulin secretion and its modification by I_{NaL} modulators. **a** Effect of TTX, RAN, and VERA (N=9) on insulin secretion during exposure to 20 mM glucose; substances were applied at the same concentration used for electrophysiology. *p<0.05 vs CTRL; #p<0.05 vs VERA. **b** Insulin secretion at 2.5 mM (*white bars*) and 20 mM (*gray bars*) glucose after chronic incubation in 10 mM glucose (*CNG*), 33 mM glucose (*CHG*) alone, CHG+RAN, and CHG+TTX. N= 6 for each group; Δ_{Ins} = change in insulin concentration between 2.5 and 20 mM glucose; *p<0.05 vs CNG; °p<0.05 vs CHG. For each condition, the statistical comparison between 2.5 and 20 mM glucose is given *above the bars*

through Na^+ influx, to a K^+ conductance (I_{KNa}), putatively mediated by *Slack* channels, which were robustly expressed in INS-1E cells; (3) during cell activation, I_{Na} blockade (by RAN or TTX) caused slight V_m hyperpolarization and a decrease in AP firing rate, both accompanied by decreases in $[Ca]_I$; (4) I_{Na} blockade reduced $[Ca^{2+}]_I$ also under V-clamp; therefore, $[Ca]_I$ decrement was independent of V_m changes; (5) I_{NaL} was permanently enhanced by CHG, a condition relevant to diabetes; and (6) I_{Na} blockade marginally affected absolute insulin secretion in all conditions except pharmacological I_{NaL} enhancement; nevertheless, RAN and TTX countered CHG-induced increment in basal insulin "leak," thus restoring the secretory response to glucose challenge.

Effect of RAN and TTX on membrane potential

During glucose- or TOLB-induced activation, both TTX and RAN hyperpolarized V_m and reduced AP firing. While the former effect can be readily attributed to I_{NaL} inhibition, AP firing is supported by I_{NaT} instead; thus, its inhibition argues against selective I_{NaL} blockade by RAN in the present setting. The easiest explanation for this is the rather positive V_m at which AP firing occurs and the known loss of RAN selectivity for I_{NaL} when Na^+ channels are partially inactivated [9]. Therefore, for what concerns modulation of electrical activity in insulin-secreting cells, RAN might act as an outright I_{Na} blocker, rather than a selective I_{NaL} one. On the other hand, the observation that RAN (or TTX) affected $[Ca]_I$ irrespective of the presence of AP suggests that I_{NaL} selectivity may not be crucial in this case. This view is consistent with the notion that AP firing is not crucial for insulin secretion [20]. Nevertheless, because of selectivity in cardiac muscle, I_{NaL} inhibition achievable in islet cells at therapeutic concentration might be still stronger for RAN than for other agents.

Expression of Na_V isoforms

INS-1E cells expressed transcripts for several TTX-sensitive channels (Na_V 1.1 to 1.4, 1.6, and 1.7) (Fig. 2) [10]; among them, Na_V 1.3 to 1.7 are also RAN-sensitive [21, 35, 43]. Such Na_V expression pattern is closer to that of human islets than to that of rat islets [12]. Consistent with Na_V expression pattern, I_{TTX} was similar between INS-1E and human islet cells (Fig. 3), with the exception of E_{TH}, slightly more negative in human islet cells. In human islets, inward I_{RAN} was smaller, but the current profile was otherwise similar, to I_{TTX}. The notion that I_{TTX} or I_{RAN} actually result from a balance between inward and outward components should be kept in mind while interpreting differences in inward current density.

Similarity of Na_V expression pattern and current profiles between INS-1E and human islet cells supports suitability of

this cell line as an experimental model I_{Na} modulation in insulin-secreting cells.

I_{NaL}–I_{KNa} coupling

Tight functional coupling between I_{NaL} and I_{KNa} has been previously described in central neurons [8] and recently confirmed in olfactory neurons [19]. These studies converge to suggest that channel co-localization may underlie the crosstalk.

The E_{REV} of I_{TTX} and I_{RAN} was largely negative to the value expected for selective Na^+ currents; Na^+ substitution with Li^+ or wide-spectrum blockade of K^+ channels (KBK solution) strongly shifted E_{REV} to approach the theoretical E_{Na} (Figs. 4 and S3). Altogether, these findings point to the presence of a K^+ current carried by Na^+-sensitive K^+ channels (I_{KNa}). Unlike TTX, RAN also blocks ERG-type K^+ current (I_{ERG}) [36], which is expressed in pancreatic β-cells [37]. I_{RAN} did include a TTX-insensitive outward component (Fig. S4a), but such component became negligible when intracellular Na^+ was removed (Fig. S4b) and is thus unlikely to reflect I_{ERG}. Failure of I_{ERG} to contribute to I_{RAN} may be due to its substantial inactivation during the ramp protocol and does not argue against I_{ERG} contribution to "phasic" electrical activity (e.g., AP repolarization).

Bithionol, albeit strongly shifting the E_{REV} of I_{TTX}, failed to change its E_{TH} (Fig. 4e), consistent with the intrinsic V dependency of I_{KNa}, reported to activate around 0 mV in auditory neurons [47].

Coupling to I_{KNa} may limit the impact of I_{NaL} changes on V_m and, with it, the effect of its blockade on electrical activity and $[Ca]_I$ balance. On the other hand, I-clamp experiments showed that, in normal conditions, I_{NaL} blockade hyperpolarized V_m by several millivolts and slightly decreased $[Ca]_I$ during activation, an action expected to reduce insulin secretion. Since selective I_{KNa} blockers are unavailable, transgenic animal models are required to fully define the physiological relevance of I_{NaL}–I_{KNa} coupling to insulin secretion.

The expression of channels potentially accounting for I_{KNa} was investigated using RT-qPCR and Western blot analysis. *Slick* and *Slack* transcripts were similarly detected, and the respective proteins were robustly expressed in the membrane fraction. These are widely expressed in the nervous system [5, 6, 18, 47]. Only *Slack* is sensitive to enhancement by bithionol [48]. Thus, bithionol effect proves *Slack*'s contribution to I_{KNa} in the present setting; nevertheless, *Slick* contribution cannot be ruled out.

I_{NaL} is enhanced by long-term exposure to high glucose

A central finding of this work is constitutive enhancement of I_{TTX} and I_{RAN} after chronic exposure to 33 mM glucose (Fig. 6). The term "constitutive" refers to the observation that, once induced by CHG, the enhancement persisted in the presence of low glucose and may thus represent a long-lasting channel modification. The mechanism underlying I_{NaL} enhancement by chronic exposure to high glucose was not investigated in the present study; however, multiple candidate mechanisms are suggested by previous ones. Chronic exposure to high glucose enhances production of reactive oxygen species [23], a well-known cause of I_{NaL} enhancement [34, 38]. Moreover, it has been recently shown that hyperglycemic stress directly activates Ca-calmodulin-kinase II (CaMKII) [16], probably the ultimate molecular trigger of I_{NaL} enhancement by various conditions [42]. Increased firing and prolonged AP, suggestive of I_{NaL} enhancement, have been actually described in α-cells of diabetic rats [22].

I_{NaL} is linked to Ca^{2+} homeostasis, which may thus be chronically perturbed by CHG-induced I_{NaL} enhancement. Whereas acute increment of $[Ca^{2+}]_I$ is expected to stimulate insulin secretion [14], the only previous information on the effect of persistently elevated $[Ca^{2+}]_I$ levels concerned prevention of CHG-induced apoptosis by nifedipine [45]. The observation that RAN prevented β-cell loss in mice with streptozotocin-induced diabetes [32] is in line with this observation and conceptually reminiscent of myocardial response to persistent I_{NaL} enhancement, i.e., transient increase in contractility followed by maladaptive remodeling [49]. The present observations add to this picture by showing that I_{NaL} enhancement by CHG may impair the secretory response to glucose also through a functional mechanism (see below).

Modulation of insulin secretion

Na^+ channels were first described in pancreatic β-cells in 1977 [13]; nevertheless, their functional impact on insulin secretion is still debated. Theoretically, I_{Na} might contribute to the voltage-triggered component of glucose-stimulated insulin secretion in two ways: (1) its transient component (I_{NaT}) may support AP firing, triggering Ca^{2+} influx through high threshold Ca^{2+} channels; (2) Na^+ influx, also supported by non-inactivating components (I_{NaL}) potentially unrelated to action potential firing, may contribute to Ca^{2+} loading through the Na^+/Ca^{2+} exchanger (NCX). Global I_{Na} blockade by TTX (at concentrations blocking TTX-sensitive channels only) had negligible effects on insulin secretion from mouse pancreatic islets [29] but inhibited insulin secretion from human islets [3]. Overall, action potential firing does not seem to be essential for V-triggered insulin secretion [20], and its quantitative contribution may be species-dependent.

On the other hand, insulin secretion was found to be positively correlated with intracellular Na^+ levels during acute exposure to a range of experimental conditions [13]. Consistent with this view, I_{Na} blockade by reduced insulin secretion (at 20 mM glucose) marginally under normal conditions and more substantially after it had been increased by VERA (Fig. 7). This effect is

paradoxically opposite to that required to explain RAN-induced insulin secretion in diabetic rats [32]. However, the pattern of secretory responses was quite different in the CHG group. As expected from constitutive I_{NaL} enhancement, CHG increased insulin secretion, but it did so mostly under unstimulated conditions (2.5 glucose), at the same time abolishing the secretory response to 20 mM glucose (Δ_{Ins}, Fig. 7b). CHG effect was largely reversed by incubation with both RAN and TTX, thus suggesting I_{NaL} involvement. Even if magnitude is potentially insufficient to fully account for improved glycemic control, the effects of I_{Na} blockade in the CHG group are at least suitable to contribute. One caveat inherent to this interpretation is that, even if enhanced by CHG, I_{NaL} threshold remains far positive to the V_m present at 2.5 mM glucose (−60 to −50 mV); thus, it cannot directly contribute to baseline insulin release. This implies that the I_{NaL}-dependent derangements leading to baseline insulin leak must have taken place during exposure to 33 mM glucose, when V_m was likely in the range appropriate for I_{NaL} activation, to persist after cell activation subsided. Such derangements may be part of a process ultimately leading to islet cell death [32]. However, prevention of increased cell loss in the CHG group is an unlikely explanation for the present observations, because it would be hard to reconcile with increased baseline insulin secretion; furthermore, secreted insulin was normalized to total protein content of the preparations, which is likely to compensate for cell loss. Because cell death cannot be reversed, functional effects, as those described here and by Dhalla and coworkers [12], are required to account for improvement of glycemic control in diabetic patients.

RAN has been shown to promote glucose utilization in muscle cells by activating the Randle cycle [17]. If extended to β-cells, this action might possibly affect insulin secretion independently of I_{NaL} blockade; however, at least in the present setting, RAN effects were shared by TTX, which is devoid of metabolic ancillary actions.

Limitations

The majority of experiments in this study were performed on rat INS-1E cells and extrapolation to native human β-cells requires caution; nevertheless, steady-state I_{TTX} and I_{RAN} were substantially similar between INS-1E and human islet cells, as discussed above. Moreover, it should be stressed that RAN amelioration of glycemic control has already been reported in patients [30], the scope of the present study being limited to test whether I_{NaL} of β-cells could be one molecular target for that effect. The choice to use a pure β-cell preparation (as INS-1E) in secretion studies was primarily motivated by the need to rule out paracrine crosstalk between cell types, which would take place if pancreatic islets were used instead.

Conclusions and translational relevance

This work aimed to test the hypothesis that I_{NaL} might contribute to islet β-cell pathophysiology, as suggested by RAN efficacy to increase insulin secretion from diabetic rat islets [32]. Although confirming such hypothesis, the present results are fully compatible with the contribution of other mechanisms, such as inhibition of glucagon secretion in islet α-cells [12], to RAN action on glucose homeostasis. Physiological response to glycemia perturbation involves paracrine crosstalk between α- and β-cells within the islet environment, dominated by tonic insulin restraint of glucagon secretion [2]. Thus, even if not detectable at plasma level, I_{NaL}-dependent insulin leak during fasting might impair α-cell response to hypoglycemia, a defect that would be countered by I_{NaL} blockade.

Disclosure of I_{Na} functional coupling to I_{KNa} suggests that abnormalities of the latter might impact on the electrical activity of insulin-secreting cells. This may justify inclusion of *Slack* among candidate genes in the screening of abnormalities of glycemic control.

The observation that long-term exposure to high glucose caused I_{NaL} enhancement and adversely affected function of β-cells suggests that the paradigm of I_{NaL} enhancement as cause of disease progression may apply to many cell types [50].

Acknowledgments This work was funded by grants from Gilead, Inc. (Fremont, CA) and Network Enabled Drug Design (NEDD from Regione Lombardia) to A. Zaza.

We thank Dr. Claes Wollheim and coworkers (University of Geneva, Switzerland) for kindly supplying the INS-1E cell line. We are also grateful to Drs. Luiz Belardinelli, Arvinder Dhalla, and Sridhar Rajamani of Gilead, Inc. for reading the manuscript and providing constructive comments and suggestions.

Ethical standards The study was previously reviewed and approved by the Ethical and Scientific Committees of Azienda Ospedaliera-Ospedale Niguarda Ca' Granda (Milan) and the University of Milano-Bicocca. Human islet donors, or their relatives on behalf, gave written consent for collection of organs and cells for transplant and research, following the statements by the Italian Ministry of Health (art. 23, law n. 91 of 1 April 1999).

Conflict of interest The study has been partially funded by Gilead, Inc. (Fremont, CA). All authors declare the absence of further conflict of interest.

References

1. Aoki K, Kosakai K, Yoshino M (2008) Monoaminergic modulation of the Na+-activated K+ channel in Kenyon cells isolated from the mushroom body of the cricket (Gryllus bimaculatus) brain. J Neurophysiol 100:1211–1222
2. Bansal P, Wang Q (2008) Insulin as a physiological modulator of glucagon secretion. Am J Physiol Endocrinol Metab 295:E751–E761
3. Barnett DW, Pressel DM, Misler S (1995) Voltage-dependent Na+ and Ca2+ currents in human pancreatic islet beta-cells: evidence for

roles in the generation of action potentials and insulin secretion. Pflugers Arch 431:272–282
4. Belardinelli L, Shryock JC, Fraser H (2006) Inhibition of the late sodium current as a potential cardioprotective principle: effects of the late sodium current inhibitor ranolazine. Heart 92(Suppl 4):iv6–iv14
5. Bhattacharjee A, Gan L, Kaczmarek LK (2002) Localization of the Slack potassium channel in the rat central nervous system. J Comp Neurol 454:241–254
6. Bhattacharjee A, von Hehn CA, Mei X, Kaczmarek LK (2005) Localization of the Na+-activated K+ channel Slick in the rat central nervous system. J Comp Neurol 484:80–92
7. Braun M, Ramracheya R, Bengtsson M, Zhang Q, Karanauskaite J, Partridge C, Johnson PR, Rorsman P (2008) Voltage-gated ion channels in human pancreatic beta-cells: electrophysiological characterization and role in insulin secretion. Diabetes 57:1618–1628
8. Budelli G, Hage TA, Wei A, Rojas P, Jong YJ, O'Malley K, Salkoff L (2009) Na+-activated K+ channels express a large delayed outward current in neurons during normal physiology. Nat Neurosci 12:745–750
9. Burashnikov A, Di Diego JM, Zygmunt AC, Belardinelli L, Antzelevitch C (2007) Atrium-selective sodium channel block as a strategy for suppression of atrial fibrillation: differences in sodium channel inactivation between atria and ventricles and the role of ranolazine. Circulation 116:1449–1457
10. Catterall WA, Goldin AL, Waxman SG (2003) International Union of Pharmacology. XXXIX. Compendium of voltage-gated ion channels: sodium channels. Pharmacol Rev 55:575–578
11. Chen WJ, Liu XY, Wang LX, Wang YP, Liu XH, Liu LB (2011) Oxidative damage to the endoplasmic reticulum stress pathway of apoptosis-related molecules expression in MIN6 cell. Xi Bao Yu Fen Zi Mian Yi Xue Za Zhi 27:249–252, 256
12. Dhalla AK, Yang M, Ning Y, Kahlig KM, Krause M, Rajamani S, Belardinelli L (2014) Blockade of Na+ channels in pancreatic alpha-cells has anti-diabetic effects. Diabetes. doi:10.2337/db13-1562
13. Donatsch P, Lowe DA, Richardson BP, Taylor P (1977) The functional significance of sodium channels in pancreatic beta-cell membranes. J Physiol 267:357–376
14. Eberhardson M, Grapengiesser E (1999) Role of voltage-dependent Na+ channels for rhythmic Ca2+ signalling in glucose-stimulated mouse pancreatic beta-cells. Cell Signal 11:343–348
15. Egan TM, Dagan D, Kupper J, Levitan IB (1992) Properties and rundown of sodium-activated potassium channels in rat olfactory bulb neurons. J Neurosci 12:1964–1976
16. Erickson JR, Pereira L, Wang L, Han G, Ferguson A, Dao K, Copeland RJ, Despa F, Hart GW, Ripplinger CM, Bers DM (2013) Diabetic hyperglycaemia activates CaMKII and arrhythmias by O-linked glycosylation. Nature 502:372–376
17. Fang YH, Piao L, Hong ZG, Toth PT, Marsboom G, Bache-Wiig P, Rehman J, Archer SL (2012) Therapeutic inhibition of fatty acid oxidation in right ventricular hypertrophy: exploiting Randle's cycle. J Mol Med-JMM 90:31–43
18. Gao SB, Wu Y, Lu CX, Guo ZH, Li CH, Ding JP (2008) Slack and Slick KNa channels are required for the depolarizing afterpotential of acutely isolated, medium diameter rat dorsal root ganglion neurons. Acta Pharmacol Sin 29:899–905
19. Hage TA, Salkoff L (2012) Sodium-activated potassium channels are functionally coupled to persistent sodium currents. J Neurosci 32: 2714–2721
20. Hatlapatka K, Willenborg M, Rustenbeck I (2009) Plasma membrane depolarization as a determinant of the first phase of insulin secretion. Am J Physiol Endocrinol Metab 297: E315–E322
21. Hirakawa R, El Bizri N, Shryock JC, Belardinelli L, Rajamani S (2012) Block of Na+ currents and suppression of action potentials in embryonic rat dorsal root ganglion neurons by ranolazine. Neuropharmacology 62:2251–2260
22. Huang YC, Rupnik MS, Karimian N, Herrera PL, Gilon P, Feng ZP, Gaisano HY (2013) In situ electrophysiological examination of pancreatic alpha cells in the streptozotocin-induced diabetes model, revealing the cellular basis of glucagon hypersecretion. Diabetes 62:519–530
23. Kaneto H, Katakami N, Matsuhisa M, Matsuoka TA (2010) Role of reactive oxygen species in the progression of type 2 diabetes and atherosclerosis. Mediat Inflamm 2010:453892
24. Kim YC, Sim JH, Kang TM, Suzuki H, Kim SR, Kwon SC, Xu WX, Lee SJ, Kim KW (2007) Sodium-activated potassium current in guinea pig gastric myocytes. J Korean Med Sci 22:57–62
25. Livak KJ, Schmittgen TD (2001) Analysis of relative gene expression data using real-time quantitative PCR and the 2(−delta delta C(T)) method. Methods 25:402–408
26. Lu BX, Liu LY, Liao L, Zhang ZH, Mei YA (2005) Inhibition of Na+ channel currents in rat myoblasts by 4-aminopyridine. Toxicol Appl Pharmacol 207:275–282
27. McCormack JG, Barr RL, Wolff AA, Lopaschuk GD (1996) Ranolazine stimulates glucose oxidation in normoxic, ischemic, and reperfused ischemic rat hearts. Circulation 93:135–142
28. Mei YA, Wu MM, Huan CL, Sun JT, Zhou HQ, Zhang ZH (2000) 4-Aminopyridine, a specific blocker of K(+) channels, inhibited inward Na(+) current in rat cerebellar granule cells. Brain Res 873:46–53
29. Meissner HP, Schmelz H (1974) Membrane potential of beta-cells in pancreatic islets. Pflugers Arch 351:195–206
30. Morrow DA, Scirica BM, Chaitman BR, McGuire DK, Murphy SA, Karwatowska-Prokopczuk E, McCabe CH, Braunwald E (2009) Evaluation of the glycometabolic effects of ranolazine in patients with and without diabetes mellitus in the MERLIN-TIMI 36 randomized controlled trial. Circulation 119:2032–2039
31. Nesher R, Anteby E, Yedovizky M, Warwar N, Kaiser N, Cerasi E (2002) Beta-cell protein kinases and the dynamics of the insulin response to glucose. Diabetes 51(Suppl 1):S68–S73
32. Ning Y, Zhen W, Fu Z, Jiang J, Liu D, Belardinelli L, Dhalla AK (2011) Ranolazine increases beta-cell survival and improves glucose homeostasis in low-dose streptozotocin-induced diabetes in mice. J Pharmacol Exp Ther 337:50–58
33. Pressel DM, Misler S (1990) Sodium channels contribute to action potential generation in canine and human pancreatic islet B cells. J Membr Biol 116:273–280
34. Qian C, Ma J, Zhang P, Luo A, Wang C, Ren Z, Kong L, Zhang S, Wang X, Wu Y (2012) Resveratrol attenuates the Na(+)-dependent intracellular Ca(2+) overload by inhibiting H(2)O(2)-induced increase in late sodium current in ventricular myocytes. PLoS One 7:e51358
35. Rajamani S, Shryock JC, Belardinelli L (2008) Block of tetrodotoxin-sensitive, Na(V)1.7 and tetrodotoxin-resistant, Na(V)1.8, Na+ channels by ranolazine. Channels (Austin) 2:449–460
36. Rajamani S, Shryock JC, Belardinelli L (2008) Rapid kinetic interactions of ranolazine with HERG K+ current. J Cardiovasc Pharmacol 51:581–589
37. Rosati B, Marchetti P, Crociani O, Lecchi M, Lupi R, Arcangeli A, Olivotto M, Wanke E (2000) Glucose- and arginine-induced insulin secretion by human pancreatic beta-cells: the role of HERG K(+) channels in firing and release. FASEB J 14:2601–2610
38. Song Y, Shryock JC, Wagner S, Maier LS, Belardinelli L (2006) Blocking late sodium current reduces hydrogen peroxide-induced arrhythmogenic activity and contractile dysfunction. J Pharmacol Exp Ther 318:214–222
39. Stafstrom CE (2007) Persistent sodium current and its role in epilepsy. Epilepsy Curr 7:15–22
40. Undrovinas A, Maltsev VA (2008) Late sodium current is a new therapeutic target to improve contractility and rhythm in failing heart. Cardiovasc Hematol Agents Med Chem 6:348–359
41. Undrovinas NA, Maltsev VA, Belardinelli L, Sabbah HN, Undrovinas A (2010) Late sodium current contributes to diastolic cell Ca2+ accumulation in chronic heart failure. J Physiol Sci 60: 245–257

42. Wagner S, Dybkova N, Rasenack EC, Jacobshagen C, Fabritz L, Kirchhof P, Maier SK, Zhang T, Hasenfuss G, Brown JH, Bers DM et al (2006) Ca/calmodulin-dependent protein kinase II regulates cardiac Na channels. J Clin Invest 116:3127–3138
43. Wang GK, Calderon J, Wang SY (2008) State- and use-dependent block of muscle Nav1.4 and neuronal Nav1.7 voltage-gated Na+ channel isoforms by ranolazine. Mol Pharmacol 73:940–948
44. Wang M, Crager M, Pugazhenthi S (2012) Modulation of apoptosis pathways by oxidative stress and autophagy in beta cells. Exp Diabetes Res 2012:647914
45. Wang Y, Gao L, Li Y, Chen H, Sun Z (2011) Nifedipine protects INS-1 beta-cell from high glucose-induced ER stress and apoptosis. Int J Mol Sci 12:7569–7580
46. Wang Z, Thurmond DC (2009) Mechanisms of biphasic insulin-granule exocytosis—roles of the cytoskeleton, small GTPases and SNARE proteins. J Cell Sci 122:893–903
47. Yang B, Desai R, Kaczmarek LK (2007) Slack and Slick K(Na) channels regulate the accuracy of timing of auditory neurons. J Neurosci 27:2617–2627
48. Yang B, Gribkoff VK, Pan J, Damagnez V, Dworetzky SI, Boissard CG, Bhattacharjee A, Yan Y, Sigworth FJ, Kaczmarek LK (2006) Pharmacological activation and inhibition of Slack (Slo2.2) channels. Neuropharmacology 51:896–906
49. Zaza A, Belardinelli L, Shryock JC (2008) Pathophysiology and pharmacology of the cardiac "late sodium current". Pharmacol Ther 119:326–339
50. Zaza A, Rocchetti M (2013) The late Na+ current—origin and pathophysiological relevance. Cardiovasc Drugs Ther 27:61–68
51. Zhu HL, Wassall RD, Takai M, Morinaga H, Nomura M, Cunnane TC, Teramoto N (2009) Actions of veratridine on tetrodotoxin-sensitive voltage-gated Na currents, Na1.6, in murine vas deferens myocytes. Br J Pharmacol 157:1483–1493

Cardiovascular Research (2015) **105**, 223–232
doi:10.1093/cvr/cvu250

Marine n-3 PUFAs modulate I_{Ks} gating, channel expression, and location in membrane microdomains

Cristina Moreno[1*†‡], Alicia de la Cruz[1‡], Anna Oliveras[2], Sanjay R. Kharche[3], Miriam Guizy[1], Nùria Comes[2], Tomáš Starý[3], Carlotta Ronchi[4], Marcella Rocchetti[4], Isabelle Baró[5], Gildas Loussouarn[5], Antonio Zaza[4], Stefano Severi[3], Antonio Felipe[2], and Carmen Valenzuela[1*]

[1]Instituto de Investigaciones Biomédicas 'Alberto Sols' CSIC-UAM, C/Arturo Duperier 4, 28029 Madrid, Spain; [2]Molecular Physiology Laboratory, Departament de Bioquímica i Biologia Molecular, Institut de Biomedicina (IBUB), Universitat de Barcelona, Barcelona, Spain; [3]Biomedical Engineering Laboratory D.E.I.S., University of Bologna, 47521 Cesena, Italy; [4]Department of Biotechnologies and Biosciences, University of Milano-Bicocca, Milan, Italy; and [5]L'Institut du Thorax, Unité Inserm UMR 1087/CNRS UMR 6291, Nantes, France

Received 9 September 2014; revised 19 November 2014; accepted 21 November 2014; online publish-ahead-of-print 11 December 2014

Time for primary review: 29 days

Aims Polyunsaturated fatty n-3 acids (PUFAs) have been reported to exhibit antiarrhythmic properties. However, the mechanisms of action remain unclear. We studied the electrophysiological effects of eicosapentaenoic acid (EPA) and docosahexaenoic acid (DHA) on I_{Ks}, and on the expression and location of K_v7.1 and KCNE1.

Methods and results Experiments were performed using patch-clamp, western blot, and sucrose gradient techniques in COS7 cells transfected with K_v7.1/KCNE1 channels. Acute perfusion with both PUFAs increased K_v7.1/KCNE1 current, this effect being greater for DHA than for EPA. Similar results were found in guinea pig cardiomyocytes. Acute perfusion of either PUFA slowed the activation kinetics and EPA shifted the activation curve to the left. Conversely, chronic EPA did not modify K_v7.1/KCNE1 current magnitude and shifted the activation curve to the right. Chronic PUFAs decreased the expression of K_v7.1, but not of KCNE1, and induced spatial redistribution of K_v7.1 over the cell membrane. Cholesterol depletion with methyl-β-cyclodextrin increased K_v7.1/KCNE1 current magnitude. Under these conditions, acute EPA produced similar effects than those induced in non-cholesterol-depleted cells. A ventricular action potential computational model suggested antiarrhythmic efficacy of acute PUFA application under I_{Kr} block.

Conclusions We provide evidence that acute application of PUFAs increases K_v7.1/KCNE1 through a probably direct effect, and shows antiarrhythmic efficacy under I_{Kr} block. Conversely, chronic EPA application modifies the channel activity through a change in the K_v7.1/KCNE1 voltage-dependence, correlated with a redistribution of K_v7.1 over the cell membrane. This loss of function may be pro-arrhythmic. This shed light on the controversial effects of PUFAs regarding arrhythmias.

Keywords K_v7.1 • KCNE1 • I_{Ks} • PUFAs • DHA • EPA • Lipid rafts

1. Introduction

A large amount of evidence from cellular and animal studies,[1] and from clinical trials,[2–5] suggested that an increased intake of fish oil fatty acids has favourable effects on cardiovascular health. Analyses of these trials concluded that these beneficial effects mainly occur through the prevention of sudden cardiac death, which is often preceded by ventricular arrhythmias, indicating that polyunsaturated fatty n-3 acids (PUFAs) are antiarrhythmic.[3,6] However, not all studies have demonstrated the cardioprotective effects on cardiovascular diseases of PUFA

* Corresponding author. Tel: +34 91 585 4493; fax: +34 91 585 4401, Email: cvalenzuela@iib.uam.es (C.V.); Email: c.moreno@maastrichtuniversity.nl (C.M.).
† Present address. Department of Cardiology, Cardiovascular Research Institute Maastricht, Maastricht University Medical Centre, Maastricht, The Netherlands.
‡ C.M. and A.d.l.C. equally contributed to this work.

consumption. Pro-arrhythmic actions have been described for PUFAs in animal models during acute regional myocardial ischaemia.[7] Moreover, the recent Alpha OMEGA and OMEGA randomized trials, involving patients who suffered myocardial infarction, did not show any improvement in the clinical results following PUFA supplementation,[8,9] and even a deleterious effect due to an increased risk of cardiac death was reported in men with stable angina who were advised to eat fish,[10] or in patients with implantable cardioverter defibrillators.[11] These differences could be explained by the fact that a diet rich in fish oil could be pro- or antiarrhythmic depending on the underlying arrhythmogenic mechanism.[12] In any case, the mechanism underlying the pro- or antiarrhythmic effect after supplementation is thought to be related to the modulation of the cardiac ion channels involved in the genesis and/or maintenance of cardiac action potentials (APs). Indeed, PUFAs decrease I_{Na}, I_{Kur}, I_{to}, I_{Kr}, I_{CaL}, and I_{NCX}, and enhanced I_{Ks} and I_{K1}.[13–19]

K_v7.1 and KCNE1 are the two major pore-forming and ancillary subunits, respectively, responsible for the biophysical properties of I_{Ks} channels.[20] Doolan *et al.* demonstrated that eicosapentaenoic acid (EPA) and docosahexaenoic acid (DHA) do not modify the electrophysiological characteristics of K_v7.1 channels, although DHA, but not EPA, increases the magnitude of the K_v7.1/KCNE1 current in *Xenopus* oocytes, effect mediated by the KCNE1 subunit.[16] In cardiac myocytes from pigs fed with a PUFA enriched-diet, I_{Ks} magnitude was greater than that recorded in myocytes from control animals.[21] However, the precise mechanism by which PUFAs produce these effects on K_v7.1/KCNE1 channels remains to be elucidated.

2. Methods

2.1 Cell transfection

In acute experiments, transfection of pCDNA3.1 KCNQ1/KCNE1 concatemer (human KCNE1 linked to the N-terminus of the human KCNQ1) in COS7 cells was performed with Fugene6, following manufacturer's instructions. In the rest of experiments, cells were transfected with KCNQ1-YFP and KCNE1-CFP.

2.2 Preparation of cell extracts

COS7 cultures were washed twice with ice-cold PBS. Cells were homogenized and cell extracts were prepared as described in Supplementary material online, Methods.

2.3 Western blot analysis

Samples of cell extracts containing equal amounts of protein were boiled in Laemmli SDS loading buffer (250 mM Tris–HCl, pH 6.8, 2% SDS, 10% glycerol, and 2% β-mercaptoethanol) and size-separated in 7–10% SDS–PAGE. The gels were blotted onto PVDF or nitrocellulose membranes and processed as recommended by the supplier of the antibodies (see Supplementary material online, Methods).

2.4 Lipid rafts

Low-density, Triton-insoluble complexes were isolated as previously described from transfected COS7 cells.[22] Cells were homogenized in 1 mL of 1% Triton X-100 and sucrose was added to a final concentration of 40%. A 5–30% linear sucrose gradient was layered on top and further centrifuged (260 000 *g*) for 20–22 h at 4°C in a Beckman SW41 rotor. Gradient fractions (1 mL) were collected from the top and analysed by western blotting.

2.5 Electrophysiological recordings

Currents were recorded using the perforated amphotericin B or whole-cell patch-clamp technique with an Axopatch 200B amplifier (Axon instruments) as described.[23,24] The investigation conforms to the NIH guidelines (Guide for the Care and Use of Laboratory Animals; NIH publications number 23–80) revised in 2011; and from Directive 2010/63/EU of the European Parliament on the protection of animals used for scientific purposes and approved by the University of Milano-Bicocca ethics review board. Adult Dunkin-Hartley guinea pig was anesthetized by 100 mg/kg sodium thiopental (Sigma Aldrich, St Louis, MO, USA) and euthanized by cervical dislocation. Guinea pig ventricular myocytes were isolated as previously described.[25] Membrane cholesterol depletion was achieved by methyl-β-cyclodextrin (MβCD) treatment (2 μM).

2.6 Statistical analysis

Data are presented as mean values ± SEM. Paired or unpaired Student's *t*-test or repeated-measures ANOVA followed by the Bonferroni test. A value of $P < 0.05$ was considered statistically significant.

2.7 Computational modelling

The K_v7.1/KCNE1 current was described by a Markov model, whose transition rates were set by fitting the experimental recordings obtained in the different conditions. The current formulation was then inserted into the O'Hara–Rudy model of human ventricular action potential. An expanded description is available in Supplementary material online, Methods.

3. Results

3.1 EPA and DHA increase K_v7.1/KCNE1 current

EPA or DHA concentration (20 μM) used in this study was selected on the basis of the free fatty acid levels in the plasma of six patients included in the SOFA trial[26] who were taking 2 g/day fish oil. They exhibited concentrations of free EPA and DHA of ~10 μM (5.0–16.4 μM) that accumulate in atria at expenses of arachidonic acid from phospholipids. *Figure 1A* shows K_v7.1/KCNE1 recordings obtained after applying 12 s pulses from a holding potential of −80 to +60 mV in the absence and in the presence of EPA or DHA. Both PUFAs increased the current by 37.3 ± 6.2% ($P < 0.05$, $n = 13$) and 82.8 ± 27.0% ($P < 0.05$, $n = 13$) for EPA and DHA, respectively. The increase induced by EPA was time-dependent, this effect being greater after longer depolarizing times (3.6 ± 6.2, 28.4 ± 5.3, and 37.3 ± 6.2% after 1.5, 5.5 and 12 s, respectively, $P < 0.05$, $n = 5–13$). However, the DHA-induced increase was not time-dependent (91.8 ± 19.3, 92.7 ± 23.8, and 82.8 ± 26.9%, when measured after 1.5, 5.5, or 12 s pulses, respectively, $P > 0.05$, $n = 4–13$).

The K_v7.1/KCNE1 activation kinetics was described by a biexponential process. *Figure 1B* shows the normalized currents obtained under control conditions and after exposure to EPA or DHA. Under control conditions, the activation time constants arose mean values of $\tau_f = 737 \pm 53$ ms and $\tau_s = 4604 \pm 542$ ms ($n = 16$). EPA slowed the activation kinetics due to an increased contribution of the slow component to the activation process [$A_s/(A_s + A_f) = 0.23 \pm 0.04$ vs. $A_s/(A_s + A_f) = 0.64 \pm 0.05$, $P < 0.05$, $n = 8$; *Figure 1B* inset]. The time constants were not modified after perfusing cells with EPA ($\tau_f = 653 \pm 56$ ms and $\tau_s = 4106 \pm 796$ ms, $P > 0.05$, $n = 8$). Similar results in the activation kinetics were observed for DHA [$A_s/(A_s + A_f) = 0.19 \pm 0.04$ vs.

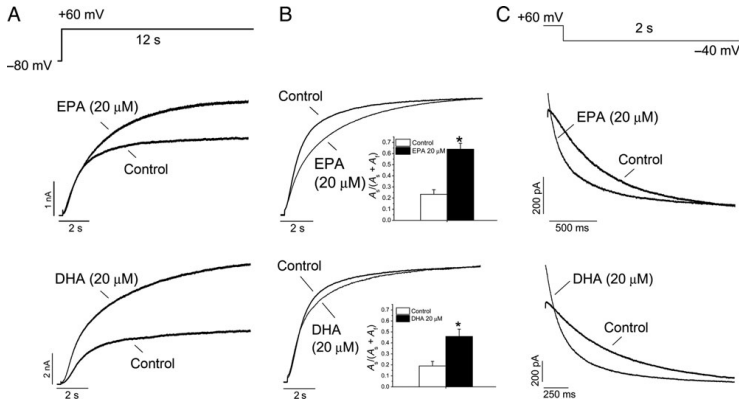

Figure 1 EPA and DHA effects on $K_v7.1$/KCNE1 currents. (*A*) Original traces of $K_v7.1$/KCNE1 current obtained in the absence and in the presence of EPA or DHA. (*B*) Normalized traces. The inset represents the plot of the $A_f/(A_f + A_s)$ in control and in the presence of either PUFA. (*C*) Tail currents recorded at −40 mV after 5.5 s pulses to +60 mV in the absence and in the presence of each PUFA.

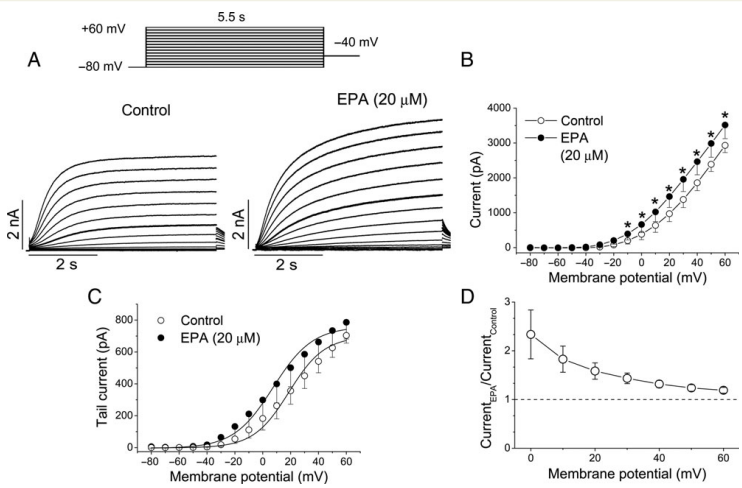

Figure 2 EPA acute effects on $K_v7.1$/KCNE1 channels. (*A*) Traces obtained after applying the pulse protocol shown in the top in the absence and in the presence of EPA. (*B*) *I*–*V* relationship obtained under control conditions and after perfusion with EPA. (*C*) Activation curves obtained under control conditions and after perfusion with EPA. (*D*) Graph showing the ratio between the current obtained in the presence of EPA and that under control conditions.

$A_s/(A_s + A_f) = 0.46 \pm 0.07$, $P < 0.05$, $n = 8$]. However, DHA accelerated the fast component of activation ($\tau_f = 737 \pm 53$ ms vs. $\tau_f = 592 \pm 52$ ms, $P < 0.05$, $n = 8$).

Tail currents were elicited upon repolarization to −40 mV after each voltage step. An increase in the tail current magnitude of 26.5 ± 14.6% ($P < 0.05$, $n = 14$) and 27.3 ± 13.3% ($P < 0.05$, $n = 9$) after exposure

to EPA or DHA was observed (*Figure 1C*). Under control conditions, the deactivation exhibited monoexponential kinetics. However, in the presence of either PUFA, this kinetics became biexponential (see Supplementary material online, *Table S1*).

Figure 2A shows current recordings obtained in the absence and presence of EPA when applying 5.5 s pulses from −80 to +60 mV in 10 mV steps from a holding potential of −80 mV. EPA (20 μM) increased the amplitude of the current at all membrane potentials tested positive to −10 mV (*Figure 2B*) and shifted the V_{mid} of the activation curve towards more negative potentials (+22.3 ± 6.6 vs. +13.5 ± 5.5 mV, $P < 0.05$, $n = 5$) without modifying the slope (16.7 ± 1.3 vs. 18.6 ± 1.7 mV, $P > 0.05$, $n = 5$; *Figure 2C*). *Figure 2D* shows the relative current in the presence of EPA vs. the membrane potential. The maximal increase occurred at ∼0 mV. This effect might be due to the negative shift of the activation curve, suggesting that the primary mechanism of the increased magnitude of K_v7.1/KCNE1 may be due to an effect on channel gating. Similar qualitative effects were produced by DHA (see Supplementary material online, *Figure S1*).

It has been described that the slow gating of I_{Ks} is likely due to the fact that KCNE1 accessory subunit slows the movement of the voltage sensors. To determine that the concatemeric construction does not interfere with the normal properties of I_{Ks} and also to analyse the effects of EPA and DHA, a series of experiments in which the currents were recorded in COS7 cells co-transfected with KCNQ1-YFP and KCNE1-CFP were performed. As shown in Supplementary material online, *Figure S2*, the effects produced by EPA/DHA on I_{Ks} were similar than those observed in cells transfected with the concatemer KCNQ1/KCNE1 subunits. The only difference observed was that the activation kinetics of the K_v7.1/KCNE1 current became monoexponential (see Supplementary material online, *Tables S2–S4*).

Effects of PUFAs were also evaluated on native I_{Ks} recorded in guinea pig ventricular myocytes at 36°C. I_{Ks} was recorded at +20 mV under I_{CaL} and I_{Kr} blockade by nifedipine (10 μM) and E-4031 (5 μM), respectively. A total of 14 myocytes were analysed. In 11 myocytes, DHA (10 μM) increased I_{Ks} amplitude (+37.7 ± 6%, $P < 0.05$) and accelerated its deactivation at −40 mV ($t_{1/2}$ −19.1 ± 8%, $P < 0.05$, see Supplementary material online, *Figure S3*). However, in 5 of 11 myocytes, during long-time recordings, the initial increase of I_{Ks} was followed by a progressive decrease in the current. Moreover, in three myocytes, exposure to 10 μM DHA was directly followed by a decline in I_{Ks} amplitude (data not shown).

3.2 Acute vs. chronic effects of EPA and DHA on K_v7.1/KCNE1 current

An increased consumption of PUFAs leads to increased blood and tissue levels of PUFAs.[26] However, the relative contribution of short- and long-term administration on the electrophysiological effects on ion currents has not been determined. Since we wished to analyse and relate the electrophysiological effects with the effects on the levels of expression and also targeting to the lipid rafts, the same conditions were used in all these experiments: COS7 were co-transfected with KCNQ1-YFP and KCNE1-CFP for 48 h with 20 μM EPA/DHA in serum-free medium. Controls of these experiments were COS7 cells cotransfected with KCNQ1-YFP and KCNE1-CFP incubated for 48 h in serum-free medium without EPA/DHA. To differentiate the acute from the possible chronic effects of EPA and DHA, three different approaches were used. First, we analysed the electrophysiological properties of K_v7.1/KCNE1 currents. Incubation with EPA did not alter the activation kinetics of K_v7.1/KCNE1 (*Figure 3*; $\tau_f = 649 \pm 42$ ms and $\tau_s = 5151 \pm 788$ ms vs. $\tau_f = 771 \pm 89$ ms and $\tau_s = 5112 \pm 1091$ ms, $P > 0.05$, $n = 9–18$, for control conditions and chronic EPA, respectively). DHA accelerated the activation τ_s ($\tau_f = 649 \pm 42$ ms and $\tau_s = 5151 \pm 788$ ms vs. $\tau_f = 587 \pm 74$ ms, $P > 0.05$ and $\tau_s = 3100 \pm 4291$ ms, $P < 0.05$, $n = 9–18$, for control conditions and chronic DHA, respectively, see Supplementary material online, *Figure S4*). The deactivation kinetics was faster than under control conditions, becoming biexponential ($\tau_f = 266 \pm 40$ ms and $\tau_s = 847 \pm 108$ ms for chronic EPA, $n = 9$; and $\tau_f = 296 \pm 26$ ms and $\tau_s = 1235 \pm 171$ ms in serum-free control conditions, $n = 18$), but slower than for acute EPA ($P < 0.05$), without changes in the $A_f/(A_f + A_s)$ relation. Similar effects on the deactivation were observed with chronic DHA ($\tau_f = 266 \pm 40$ ms and $\tau_s = 802 \pm 83$ ms for chronic DHA, $n = 12$; and $\tau_f = 296 \pm 26$ ms and $\tau_s = 1235 \pm 171$ ms in serum-free control conditions, $n = 18$). Chronic EPA or DHA did not modify the current magnitude (*Figure 3C* and see Supplementary material online, *Figure S4C*). EPA induced a positive shift of the activation curve ($V_{mid} = 21 \pm 3$ vs. 31 ± 3 mV, $P < 0.05$, $n = 14–7$, for control and chronic EPA, respectively; *Figure 3D*). However, DHA shifted the activation curve to negative potentials ($V_{mid} = 21 \pm 3$ vs. 13 ± 4 mV, $P < 0.05$, $n = 14–12$, for control and chronic DHA, respectively). Thus, chronic EPA and DHA produce different effects in the channel voltage-dependence.

Chronic treatment with EPA and DHA, but not with α-linolenic acid, decreases the protein levels of K_v1.5 in L-cells.[19] Thus, our second approach was to analyse whether chronically applied EPA and DHA modified the expression pattern of K_v7.1 and KCNE1 subunits. To that end, COS7 cells were transfected with K_v7.1-YFP alone or together with KCNE1-CFP, and the levels of K_v7.1 and KCNE1 were measured by western blot. Under both experimental conditions, EPA reduced the protein levels of K_v7.1 in a concentration-dependent manner (*Figure 4A*), but not those of KCNE1 (*Figure 4C*). Internalization and stability of K_v7.1 is regulated by ubiquitylation,[27] and PUFAs are able to modify the activity of the proteasome. Thus, the decrease in K_v7.1 protein level might be due to a higher degree of K_v7.1 degradation via proteasome. Hence, a series of experiments in the presence of 2 μM MG132 (proteasome inhibitor) were performed. Under these experimental conditions, EPA did not produce any change in the protein levels of K_v7.1, thus suggesting that EPA induces degradation of K_v7.1 via proteasome (*Figure 4B*). Similar results were obtained for DHA (see Supplementary material online, *Figure S5*).

K_v7.1 and KCNE1 subunits partially target to lipid rafts in HEK-293 cells and ventricular myocytes.[22,28] Dietary PUFAs incorporate into the cell membrane and, by altering the lipid composition and protein distribution of lipid raft microdomains, may affect ion channel function.[21] Therefore, the third approach was to analyse whether EPA and DHA modified the location of K_v7.1 and/or KCNE1 in lipid rafts. *Figures 4D* and see Supplementary material online, *Figure S5D* show the distribution of K_v7.1 and KCNE1 over the sucrose gradient under control conditions and after incubation with EPA or DHA for 48 h. Both PUFAs altered the buoyancy of cholesterol-enriched domains as indicated by a redistribution of caveolin thorough the gradient. Concomitantly, the localization of K_v7.1 and KCNE1 was also varied, indicating different channel localization in membrane microdomains. A spatial redistribution of K_v7.1 and KCNE1 in the membrane surface can account for some of the electrophysiological changes observed on K_v7.1/KCNE1.

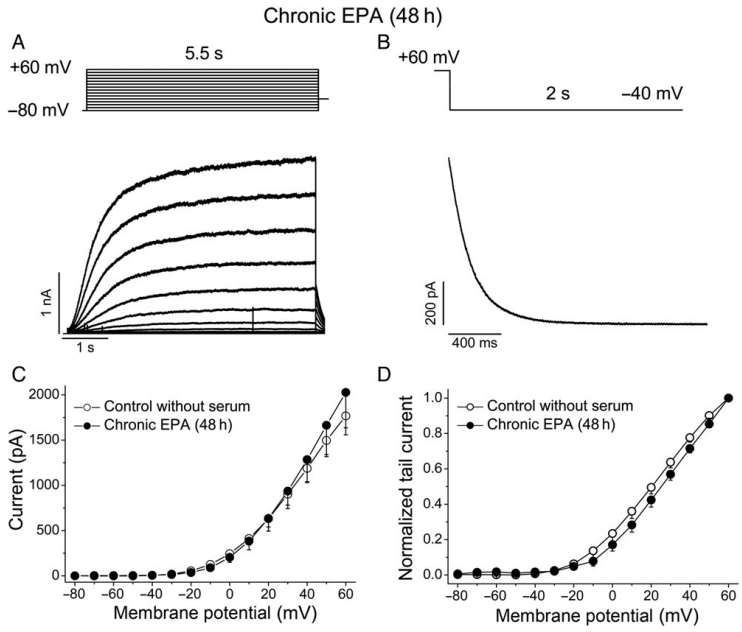

Figure 3 EPA chronic effects on $K_v7.1$/KCNE1 channels. (*A*) Currents are shown for pulses from −80 mV to voltages between −80 and +60 mV in steps of 10 mV. (*B*) Original tail currents recorded at −40 mV after a 5.5 s depolarization to +60 mV. (*C*) *I–V* relationship obtained after measuring the current after 5.5 s. (*D*) Activation curves of $K_v7.1$/KCNE1 current obtained after representing the maximum tail current amplitude vs. the previous step potential recorded in cells incubated for 48 h with EPA.

3.3 Effects of cholesterol depletion on $K_v7.1$/KCNE1 current

Association with lipid rafts is an important signalling mechanism for ion channel function and changes and disruption of these microdomains modify the activity of ion channels.[29]

Because PUFAs modified the localization of $K_v7.1$ channels in lipid microdomains, we analysed the electrophysiological consequences of the disruption of these structures (by removing cholesterol from the membrane with MβCD) on $K_v7.1$/KCNE1. COS7 cells were sequentially perfused with different external solutions in the following order: (i) normal external solution; (ii) 10 mM MβCD; (iii) 10 mM MβCD + 20 μM EPA, and (iv) drug-free external solution with 10 mM MβCD. MβCD triggered an increase in the $K_v7.1$/KCNE1 current at potentials positive to +30 mV and a decrease in the current at potentials negative to +30 mV (*Figure 5A–D*). Concomitantly, a positive shift of the activation curve approximately +23 mV ($P < 0.05$, $n = 4$) was observed (*Figure 5D* and *E*; see Supplementary material online, *Table S5*). Under these conditions, perfusion with EPA produced similar effects than those observed in cells non-treated with MβCD. Thus, (i) an increase in the current at potentials negative to +40 mV; (ii) no changes in the midpoint of the activation curve compared with that obtained in the presence of MβCD; and (iii) an increased slope factor. EPA effects were accompanied by the typical slowing of the activation kinetics that was due to the abolishment of the fast component of the activation process (see Supplementary material online, *Table S6*) and the appearance of a second component in the deactivation processes, becoming again biexponential. EPA effects produced in cholesterol-depleted cells with MβCD were reversible, not only in the magnitude of the current, but also in the kinetics and in the activation curve (*Figure 5*).

3.4 Computational modelling of the experimental results

A Markov model of the human $K_v7.1$/KCNE1 channel[30,31] was optimized to reproduce PUFA acute effects observed in $K_v7.1$/KCNE1, within the same model structure, by adjusting the parameters governing the transitions between the different channel states (see Supplementary material online, *Figures S6–S8*) and, for the case of chronic exposure to EPA, the maximal current conductance (see Supplementary material online, *Figure S6D*). Model simulations of $K_v7.1$/KCNE1 current reproduced accurately the experimental current traces under voltage clamp (see Supplementary material online, *Figure S6*) as well as current–voltage and tail current–voltage relationships (see Supplementary material

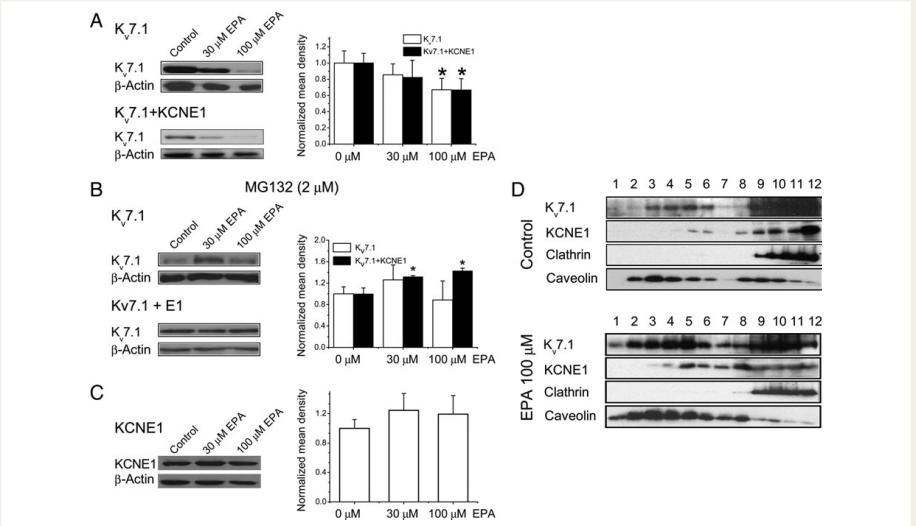

Figure 4 EPA decreases the $K_v7.1$ protein expression in COS7 cells. (*A*) Left: representative western blots illustrating treatments with EPA. Note that EPA induces dose-dependent reductions of $K_v7.1$ protein. Cellular lysates were prepared from COS7 cells transiently expressing $K_v7.1$ and incubated for 48 h with 30 and 100 μM EPA. Samples were subjected to SDS–PAGE, transferred to PVDF, and probed with an anti-$K_v7.1$ antibody. Right: Bar graph summarizing densitometry measurements used to compare protein levels for the treatments of EPA for 48 h. β-Actin levels were used as a loading control ($n = 3$ or 4; $^*P < 0.05$). (*B*) Representative western blots and graph showing the effects of EPA (0, 30, and 100 μM) on $K_v7.1$ in cells transfected with $K_v7.1$ or $K_v7.1$/KCNE1 in the presence of MG132 (proteasome inhibitor). (*C*) Representative western blots and graph showing the effects of EPA (0, 30, and 100 μM) on $K_v7.1$ in cells transfected with KCNE1. (*D*) Sucrose density gradient fractions of cells expressing $K_v7.1$ and KCNE1 in the absence or the presence of EPA. While caveolin indicated floating lipid rafts with low-density, clathrin-labelled non-raft fractions. $K_v7.1$ and KCNE1 co-localized with caveolin in low-buoyant density fractions (fractions 2–6) in control experiments, whereas EPA triggered a wider distribution of proteins (fractions 1–12) and rafts. Pictures are representative images of at least three independent lipid raft extractions analysed by western blot.

online, *Figure S8*). The $K_v7.1$/KCNE1 current model was incorporated into a biophysically detailed model for human ventricular epicardial cell AP by O'Hara *et al.*,[32] which has a basal AP duration measured at the 90% repolarization (APD_{90}) of 226 ms.

The main effects of the altered parameters during an AP are shown in *Figure 6*, and the effects on the closed zones occupancy are detailed in Supplementary material online, *Figure S9*. PUFAs increased the open state probability of the $K_v7.1$/KCNE1 channel, leading to an elevated $K_v7.1$/KCNE1 current during the AP, and slightly shortened the APD_{90} (*Figure 6*). The APD_{90} in the presence of EPA and DHA was 214 and 217 ms, respectively. These observations are also reflected in the simulated S1–S2 restitution (*Figure 6A*). On the contrary, chronic EPA did not significantly altered $K_v7.1$/KCNE1 when compared with control, and therefore expectedly did not alter the APD_{90}.

PUFA effects on $K_v7.1$/KCNE1 current were simulated in a condition in which the contribution of $K_v7.1$/KCNE1 channels to repolarization can be more critical. Indeed, along with their effects on $K_v7.1$/KCNE1 channels, acute and chronic exposure to PUFAs affects $K_v11.1$ current. The effects of a graded reduction in $K_v11.1$ were simulated. $K_v7.1$/KCNE1 and $K_v11.1$ current profiles during AP and APD_{90} are illustrated in *Figure 7*. EPA and DHA partially compensated the AP prolongation due to $K_v11.1$ reduction, whereas the chronic exposure had negligible effects for $K_v11.1$ reductions up to 60% but led further AP prolongation for 80% $K_v11.1$ block. The relative shortening of APD_{90} due to EPA in comparison with control APD_{90} was greater as the $K_v11.1$ block was increased. At a 20% block of $K_v11.1$, EPA reduced APD_{90} to 93.1%, whereas DHA reduced APD_{90} to 95.3%. At 80% block of $K_v11.1$, EPA reduced APD_{90} to 83.7%, whereas DHA reduced APD_{90} to 94.1%.

4. Discussion

In this study, we investigated the effects of two n-3 PUFAs from marine origin (EPA and DHA) on $K_v7.1$/KCNE1 channels expressed in COS7 cells and on I_{Ks} in guinea pig cardiomyocytes. We demonstrated that: (i) at physiological concentrations, both PUFAs increase the magnitude of $K_v7.1$/KCNE1 current after acute, but not after chronic, exposition, DHA being more potent than EPA. (ii) The response pattern of DHA in ventricular myocytes was complex but mainly consistent with that observed in COS7 cells. (iii) Acute and chronic effects of EPA were time- and voltage-dependent. (iv) Chronic application of either PUFAs reduced the expression of $K_v7.1$, but not that of KCNE1 due to an

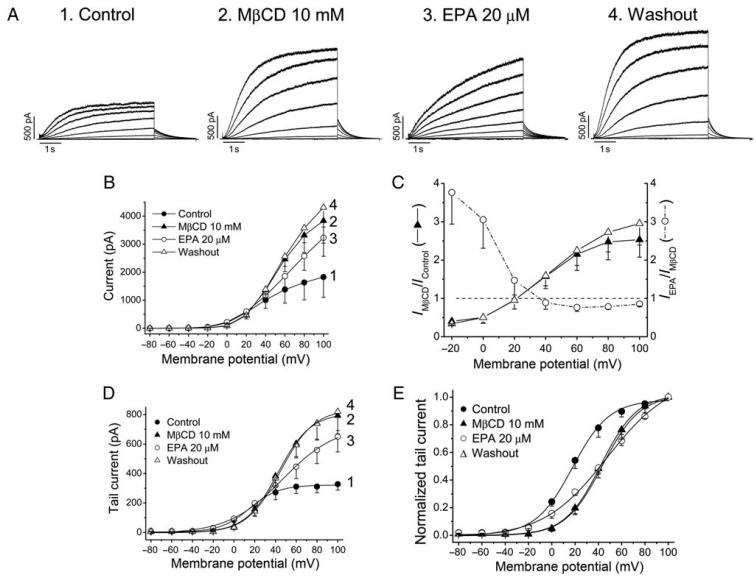

Figure 5 EPA effects in membrane cholesterol-depleted cells. (*A*) Traces of $K_v7.1$/KCNE1 current under control conditions, after perfusion with MβCD for 40 min, with EPA and washout with EPA-free external solution. All recordings were obtained from the same cell. (*B*) *I–V* relationships. (*C*) Graph showing the ratio between the current obtained after perfusion with MβCD (filled triangle) or after washout (open triangle) and that recorded under control conditions, as well as the current recorded in the presence of EPA and after perfusion with MβCD (open circle). (*D*) Activation curves. (*E*) Normalized activation curves.

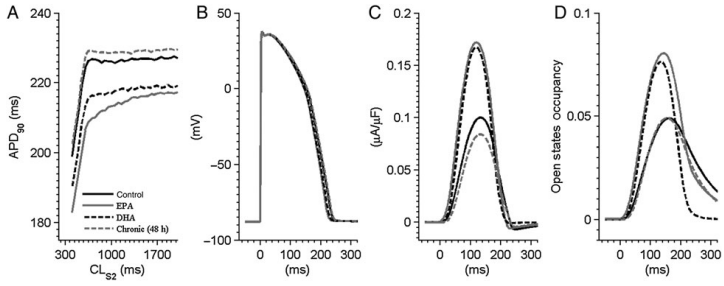

Figure 6 n-3 PUFA effects in the human ventricle O'Hara cell model.[32] (*A*) APD as a function of premature stimulus. (*B*) Action potential. (*C*) I_{Ks} profile during AP, and (*D*) occupancy of open states of the I_{Ks} model (see Supplementary material online, *Figure S9*).

enhanced degradation of $K_v7.1$ via proteasome. (v) Chronic application of either PUFAs modified the $K_v7.1$ channel distribution in membrane microdomains, and (vi) Acute EPA effects on $K_v7.1$/KCNE1 current recorded in cholesterol-depleted cells were similar to those observed without cholesterol depletion, consistent with a direct interaction with the channel during acute application.

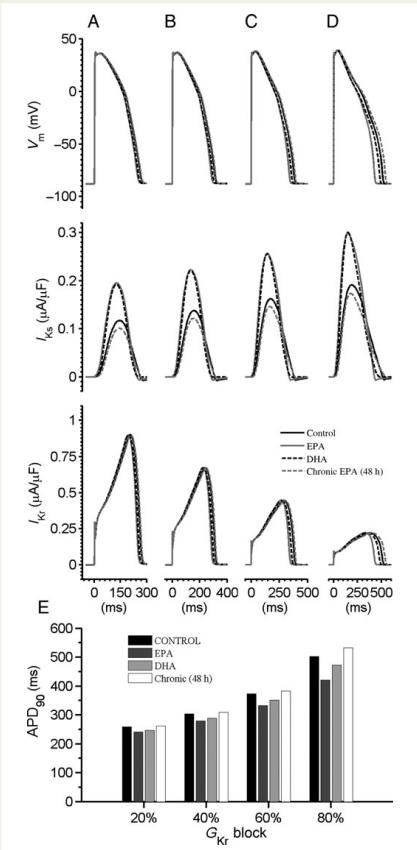

Figure 7 Effect of I_{Kr} block on simulated action potential (first row), I_{Ks} (second row), and I_{Kr} (third row). (*A*) 20% G_{Kr} block. (*B*) 40% G_{Kr} block. (*C*) 60% G_{Kr} block. (*D*) 80% G_{Kr} block. (*E*) Action potential duration (APD_{90}) as a function of G_{Kr} block. G_{Kr}, Maximum conductance of Kr channels.

4.1 Acute and chronic effects of n-3 PUFAs

In this study, we demonstrated that acute perfusion of EPA or DHA increased to a different extent the magnitude of K_v7.1/KCNE1 current. EPA and DHA increased the current and slowed its activation kinetics. Moreover, their effects on the electrophysiological properties of this current exhibited some differences, which are consistent with a direct effect of both PUFAs with these channels. These results can be due to a modification of the interaction between KCNE1 and K_v7.1 subunits, without changes in stoichiometry, since similar effects were observed in cells transfected with the concatemer KCNQ1/KCNE1 construction and cells co-transfected with the two subunits separately. Also, as previously described,[16] neither EPA nor DHA modified the properties of K_v7.1 channels when expressed alone (see Supplementary material online, *Figure S10*). Thus, the presence of KCNE1 subunits is essential for the observed electrophysiological effects of acutely applied PUFAs.

Dietary administration of fish oil leads to the incorporation of PUFAs into the cell membranes.[21] It has been reported that long-term PUFA intake modulates the activity of several cardiac ion channels. However, the effects of long-term administration of PUFAs differ from those observed after acute administration. In this line of evidence, the effects of long-term administration of EPA and DHA (48 h) on COS7 cells expressing K_v7.1/KCNE1 channels were different compared with those produced acutely. Chronic application of EPA or DHA did not increase the current magnitude, but it accelerated the activation process compared with acutely EPA effects. Surprisingly, EPA and DHA shifted the activation curve towards opposite directions, suggesting that the mechanism by which acute or chronic PUFA modulates the electrophysiological properties of K_v7.1/KCNE1 channels is different.

4.2 Direct and indirect effects on K_v7.1/KCNE1 channels

Several hypothesis have been proposed to explain the electrophysiological differences between acute and long-term administration of PUFAs. Some authors explain PUFA effects by a direct interaction between fatty acid and the ion channel. This hypothesis is supported by the observation that substitutions of a single amino acid in the Na_v1.5 channel diminished the inhibitory effect of acutely administered EPA.[33] Our results showing differences between EPA and DHA effects on K_v7.1/KCNE1 channels are consistent with a direct effect between PUFAs and ion channels. However, their effects were not washed-out and thus, we cannot rule out an indirect effect.

Others suggest that PUFA effects are the result of an alteration of the membrane properties rather than a direct interaction with the ion channel. It was reported that PUFAs alter the composition and order of the plasmalema.[12] In this line of evidence, it has been proposed that the potency of PUFAs to inhibit cardiac I_{Na} is correlated with their ability to increase membrane fluidity measured by steady-state fluorescence anisotropy.[34] In addition, changes in cellular redox status, metabolism of phospholipids, and modulation of gene expression are other processes, implying PUFAs that might modulate indirectly ion channel function.[35]

To further explore the mechanisms by which acute and chronic PUFAs exert their actions on K_v7.1/KCNE1 channels, three different approaches were used. First, the effects of chronic administration of EPA were analysed on the expression levels of K_v7.1 and KCNE1. In addition to their ability to modulate the electrophysiological properties of ion channels, it was reported that PUFAs decrease the expression levels of K_v1.5 channels.[19] Our data showed that long-term administration (48 h) of PUFAs decreased the protein levels of K_v7.1, but not those of KCNE1, in a concentration-dependent manner. It was established that internalization and stability of K_v7.1 is regulated through ubiquitinylation by Nedd4–2 and posterior degradation in the proteasome.[27] The decreased K_v7.1 expression was prevented by a proteasome inhibitor, suggesting that PUFAs promote K_v7.1 degradation via proteasome. Secondly, targeting of K_v7.1/KCNE1 to lipid rafts during chronic administration of PUFAs was analysed. K_v7.1 channels partially target lipid rafts in ventricular myocytes,[28] whereas KCNE1 localizes in low-buoyancy fractions only in association with K_v7.1.[22] Our results demonstrated that

chronic administration of EPA and DHA delocalized $K_v7.1$ in the cell membrane. This suggests an indirect effect of chronic application PUFAs on channel properties, through a change in its membrane environment.

It has been proposed that lipid rafts form signalling platforms in which ion channels, regulatory subunits, scaffolding proteins, kinases, and other modulatory proteins interact.[36] Differential targeting of $K_v7.1$ and KCNE1 subunits to lipid rafts might represent a critical mechanism of spatial regulation of channel properties as described for other ion channels.[29,37] Correlated changes in $K_v7.1$ and KCNE1 location in specific microdomains and in their functional properties were shown in the third set of experiments: lipid raft disruption, triggered by MβCD, was followed by measurements of $K_v7.1$/KCNE1 current, before and after acute application of EPA. Lipid raft disruption (via membrane cholesterol depletion) increased the current magnitude of $K_v7.1$/KCNE1 at potentials positive to +30 mV and shifted the activation curve towards positive potentials. This observation emphasizes the impact of membrane environment on channel properties. Most importantly, in these conditions, acute EPA application produced similar effects than those observed in non-cholesterol-depleted cells. This suggests a direct effect of EPA during acute application.

Chronic EPA shifts the activation curve to positive potentials, similar to that observed after MβCD treatment. Hence, at least some of the electrophysiological changes on $K_v7.1$/KCNE1 current after the chronic treatment with EPA might be due to a different location of both subunits on the plasma membrane microdomains. The precise mechanism involved in lipid raft modulation of channel activity is not fully understood. Three different explanations have been proposed: (i) by affecting the biophysical properties of the membrane. Lipid rafts represent thicker and less fluid parts of the membrane than non-raft domains. Changes in the membrane fluidity may modulate ion channel activity. Indeed, it has been described that TRPM8 channel agonists, such as menthol, geraniol, and monoterpenes, enhance the membrane fluidity and increase the ion current.[29] Conversely, increasing the order of the membrane after enrichment with cholesterol inhibits $K_v11.1$ and K_v7 currents.[38] We can speculate that the location of $K_v7.1$ and KCNE1 subunits in a thicker and less deformable membrane will increase the energy required for the transition from the closed to the open state. (ii) By specific lipid–protein interactions occurring at raft microdomains. A growing number of studies have demonstrated that cholesterol and PIP_2, major components of the lipid rafts, modulate the activity of several ion channels.[39–41] Moreover, it has been recently reported the binding site for fatty acids in the cavity of the prokaryotic potassium channel KcsA.[42] (iii) By protein–protein interactions. Lipid rafts are enriched in multiple signalling molecules such as G-proteins, protein kinases, phosphatases, etc. It was reported that inhibition of K_v7 channels by cholesterol involves the activity of PKC.[43] Following this reasoning, an impaired interaction between $K_v7.1$/KCNE1 with adjacent proteins could have an effect on the current magnitude. These three mechanisms are not mutually exclusive.

Overall, our results suggest that PUFAs act on Kv7.1/KCNE1 channels following two mechanisms: (i) a direct one on the channel protein and (ii) an indirect one through rupturing lipid rafts.

4.3 Clinical implications

Acutely applied, PUFAs increased I_{Ks} magnitude by enhancing channel's propensity to remain open. This increased probability of I_{Ks} current remaining open under voltage clamp protocols led to increased I_{Ks} during AP. The reduction of APD was quite small (12 ms for EPA), given the limited role that I_{Ks} has in modulating repolarization under basal physiological conditions. This AP modification *per se* is not likely to have pro- or antiarrhythmic significance. But, the I_{Ks} gain of function could play a relevant role when all the contrasting PUFA effects on cardiac electrophysiology are taken into account. Because such effects are not completely characterized in a quantitative way, we only considered, as a proof of concept, a concomitant I_{Kr} reduction. In this condition, acute PUFA exposure seems to play a significant protective role, by partially compensating the AP prolongation.

On the other hand, the AP simulations also show that chronic exposure to PUFAs does not affect APD_{90}, so that the protective role seems lost in this condition. On the contrary, under extreme I_{Kr} inhibition conditions (80% block), EPA exacerbates the lengthening of the APD. This is a potentially important issue, since it was demonstrated that PUFAs decrease I_{Kr} by 75%.[18]

PUFA antiarrhythmic effects are controversial and some of the reasons contributing to this variability might be the following. First, at the cellular level, PUFAs modify ion channel function through different mechanisms: (i) directly through specific interactions, (ii) modifying the ion channel levels of expression, and (iii) indirectly after rupturing lipid rafts. Secondly, at the population level, different ways of administration and different doses could influence the variability observed in many clinical trials. Other parameters, such as life style or the total amount of fat ingestion, would also modify the risk of cardiovascular events. Finally and more important, it has been demonstrated that PUFA antiarrhythmic potential depends on the subjacent arrhythmogenic mechanism, being antiarrhythmic in triggered activity-induced arrhythmias but deleterious in re-entry arrhythmias.

Supplementary material

Supplementary material is available at *Cardiovascular Research* online.

Acknowledgements

The authors thank T. González and A. Macías for their helpful suggestions. We thank Barhanin for kindly provide us with the pCDNA3.1 KCNQ1/KCNE1 concatemer construction.

Conflict of interest: none declared.

Funding

This work was supported by grants from CICYT (SAF2010-14916 and SAF2013-45800-R to C.V.; BFU2011-23268 and CSD2008-00005 to A.F.) and FIS (PI11/02459, RD06/0014/0006, and RD12/0042/0019 to C.V.). C.M. and M.G. hold FPI grants. N.C. and A.d.l.C. hold Juan de la Cierva and RIC contracts, respectively.

References

1. Moreno C, Macias A, de la Cruz A, Prieto A, Gonzalez T, Valenzuela C. Effects of n-3 polyunsaturated fatty acids on cardiac ion channels. *Front Physiol* 2012;**3**:245.
2. Burr ML, Fehily AM, Gilbert JF, Rogers S, Holliday RM, Sweetnam PM, Elwood PC, Deadman NM. Effects of changes in fat, fish, and fibre intakes on death and myocardial reinfarction: diet and reinfarction trial (DART). *Lancet* 1989;**2**:757–761.
3. GISSI-Prevenzione Investigators. Dietary supplementation with n-3 polyunsaturated fatty acids and vitamin E after myocardial infarction: results of the GISSI-Prevenzione trial. Gruppo Italiano per lo Studio della Sopravvivenza nell'Infarto miocardico. *Lancet* 1999;**354**:447–455.
4. Tanaka K, Ishikawa Y, Yokoyama M, Origasa H, Matsuzaki M, Saito Y, Matsuzawa Y, Sasaki J, Oikawa S, Hishida H, Itakura H, Kita T, Kitabatake A, Nakaya N, Sakata T, Shimada K, Shirato K. Reduction in the recurrence of stroke by eicosapentaenoic acid for hypercholesterolemic patients: subanalysis of the JELIS trial. *Stroke* 2008;**39**:2052–2058.

5. Tavazzi L, Maggioni AP, Marchioli R, Barlera S, Franzosi MG, Latini R, Lucci D, Nicolosi GL, Porcu M, Tognoni G. Effect of n-3 polyunsaturated fatty acids in patients with chronic heart failure (the GISSI-HF trial): a randomised, double-blind, placebo-controlled trial. *Lancet* 2008;**372**:1223–1230.
6. Marchioli R, Barzi F, Bomba E, Chieffo C, Di GD, Di MR, Franzosi MG, Geraci E, Levantesi G, Maggioni AP, Mantini L, Marfisi RM, Mastrogiuseppe G, Mininni N, Nicolosi GL, Santini M, Schweiger C, Tavazzi L, Tognoni G, Tucci C, Valagussa F. Early protection against sudden death by n-3 polyunsaturated fatty acids after myocardial infarction: time-course analysis of the results of the Gruppo Italiano per lo Studio della Sopravvivenza nell'Infarto Miocardico (GISSI)-Prevenzione. *Circulation* 2002;**105**: 1897–1903.
7. Coronel R, Wilms-Schopman FJ, Den Ruijter HM, Belterman CN, Schumacher CA, Opthof T, Hovenier R, Lemmens AG, Terpstra AH, Katan MB, Zock P. Dietary n-3 fatty acids promote arrhythmias during acute regional myocardial ischemia in isolated pig hearts. *Cardiovasc Res* 2007;**73**:386–394.
8. Kromhout D, Giltay EJ, Geleijnse JM. n-3 fatty acids and cardiovascular events after myocardial infarction. *N Engl J Med* 2010;**363**:2015–2026.
9. Rauch B, Schiele R, Schneider S, Diller F, Victor N, Gohlke H, Gottwik M, Steinbeck G, Del CU, Sack R, Worth H, Katus H, Spitzer W, Sabin G, Senges J. OMEGA, a randomized, placebo-controlled trial to test the effect of highly purified omega-3 fatty acids on top of modern guideline-adjusted therapy after myocardial infarction. *Circulation* 2010;**122**: 2152–2159.
10. Burr ML, Ashfield-Watt PA, Dunstan FD, Fehily AM, Breay P, Ashton T, Zotos PC, Haboubi NA, Elwood PC. Lack of benefit of dietary advice to men with angina: results of a controlled trial. *Eur J Clin Nutr* 2003;**57**:193–200.
11. Raitt MH, Connor WE, Morris C, Kron J, Halperin B, Chugh SS, McClelland J, Cook J, MacMurdy K, Swenson R, Connor SL, Gerhard G, Kraemer DF, Oseran D, Marchant C, Calhoun D, Shnider R, McAnulty J. Fish oil supplementation and risk of ventricular tachycardia and ventricular fibrillation in patients with implantable defibrillators: a randomized controlled trial. *JAMA* 2005;**293**:2884–2891.
12. Den Ruijter HM, Berecki G, Opthof T, Verkerk AO, Zock PL, Coronel R. Pro- and anti-arrhythmic properties of a diet rich in fish oil. *Cardiovasc Res* 2007;**73**:316–325.
13. Honoré E, Barhanin J, Attali B, Lesage F, Lazdunski M. External blockade of the major cardiac delayed-rectifier K^+ channel (Kv1.5) by polyunsaturated fatty acids. *Proc Natl Acad Sci USA* 1994;**91**:1937–1941.
14. Xiao YF, Kang JX, Morgan JP, Leaf A. Blocking effects of polyunsaturated fatty acids on Na^+ channels of neonatal rat ventricular myocytes. *Proc Natl Acad Sci USA* 1995;**92**: 11000–11004.
15. Xiao YF, Gomez AM, Morgan JP, Lederer WJ, Leaf A. Suppression of voltage-gated L-type Ca^{2+} currents by polyunsaturated fatty acids in adult and neonatal rat ventricular myocytes. *Proc Natl Acad Sci USA* 1997;**94**:4182–4187.
16. Doolan GK, Panchal RG, Fonnes EL, Clarke AL, Williams DA, Petrou S. Fatty acid augmentation of the cardiac slowly activating delayed rectifier current (I_{Ks}) is conferred by hminK. *FASEB J* 2002;**16**:1662–1664.
17. Jude S, Bedut S, Roger S, Pinault M, Champeroux P, White E, Le Guennec JY. Peroxidation of docosahexaenoic acid is responsible for its effects on ITO and ISS in rat ventricular myocytes. *Br J Pharmacol* 2003;**139**:816–822.
18. Guizy M, Arias C, David M, Gonzalez T, Valenzuela C. ω-3 and ω-6 polyunsaturated fatty acids block HERG channels. *Am J Physiol Cell Physiol* 2005;**289**:C1251–C1260.
19. Guizy M, David M, Arias C, Zhang L, Cofan M, Ruiz-Gutierrez V, Ros E, Lillo MP, Martens JR, Valenzuela C. Modulation of the atrial specific $K_v1.5$ channel by the n-3 polyunsaturated fatty acid, alpha-linolenic acid. *J Mol Cell Cardiol* 2008;**44**:323–335.
20. Sanguinetti MC, Curran ME, Zou A, Shen J, Spector PS, Atkinson DL, Keating MT. Coassembly of K(V)LQT1 and minK (IsK) proteins to form cardiac I(Ks) potassium channel. *Nature* 1996;**384**:80–83.
21. Verkerk AO, van Ginneken AC, Berecki G, Den Ruijter HM, Schumacher CA, Veldkamp MW, Baartscheer A, Casini S, Opthof T, Hovenier R, Fiolet JW, Zock PL, Coronel R. Incorporated sarcolemmal fish oil fatty acids shorten pig ventricular action potentials. *Cardiovasc Res* 2006;**70**:509–520.
22. Roura-Ferrer M, Sole L, Oliveras A, Dahan R, Bielanska J, Villarroel A, Comes N, Felipe A. Impact of KCNE subunits on KCNQ1 ($K_v7.1$) channel membrane surface targeting. *J Cell Physiol* 2010;**225**:692–700.
23. Valenzuela C, Sanchez Chapula J, Delpon E, Elizalde A, Perez O, Tamargo J. Imipramine blocks rapidly activating and delays slowly activating K^+ current activation in guinea pig ventricular myocytes. *Circ Res* 1994;**74**:687–699.
24. Macias A, Moreno C, Moral-Sanz J, Cogolludo A, David M, Alemanni M, Perez-Vizcaino F, Zaza A, Valenzuela C, Gonzalez T. Celecoxib blocks cardiac $K_v1.5$, $K_v4.3$ and $K_v7.1$ (KCNQ1) channels: effects on cardiac action potentials. *J Mol Cell Cardiol* 2010;**49**: 984–992.
25. Rocchetti M, Freli V, Perego V, Altomare C, Mostacciuolo G, Zaza A. Rate dependency of beta-adrenergic modulation of repolarizing currents in the guinea-pig ventricle. *J Physiol* 2006;**574**:183–193.
26. Brouwer IA, Zock PL, Camm AJ, Bocker D, Hauer RN, Wever EF, Dullemeijer C, Ronden JE, Katan MB, Lubinski A, Buschler H, Schouten EG. Effect of fish oil on ventricular tachyarrhythmia and death in patients with implantable cardioverter defibrillators: the Study on Omega-3 Fatty Acids and Ventricular Arrhythmia (SOFA) randomized trial. *JAMA* 2006;**295**:2613–2619.
27. Jespersen T, Membrez M, Nicolas CS, Pitard B, Staub O, Olesen SP, Baro I, Abriel H. The KCNQ1 potassium channel is down-regulated by ubiquitylating enzymes of the Nedd4/Nedd4-like family. *Cardiovasc Res* 2007;**74**:64–74.
28. Balijepalli RC, Delisle BP, Balijepalli SY, Foell JD, Slind JK, Kamp TJ, January CT. Kv11.1 (ERG1) K^+ channels localize in cholesterol and sphingolipid enriched membranes and are modulated by membrane cholesterol. *Channels* 2007;**1**:263–272.
29. Morenilla-Palao C, Pertusa M, Meseguer V, Cabedo H, Viana F. Lipid raft segregation modulates TRPM8 channel activity. *J Biol Chem* 2009;**284**:9215–9224.
30. Silva J, Rudy Y. Subunit interaction determines I_{Ks} participation in cardiac repolarization and repolarization reserve. *Circulation* 2005;**112**:1384–1391.
31. Severi S, Corsi C, Rocchetti M, Zaza A. Mechanisms of beta-adrenergic modulation of I(Ks) in the guinea-pig ventricle: insights from experimental and model-based analysis. *Biophys J* 2009;**96**:3862–3872.
32. O'Hara T, Virag L, Varro A, Rudy Y. Simulation of the undiseased human cardiac ventricular action potential: model formulation and experimental validation. *PLoS Comput Biol* 2011;**7**:e1002061.
33. Xiao YF, Ke Q, Wang SY, Auktor K, Yang Y, Wang GK, Morgan JP, Leaf A. Single point mutations affect fatty acid block of human myocardial sodium channel alpha subunit Na+ channels. *Proc Natl Acad Sci USA* 2001;**98**:3606–3611.
34. Leifert WR, McMurchie EJ, Saint DA. Inhibition of cardiac sodium currents in adult rat myocytes by n-3 polyunsaturated fatty acids. *J Physiol* 1999;**520** (Pt 3):671–679.
35. Leaf A, Xiao YF, Kang JX, Billman GE. Prevention of sudden cardiac death by n-3 polyunsaturated fatty acids. *Pharmacol Ther* 2003;**98**:355–377.
36. Martens JR, O'Connell K, Tamkun MM. Targeting of ion channels to membrane microdomains: localization of KV channels to lipid rafts. *Trends Pharmacol Sci* 2004;**25**:16–21.
37. Romanenko VG, Fang Y, Byfield F, Travis AJ, Vandenberg CA, Rothblat GH, Levitan I. Cholesterol sensitivity and lipid raft targeting of Kir2.1 channels. *Biophys J* 2004;**87**: 3850–3861.
38. Chun YS, Shin S, Kim Y, Cho H, Park MK, Kim TW, Voronov SV, Di PG, Suh BC, Chung S. Cholesterol modulates ion channels via down-regulation of phosphatidylinositol 4,5-bisphosphate. *J Neurochem* 2010;**112**:1286–1294.
39. David M, Macias A, Moreno C, Prieto A, Martinez-Marmol R, Vicente R, Felipe A, Gonzalez T, Tamkun MM, Valenzuela C. PKC activity regulates functional effects of $K_v\beta1.3$ on $K_v1.5$ channels. Identification of a cardiac $K_v1.5$ channelosome. *J Biol Chem* 2012;**287**:21416–21428.
40. Loussouarn G, Park KH, Bellocq C, Baro I, Charpentier F, Escande D. Phosphatidylinositol-4,5-bisphosphate, PIP2, controls KCNQ1/KCNE1 voltage-gated potassium channels: a functional homology between voltage-gated and inward rectifier K^+ channels. *EMBO J* 2003;**22**:5412–5421.
41. Epshtein Y, Chopra AP, Rosenhouse-Dantsker A, Kowalsky GB, Logothetis DE, Levitan I. Identification of a C-terminus domain critical for the sensitivity of Kir2.1 to cholesterol. *Proc Natl Acad Sci USA* 2009;**106**:8055–8060.
42. Smithers N, Bolivar JH, Lee AG, East JM. Characterizing the fatty acid binding site in the cavity of potassium channel KcsA. *Biochem* 2012;**51**:7996–8002.
43. Lee SY, Choi HK, Kim ST, Chung S, Park MK, Cho JH, Ho WK, Cho H. Cholesterol inhibits M-type K^+ channels via protein kinase C-dependent phosphorylation in sympathetic neurons. *J Biol Chem* 2010;**285**:10939–10950.